Fakultät für Medizin

Institut für Diabetes und Adipositas

The Role of Mitochondrial Fission Protein *Drp1* in Pancreatic Islets and Beta Cells

Uma Kabra

Vollständiger Abdruck der von der Fakultät für Medizin der Technischen Universität München zur Erlangung des akademischen Grades eines

Doktors der Naturwissenschaften

genehmigten Dissertation.

Vorsitzender: Prof. Dr. Radu Roland Rad

Prüfer der Dissertation: 1. Prof. Dr. Matthias Tschöp
2. Prof. Dr. Wolfgang Wurst

Die Dissertation wurde am 20.03.2017 bei der Technischen Universität München eingereicht und durch die Fakultät für Medizin am 06.10.2017 angenommen.

Summary

The development of Type 2 Diabetes (T2D) is often associated with impaired mitochondrial dynamics and bioenergetics, particularly in pancreatic beta (β) cells. In this thesis, I show that alteration in mitochondrial dynamics affects mitochondrial bioenergetics and subsequently glucose-stimulated insulin secretion (GSIS) in pancreatic β-cells and islets. The transient phosphorylation of *Drp1*, a mitochondrial fission regulator, at its serine residues 616 and 637 in response to glucose indicates involvement of *Drp1* during GSIS. Genetic silencing of *Drp1* altered mitochondrial morphology, increased mitochondrial proton leak and decreased GSIS in mouse insulinoma MIN6 cells, consistent with another study in INS-1E cell line. Acute pharmacological inhibition of *Drp1* by mitochondrial division inhibitor (mdivi-1) mimicked genetic knockdown effects not only in MIN6 cells but also in mouse and human pancreatic islets. Surprisingly, comprehensive analysis of bioenergetics in MIN6 cells and islets revealed that *Drp1* deficiency attenuated GSIS by lowering glucose-fuelled respiration linked to ATP production, instead of its effect on proton leak as suggested previously. Strikingly, the impaired ATP output and insulin secretion was rescued by supplying fission-deficient cells and islets with pyruvate. It thus transpires that *Drp1*-dependent mitochondrial dynamics influences mitochondrial function and GSIS, both by controlling mitochondrial substrate delivery upstream of oxidative phosphorylation. Furthermore, transient *Drp1* overexpression rescued the impaired insulin secretion triggering in *Drp1* knockdown MIN6 cells. In the last part of my thesis, I explore bioenergetics of islets from diet-induced obese (DIO) and chow fed mice using respirometry as a tool to predict pancreatic β-cell function. Although there were no apparent pathologies in absolute GSIS values, I found high-fat diet-induced increase in insulin content and marked decrease in glucose-stimulated respiration, resulting in reduced ATP-linked respiration. Normalizing GSIS to insulin content uncovered compromised insulin secretion triggering in DIO islets. Additionally, I also disclose that plotting mitochondrial respiratory parameters vs. GSIS classifies dysfunctional properties of pancreatic insulin secretion. Using this prediction model, the data of DIO islets suggested defects in or upstream of oxidative phosphorylation. Moreover, internally standardizing mitochondrial respiration as coupling efficiency (CE) reveals a bioenergetic threshold for insulin triggering that can be used to address mitochondrial failure across independent studies.

Zussammenfassung (verfasst durch Mithilfe von Dr. Martin Jastroch)

Die Entwicklung der Krankheit Typ 2 Diabetes mellitus (T2D) wird oft mit gestörten morphologischen Dynamiken und Bioenergetik der Mitochondrien assoziert, insbesondere in pankreatischen beta (β) Zellen. In dieser Doktorarbeit zeige ich, daß Änderungen in der Mitochondriendynamik sowohl die mitochondrielle Bionergetik als auch die Glukose-stimulierte Insulinsekretion (*glucose-stimulated insulin secretion = GSIS*) von pankreatischen β-Zellen und Inseln beeinflussen. Das Protein *Drp1*, welches die Fragmentierung von Mitochondrien (*mitochondrial fission*) reguliert, wird transient an seinen Serinen 616 und 637 bei Glukosegabe phosphoryliert und impliziert dadurch eine direkte Beteiligung des Proteins während der Glukoseaktivierung der β-Zellen. Die genetische manipulierte Reduktion des *Drp1* Proteins zeigt Änderungen der Mitochondrienmorphologie, Erhöhungen des mitochondriellen Protonenlecks, sowie eine Reduktion von *GSIS* in murinen Insulinoma Zellen (MIN6), und bestätigt somit die Befunde einer früheren Studie an einer Ratten-Zellinie (INS-1E). Akute pharmakologische Inaktivierung von *Drp1* durch den Mitochondrien-Teilungs-Inhibitor 1 (*mitochondrial division inhibitor = mdivi-1*) rekapituliert die Effekte des genetischen *knockdowns* sowohl in MIN6 Zellen, als auch in murinen und humanen pankreatischen Langerhansschen Inseln. Meine umfangreiche Analyse der Bioenergetik von MIN6 Zellen und pankreatischen Inseln zeigt, dass *Drp1* Defizienz die Glukose-stimulierte Insulinsekretion abschwächt, und zwar durch die Erniedrigung der Glukose-abhängigen Atmung, welche an ATP Produktion gekoppelt ist, aber nicht durch Effekte auf das Protonenleck, wie in früheren Studien gezeigt. Dieser Mechanismus wurde eindeutig erörtert, da in fragmentierungs-defizienten beta Zellen und pankreatischen Inseln die komprimierte ATP Produktion und Insulinsekretion durch Zugabe von Pyruvat wiederhergestellt werden kann. Somit konnte ich eindeutig zeigen, daß *Drp1*-abhängige Mitochondriendynamiken die Mitochondrienfunktion und GSIS beeinflussen, beides durch die Kontrolle der mitochondriellen Substratzulieferung oberhalb der oxidativen Phosphorylierung. Zusätzlich zeige ich, daß die transiente Überexpression von *Drp1* in *Drp1 knockdown* MIN6 Zellen das Auslösen (*triggering*) der Insulinsekretion retten kann. Im letzten Teil meiner Arbeit evaluiere ich, ob mit der bioenergetischen Analyse durch Respirometrie die Funktionalität der pankreatischen Inseln von diät-induzierten gegen normalgefütterten Mäusen

vorhergesagt werden kann. Obwohl die absoluten Insulinsekretionswerte keine Pathologien zeigen, gibt es eine diät-induzierte Erhöhung des Insulingehaltes und eine signifikanter Erniedrigung der Glukose-induzierten Atmung, welche in reduzierter ATP-produzierender Atmung resultiert. Durch die konventionelle Normalisierung der Insulinsekretion zum Insulingehalt ist erkenntlich, daß der Auslöser von Insulinsekretion in der Tat kompromittiert ist. Ich zeige, daß die Korrelationen von Atmungsparametern genutzt werden können, um Störungen der pankreatischen Insulinsekretion zu klassifizieren. Dieses Klassifizierungsmodell prognostiziert, daß *DIO* Effekte insbesondere oberhalb oder innerhalb der oxidativen Phosphorylierung zu finden sind. Des Weiteren zeigen diese Modellanalysen, daß der intern standardisierende Faktor Kopplungseffizienz (*CE = coupling efficiency*) einen bioenergetischen Schwellwert für das Auslösen der Insulinsekretion bestimmt, welcher benutzt werden kann um mitochondrielle Dysfunktionen aufzuzeigen, und zwar vergleichend über unabhängige Studien.

Acknowledgements

I would like to express my sincere gratitude to Prof. Matthias Tschöp, for giving me the opportunity to work in his research group, and for all the advice and support he has given me over the years.

I would like to express my gratefulness towards my mentor Dr. Martin Jastroch for pioneering me into the field of diabetes research, for persistent support, encouragement, optimism and never-ending enthusiasm. I really appreciate working with you and I have learnt a lot during my time as your PhD-student.

I would further like to thank my co-supervisors Dr. Charles Affourtit and Dr. Johannes Becker for their insightful discussion and guidance on my project, which has steered me towards success.

I am also grateful for our collaborators Prof. Heiko Lickert and Dr. Adriana Migliorini for generously sharing protocols, materials and valuable knowledge on confocal microscopy and human islets that aided critically in my manuscript.

I want to thank Dr. Susanne Keipert, Dr. Ruchi Jain, Katrin Pfuhlmann, Ellen Walheim, Veronica Casquero, Maria Kutschke, and Daniel Lamp for their scientific input, support and valuable assistance in the lab with experiments.

I am also grateful to my lab colleagues for the wonderful friendships I have gained over the years and all the fun we had together in and outside the lab.

To my husband, Dhiraj, for the endless love, patience and support he has given me over the years. My adorable children, Khush and Harshita, you have always brought fun and laughter to us.

Lastly but most importantly, I would like to pay regards to my parents for their unwavering love, faith, boundless encouragement and inspiration throughout my PhD study and lifting me uphill this phase of life.

Table of Contents

List of Tables

List of Figures

List of Abbreviations

^0C	Grad celsius
β	Beta
μ	Micro
ADP	Adenosine diphosphate
ATP	Adenosine triphosphate
BCA	Bicinchoninic acid
BSA	Bovine serum albumin
Ca^{2+}	Calcium ion
cAMP	Cyclic adenosine monophosphate
Cdk	Cyclin-dependent kinase
CE	Coupling efficiency
CMRL	Connaught medical research laboratories
CMT2A	Charcot Marie Tooth 2A
CO_2	Carbondiaoxide
Co-A	Coenzyme A
COS-7	Fibroblast like cell lines derived from monkey kidney tissue
C-peptide	Connecting peptide
Cys	Cysteine
2-DG	2-deoxyglucose
DMEM	Dulbecco's modified eagle medium
DMSO	Dimethyl sulfoxide
DN	Dominant negative
DNA	Deoxyribonucleic acid
DPBS	Dulbecco's phosphate buffered saline
Drp1	Dynamin related protein 1
ELISA	Enzyme-linked immunosorbent assay
ER	Endoplasmic reticulum
ETC	Electron transport chain
$FADH_2$	Flavin adenine dinucleotide (reduced form)
FBS	Fetal bovine serum
FCCP	Carbonyl cyanide-*4*-(trifluoromethoxy)phenylhydrazone
FFA	Free fatty acid

Fis1	Fission factor 1
g	Gravitational force
GCK	Glucokinase
GED	GTPase effector domain
GIP	Gastric inhibitory polypeptide
GLP1	Glucagon-like peptide 1
GLUT	Glucose transporter
G6P	Glucose-6-phosphate
GSIS	Glucose-stimulated insulin secretion
GSR	Glucose stimulated respiration
GTP	Guanosine triphosphate
h	Hour
H^+	Hydrogen ion
HCT119	Human colorectal cancer cell line
HeLa	Human cells grown from cervical cancer of african-american women
HEPES	4-(2-hydroxyethyl)-1-piperazineethanesulfonic acid
HFD	High fat diet
H_2O	Water
HPRT	Hypoxanthine-guanine phosphoribosyl transferase
HRP	Horseradish peroxidase
IMM	Inner mitochondrial membrane
IMS	Intermembrane space
Ins	Insulin
INS1	Insulinoma 1 cell line derived from rat
K^+	Potassium ion
K_{ATP}	ATP sensitive potassium channel
KDa	Kilodalton
KRH	Hepes-balanced Krebs ringer buffer
L	Liter
LB	Luria Broth
LDH	Lactate dehydrogenase
m	Milli

M	Molar
MARCH	Membrane-associated RING-CH
MAPL	Mitochondria associated protein ligase
mdivi-1	Mitochondrial division inhibitor 1
Mff	Mitochondrial fission factor
Mfn	Mitofusin
MiD	Mitochondrial dynamic protein
mins	Minutes
MIN6	Mouse insulinoma 6 cell line
MODY	Maturity onset diabetes of young
mol	Mole
mRNA	Messenger ribonucleic acid
mtDNA	Mitochondrial DNA
n	Nano
NADH	Nicotinamide-adenine dinucleotide
$NaHCO_3$	Sodium bicarbonate
OCR	Oxygen consumption rate
OMM	Outer mitochondrial membrane
Opa1	Optic atrophy 1
OXPHOS	Oxidative phosphorylation
Pdx1	Pancreatic and duodenal homebox 1 promoter
PHD	Pleckstrin homology domain
qPCR	Quantitative polymerase chain reaction
RIA	Radioimmuno assay
RIPA	Radioimmunoprecipitation assay
RNA	Ribonucleic acid
RNAi	RNA interference
ROS	Reactive oxygen species
SEM	Standard error mean
Ser	Serine
shRNA	Short hairpin RNA
siRNA	Small interference RNA
STZ	Streptozotocin

SUMO	Small ubiquitin-like modifier
T	Threonine
T1D	Type 1 Diabetes
T2D	Type 2 Diabetes
TBST	Tris-buffered saline with Tween 20
TCA	Tricarboxylic acid
TFAM	Transcription factor A, mitochondrial
Tris	Tris(hydroxymethyl)aminoethane
tRNA	Transfer RNA

1 Introduction

1.1 Diabetes and the pancreatic beta (β) cell

1.1.1 Diabetes – A worldwide problem

Diabetes (diabetes mellitus) is a complex metabolic disorder characterized by chronically high blood glucose concentration resulting from defective insulin secretion and/or action (Lin and Sun, 2010). There is a tremendous increase in the incidence of diabetes, which makes this disease one of the huge global health threats for mankind. According to International Diabetes Federation, this disease currently affects 285 million individuals in ages 20-79 years, which corresponds to 6.4% of the world's population. The disease is expected to increase by 70% in developing countries and by 20% in developed countries by the year 2030 (Green et al., 2003, Zimmet et al., 2001).

Diabetes is typically classified into two broad categories: Type 1 Diabetes (T1D) and Type 2 Diabetes (T2D). T1D, also referred to as juvenile diabetes, is characterized by absolute deficiency of insulin, which is caused by autoimmune destruction of insulin-secreting β cells of the pancreas. It represents approximately 5-10% of the diabetic cases (Kuzuya et al., 2002). On the other hand, T2D is the most prevalent form of diabetes representing 90-95% of all diabetic cases. A fasting blood glucose level of $>$ 7 mmol/L two hour postload glucose concentration is the benchmark of T2D (Kuzuya et al., 2002). It is characterized by two metabolic defects: impaired insulin secretion from the pancreatic β-cells and insulin resistance in the target tissues (DeFronzo, 2004). When insulin resistance develops, the pancreatic β-cells compensate by increasing their secretion of insulin, causing hyperinsulinemia (Weyer et al., 2001). In some individual's β-cells, genetically influenced, are unable to increase their secretion adequately to meet the requirements. This leads to hyperglycemia, the main hallmark of diabetes (Weir et al., 2001). The elevated insulin demands in T2D make it challenging for the β-cells to meet the needs and ultimately results in β-cell failure. This can be combined with decreased β-cell mass aggravating the pathology (Butler et al., 2003). Nongenetic factors also influence T2D include increasing age, central adiposity, sedentary lifestyle, high caloric intake and obesity (DeFronzo, 2004, Ridderstrale and Groop, 2009).

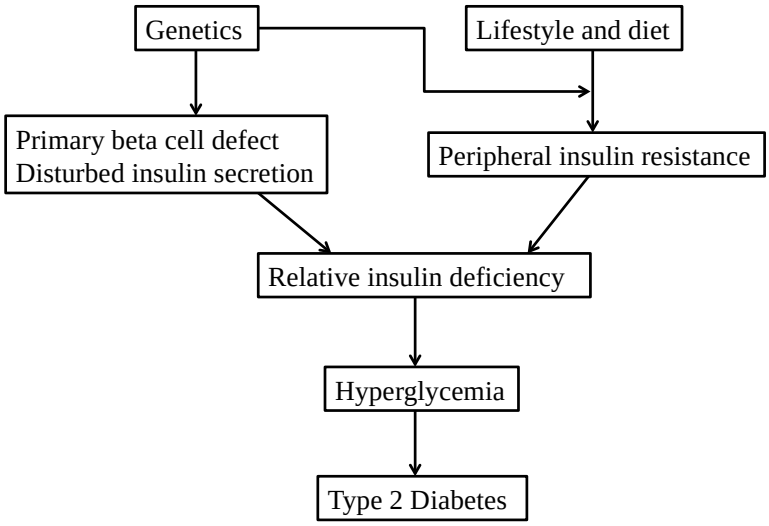

Figure 1: Pathogenesis of Type 2 Diabetes characterized by impaired insulin secretion and insulin resistance (Figure adapted from (Cheng and Fantus, 2005)).

Diabetes is also associated with long-term complications like cardiovascular diseases, retinopathy, nephropathy and neuropathy (Reasner, 2008, Soldatos and Cooper, 2008). Every year around 4 million deaths are attributable to the complication of diabetes. The overall cost of diabetes treatment, including the complications, ranges from 2.5 to 15% of the annual health care budget of a country (Gloyn, 2003, Zimmet et al., 2001).

Despite of intensive research in the field of diabetes, the triggering factors and underlying mechanisms behind the development of disease is indefinable. Therefore, in order to get better insight on the cellular and molecular aspects responsible for T2D, it is imperative to understand the concept within which glycaemia is controlled and this is discussed further below.

1.1.2 Glucose homeostasis

Glucose is the main source of energy for all types of tissues in our body. It is essential to maintain the blood glucose levels within limits of 4-7 mmol/L (DeFronzo, 2004, Kuzuya et al., 2002). In the normal physiological state, the glucose concentration is regulated by two antagonistic hormones glucagon and insulin, both secreted by the endocrine pancreas (Triplitt, 2012). Glucagon stimulates the breakdown of glycogen stored in the liver and activates hepatic gluconeogenesis, thereby increasing glucose production. Glucagon also enhances lipolysis in adipose tissue, which can be considered as an added mean of maintaining blood glucose level by providing fatty

acid fuel into the cells. In contrast, insulin lowers blood glucose levels by stimulating glycogen synthesis and inhibiting gluconeogenesis and glycogenolysis in liver. It also promotes peripheral glucose uptake by fat and muscle tissues *via* stimulation of GLUT4. On the other hand, GLUT2 in β-cells permits the entry of glucose into the cells proportionally to extracellular levels. Insulin has been shown to have an inhibitory effect on glucagon and somatostatin secretion (Schwartz et al., 2013, Triplitt, 2012, Marty et al., 2007).

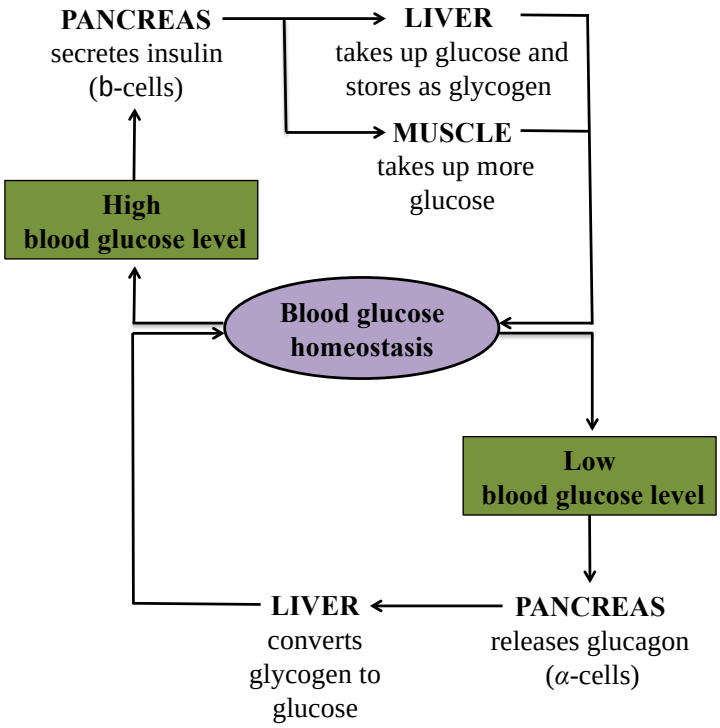

Figure 2: Glycemic control by two antagonistic hormones glucagon and insulin (Figure adapted from (James and McFadden, 2004)).

1.1.3 Islets of Langerhans

The pancreas consists of two functionally different glands that are intimately mixed together into one organ. The bulk of the pancreas is composed of exocrine cells that produce and secrete digestive enzymes and fluids like trypsin, chemotrypsin, pancreatic lipase and amylase into the upper part of small intestine. The endocrine pancreas, constituting 2-3% of total mass, are composed of several discrete clusters of cells, called the islets of Langerhans. The endocrine cells play an important role in controlling fuel storage and glucose homeostasis. Islets of Langerhans are composed of four different types of cells, existing in the ratio 68: 20: 10: 2%: β-cells (secreting insulin), alpha α-cells (glucagon), delta δ-cells (somatostatin) and *PP*-cells (pancreatic

polypeptide) (In't Veld and Marichal, 2010, Cabrera et al., 2006). Each islet structure of mice encloses β-cells in the center surrounded by layers made up of all other cell types. The highly specialized pattern of blood flow through the islet of Langerhans enables extensive exchange of molecules. However, maintenance of β-cell mass is attained by proliferation of existing β-cells, which is controlled by the various cell cycle machinery (Cabrera et al., 2006).

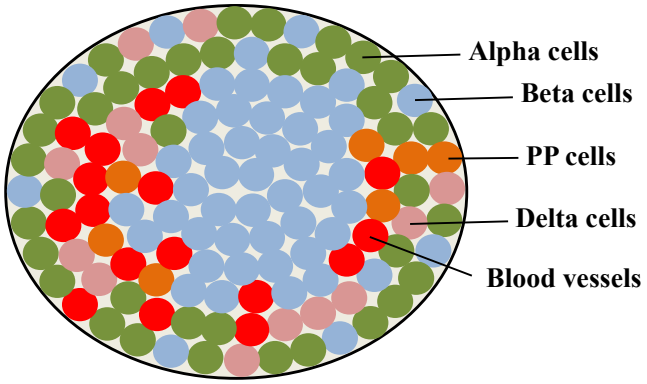

Figure 3: Physiologic anatomy of an islet of Langerhans in pancreas (Figure adapted from (Cabrera et al., 2006, Steiner et al., 2010)).

1.1.4 Glucose-Stimulated Insulin Secretion (GSIS)

Glucose is the main physiological stimulator of insulin but also increased plasma concentration of some amino acids (arginine and leucine) and neuromodulators (GLP1 and GIP) also act as stimulators (Drucker, 2001, Thorens, 2008). The main function of pancreatic β-cell is to metabolize glucose in order to secrete appropriate amount of insulin (Hiriart and Aguilar-Bryan, 2008). Each β-cell contains about 10,000 insulin granules (Leibiger et al., 2000). In response to elevated blood glucose level, e.g. after consumption of a meal, glucose is taken up by pancreatic β-cells via a facilitated glucose transporter GLUT2 (in mice) and GLUT1 (in humans) (De Vos et al., 1995, Herman and Kahn, 2006). Inside the β-cell, glucose is phosphorylated by the enzyme glucokinase forming glucose-6-phosphate (G6P). G6P is then metabolized by glycolysis in the cytoplasm forming two molecules of water (H_2O), two molecules of ATP (net), two molecules of NADH, and two molecules of pyruvate (Matschinsky, 1996). The pyruvate formed enters mitochondrial matrix where it acts either as a substrate for pyruvate carboxylase, which convert pyruvate to oxaloacetate, or for pyruvate dehydrogenase, which decarboxylates it to acetyl-CoA. Both oxaloacetate and acetyl-CoA act as a substrate for the tricarboxylic acid (TCA) cycle and serve the

generation of reducing equivalents NADH and $FADH_2$. These two compounds then donate their electrons subsequently to oxidative phosphorylation system (OXPHOS) (Fernie et al., 2004).

OXPHOS is made up of the electron transport chain (ETC) formed of five multi-subunit polypeptide complexes (I-V) together with associated mobile electron carriers, embedded within the mitochondrial inner membrane (Papa et al., 2012, Schagger and Pfeiffer, 2000). As electrons are transferred along ETC, a fixed number of protons are pumped from the mitochondrial matrix into intermembrane space (IMS). Briefly, complex I (ubiquinone NADH dehydrogenase) oxidize NADH and pumps protons ($4H^+$) into the IMS while reducing ubiquinone (Papa et al., 2008). Complex II (succinate dehydrogenase) oxidizes succinate into malate, thus liberating reducing equivalents (electrons) that are shuttled to complex III *via* ubiquinone. Complex III (ubiquinol-cytochrome-c oxidase) receives electrons and pump $4H^+$ in the process (Brzezinski and Gennis, 2008, Matsuno-Yagi and Hatefi, 2001). Complex IV (cytochrome-c oxidase) reduces molecular oxygen (O_2) to H_2O, transporting $2H^+$ in the process. This property of oxygen consumption can be used as a measure of mitochondrial ETC activity (Tsukihara et al., 2003). The proton electrochemical gradient (the proton motive force, Δp) generated is used by complex V (F1F0 ATP synthase) to drive the production of ATP from ADP + inorganic phosphate (P_i) as protons are transported back from IMS into the mitochondrial matrix (Kabaleeswaran et al., 2006). However, the consumption of NADH and $FADH_2$ and the pumping out of protons from the mitochondrial matrix are not perfectly coupled with proton re-entry and ATP synthesis. The result is a proton leak mediated by specific inner membrane proteins, the uncoupling proteins (UCPs) and dissipated as heat (Zhang et al., 2001).

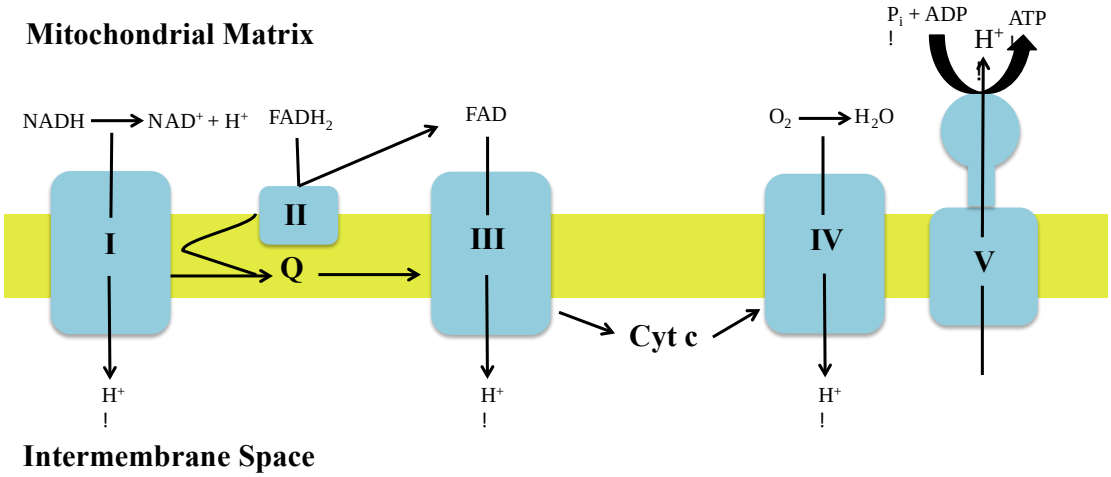

Figure 4: The Electron Transport Chain (ETC). The electron transport chain is located in the inner membrane. NADH is oxidized by Complex I to NAD^+. Electrons from Complex I are donated to Complex II. Complex II is oxidized by Complex III, which in turn reduces Complex IV. Complex IV transports electrons to molecular oxygen to form H_2O. At each complex, the energy from redox reactions is used to pump protons into the intermembrane space thereby setting up a proton motive force (PMF). PMF is used by Complex V ATP Synthase to drive the production of ATP from ADP + inorganic phosphate (P_i) (Figure adapted from (Lesnefsky and Hoppel, 2006)).

The synthesized ATP is then transported back into the cytoplasm, where it is used as source of energy, and more importantly in *β*-cells, used as a signaling molecule to stimulate insulin secretion. ATP binds to the Kir6.2 subunit of the K_{ATP} channel causing channel closure, resulting in the depolarization of the plasma membrane (Ashcroft, 2005). Depolarisation activates the opening of the L-type voltage-gated calcium channels allowing influx of Ca^{2+} ions into the cells (Bergsten et al., 1998, Yang and Berggren, 2006). Increase in intracellular free Ca^{2+} ions concentration subsequently triggers exocytosis of insulin granules. This pathway is called the K_{ATP} channel dependent insulin secretion pathway or triggering pathway (Henquin, 2000).

There is also the K_{ATP} channel independent insulin secretion pathway (termed as amplifying pathway) that involves augmented glucose-stimulated insulin release in response to increased intracellular calcium levels (Bergsten et al., 1998, Gembal et al., 1993). Although, the mechanisms of this amplification are undetermined, it is thought to involve several factors that function *via* this pathway like cAMP, phospholipase C, glutamate and plasma membrane phosphoinositides (Henquin, 2000, Warnotte et al., 1994).

GSIS is biphasic with a rapid first phase occurring within 5-10 mins, followed by a sustained second phase, which continues for the duration of the stimulus. It has been proposed that the triggering pathway is responsible for initiating the first phase and the amplifying pathway to cause the second phase. Defect in first phase of GSIS is an

early detectable sign in individuals destined to develop T2D (Henquin, 2000, Straub and Sharp, 2002).

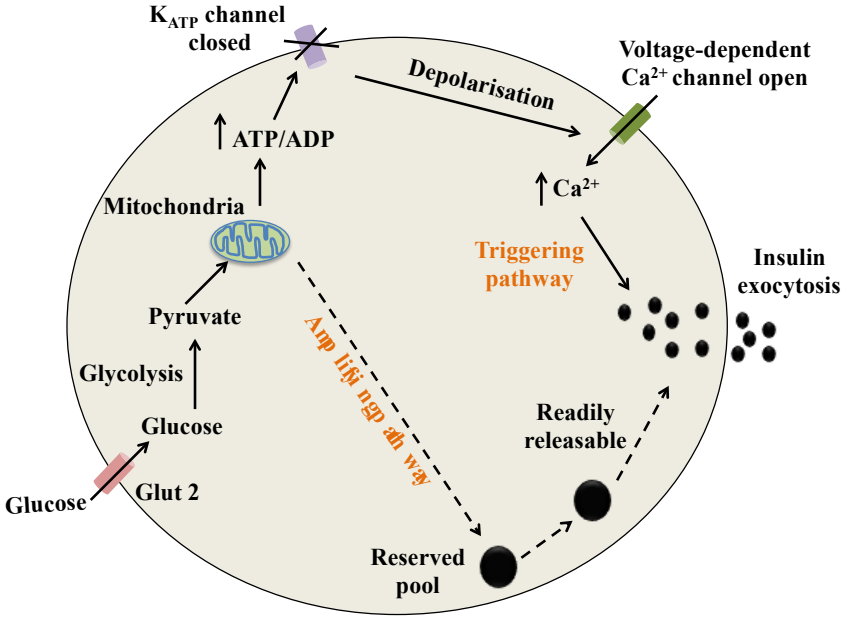

Figure 5: A simplified model of *β*-cell function. The triggering pathway begins with the uptake and catabolism of glucose generating ATP which closes the K^+ ATP-channels. This leads to membrane depolarization, which opens voltage dependent Ca^{2+} channels and Ca^{2+} flux into the cell and triggers the release of insulin granules. The amplifying pathway enhances the rate of Ca^{2+}-induced insulin release (Figure adapted from (Komatsu et al., 2013)).

From this model of the *β*-cell insulin secretory pathway, it becomes clear that many events can affect the efficiency of insulin secretion. In particular, mitochondria play an important role as it couples metabolism of glucose and other nutrients to the production of ATP and subsequently release of insulin (Kaufman et al., 2015).

1.1.5 *β*-cell mitochondria and diabetes

Mitochondria of pancreatic *β*-cell play an important role in modulating insulin secretion. Emerging evidences suggest disturbed mitochondrial function and morphology to be associated with the development of T2D (Gomez-Valades et al., 2015, Sivitz and Yorek, 2010). More than 80% of the utilized glucose is oxidized in *β*-cell. Therefore, interfering with the mitochondrial energy metabolism, for instance by blocking the respiratory chain, abolishes GSIS (Ashcroft et al., 1994, Schuit et al., 1997). The importance of mitochondria in metabolism-secretion coupling has also been exemplified by using insulin secreting Rho0 cells lacking mitochondrial DNA (mtDNA), which no longer respond to glucose. Such cells have increased NAD(P)H

levels, which inhibits glyceraldehyde phosphate dehydrogenase but facilitates lactate production by LDH. This congregating evidence emphasis the importance of hydrogen shuttles and mitochondrial respiration to effectively re-oxidize the NADH formed during glycolysis in the *β*-cell (Kennedy et al., 1998, Noda et al., 2002, Soejima et al., 1996). The effect of mitochondrial dysfunction has been demonstrated by *β*-cell specific *TFAM* knockout mice which developed mitochondrial diabetes (Maechler and Wollheim, 2001). Similarly, mutation in *Pdx1* leads to early onset diabetes of the young MODY4, one of the forms of monogenic diabetes. In addition to this, overexpression of the dominant negative version of *Pdx1* causes defective insulin secretion in *β*-cell. This can be restored by overexpression of *TFAM*. *TFAM* restores glucose-dependent ATP generation and thereby GSIS (Gauthier et al., 2004). Mitochondrial dysfunction during aging is a possible contributing factor to the development of glucose intolerance and the common forms of T2D (Maechler and Wollheim, 2001). Mitochondrial dysfunction has also been linked to impaired insulin secretion in animal models of T2D, in particular the Goto-kakisaki (GK) rat, rats injected neonatally with streptozotocin, and the 90% pancreatectomized rat (Hughes et al., 1998, Portha et al., 1988, Laybutt et al., 2002). The evidence linking mitochondrial structure with diabetes begins with the observation in type 2 diabetic patients islets that exhibited altered mitochondrial morphology, impaired glucose oxidation, reduced ATP generation, and reduced number of insulin granules explaining defective insulin secretion (Anello et al., 2005). In addition, *β*-cell isolated from Zucker diabetic fatty rat model also exhibited shorter and swollen mitochondria (Bindokas et al., 2003).

All the above observations give first insight into form-function relationship of mitochondria, pinpointing mitochondrial dynamics as an important contributing factor in upholding normal *β*-cell function. It also raises the question whether mitochondrial structure changes contribute to the *β*-cell defects in the diabetic state.

1.2 Introduction to *Drp1* (Dynamin-related protein 1)

1.2.1 Mitochondrial dynamics

The mitochondrion is a double-membrane organelle plays a central role in regulating bioenergetics, secondary metabolism, calcium homeostasis, and apoptosis in eukaryotic cells (Chan, 2006). Mitochondria exist as dynamic networks that are

constantly remodeled through the opposing actions of fusion and fission proteins. The continuous changes in mitochondrial morphology are controlled by a group of highly conserved large dynamin-related GTPases (Chen and Chan, 2005). A balance between fragmentation and fusion events is necessary for proper cell function and viability. Recent research suggests aberrant mitochondrial dynamics to be associated with the pathogenesis of several genetic and neurological disorders, cardiac dysfunction, cancer, and metabolic diseases such as diabetes and obesity (Chen et al., 2003, Davies et al., 2007, Ishihara et al., 2009, Chan, 2006).

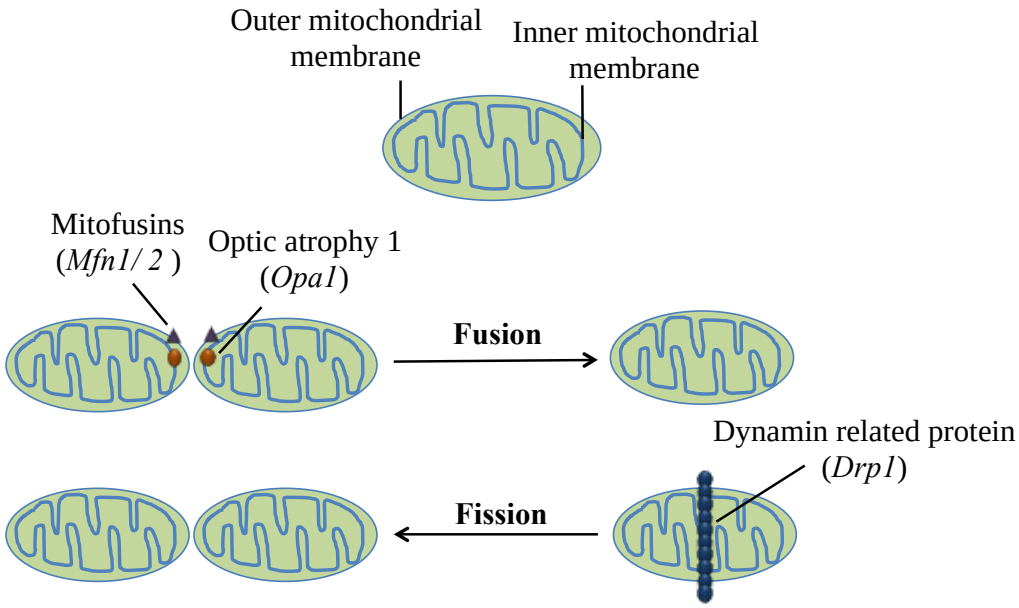

Figure 6: Regulation of mitochondrial dynamics by fusion and fission genes (Figure adapted from (Wai and Langer, 2016)).

1.2.2 Mitochondrial fusion and its machinery

Mitochondrial fusion is defined as the merger of two individual mitochondria thus forming a larger (longer) one. Fusion has been suggested as a route for the rapid exchange of metabolites, may be able to complement dysfunctional mitochondria. Recent reports have suggested that fusion is also important to maintain mitochondrial calcium buffering, propagate intra-mitochondrial Ca^{2+} waves and preserve mtDNA (Chan, 2012). Before cells enter the replication phase (S phase), mitochondria become hyperfused and increase their ATP production. Specifically in mammals, three large dynamin-family GTPases cooperates in the fusion of mitochondrial membranes: Mitofusins 1 (*Mfn1*), Mitofusins 2 (*Mfn2*) and Optic atrophy 1 (*Opa1*) (Cipolat et al., 2004, Chen et al., 2005).

Mitofusins (Mfn1 and 2)

Mitofusins regulate the fusion of the outer mitochondrial membrane (OMM) and form complexes *in-trans* that tether mitochondria together. *Mfn1* is primarily expressed on the OMM while *Mfn2* is also expressed on the endoplasmic reticulum (ER) installing trans-organelle connections (Chen et al., 2005, Chen et al., 2003, de Brito and Scorrano, 2008, Koshiba et al., 2004). Both the proteins share structural homology. *Mfn1* has higher GTPase activity and cause more efficient fusion than *Mfn2*. Moreover, *Mfn1* and *Mfn2* can functionally replace each other and deletion of both mitofusins abolishes all mitochondrial fusion. For example, fibroblasts lacking *Mfn1* and *Mfn2* completely lack mitochondrial fusion and show severe cellular defects, including poor growth, heterogeneity of mitochondrial membrane potential, and decreased respiration (DiMauro and Schon, 2003). Deletion of either *Mfn1* or *Mfn2* results in mitochondrial fragmentation (although low level of mitochondrial fusion remains), mitochondrial dysfunction, and mid-gestational lethality (Chen et al., 2003). For instance, in muscle cells glucose oxidation, oxygen consumption, and mitochondrial membrane potential are lowered by loss of *Mfn2* (Chen et al., 2010). A point mutation in the GTPase domain of *Mfn1* (*Mfn1*^{T109A}) allows the protein to act as a dominant-negative (DN), including excessive fission when overexpressed (Chen et al., 2005). Missense mutations in *Mfn2* causes Charcot-Marie-tooth disorder type 2A2 (CMT2A2), a common autosomal dominant peripheral neuropathy associated with axon degeneration (Zuchner et al., 2004). Furthermore, overexpression of fusion genes delays release of cytochrome *c* on apoptotic activation (Neuspiel et al., 2005). Overexpression of *Mfn1* induced hyperfusion leading to mitochondrial dysfunction and hypomotility, which explains impaired insulin secretion in pancreatic *β*-cell (Park et al., 2008).

Optic atrophy 1 (Opa1)

Opa1, another dynamin-related protein is embedded in the inner mitochondrial membrane (IMM) through a transmembrane domain that resides nearby the N-terminus and protrudes the major portion into the IMS. The two functions of *Opa1* consist of promoting *Mfn1*-mediated mitochondrial fusion as well as in regulating the intrinsic apoptotic pathway by impairing cristae maintenance and cytochrome *c* release (Frezza et al., 2006, Song et al., 2007). Fusion of the IMM is critical for the maintenance of mtDNA and metabolic function, and loss of *Opa1* results in

autophagic elimination of mitochondria (Chen et al., 2010). Knockdown of *Opa1* by RNA interference (RNAi) leads to mitochondrial fragmentation and deformities in cristae structure (Frezza et al., 2006). Missense mutations in *Opa1* cause autosomal dominant optic atrophy, the leading cause of hereditary blindness, followed by ataxia, deafness and a sensory-motor neuropathy (Alexander et al., 2000). Furthermore, *β*-cell lacking *Opa1* maintained normal copy number of mtDNA, however cell proliferation was impaired, whereas apoptosis was not prompted. Mice lacking *Opa1* in *β*-cell, leads to defective mitochondrial activation and GSIS, which made mice hyperglycemic (Molina et al., 2009, Zhang et al., 2011).

1.2.3 Mitochondrial fission and its machinery

Mitochondrial fission is the division of a mitochondrion to form two or more separate mitochondrial units. In mammals, mitochondrial fission is catalyzed by only one GTPase protein, namely dynamin-related protein 1 (*Drp1*). It is highly expressed in tissues, such as brain and muscle, whereas moderate to low expression levels are found in liver, lung, placenta, kidney and pancreas (Smirnova et al., 1998). *Drp1* contains four domains: an N-terminal GTP binding domain, a middle assembly domain, a variable domain, and C-terminal GTPase effector domains (GED). The molecular structure of *Drp1* lacks the C-terminal proline-rich domain termed pleckstrin homology domain (PHD), which is present in most members of the superfamily, important for dynamin-membrane interaction. Positioned like the PHD in dynamin, the variable domain of *Drp1* contains most of the post-translational modification sites. The GED domain of *Drp1* is important for mediating both intra- and intermolecular interactions and the middle domain is important for self-assembly into higher order structures (Hoppins et al., 2007, Smirnova et al., 2001, Smirnova et al., 1998).

In mice, multiple isoform of *Drp1* arise from the alternative splicing of its single gene-encoded pre-mRNA transcript. Encoded in its entirety by 20 exons, the alternative splicing of exons 3, 16 and 17, and several variations therein, gives rise to multiple *Drp1* isoforms. Among these the longer *Drp1* isoforms, expressed selectively in neurons, bear unique polypeptide sequence within their GTPase and variable domain, known as A-insert (encode for exon 3) and the B-insert (encode for exon 16 and 17) respectively. On the other hand, shorter isoforms of *Drp1* that lack A-insert but alternatively exclude either exon 16, 17 or both are variably expressed in other cell

types. It has been revealed that A and B inserts differentially alter the propensity and geometry of *Drp1* polymerization both in solution and on membranes, and additively suppress *Drp1* cooperative GTPase activity (Strack et al., 2013, Uo et al., 2009, Macdonald et al., 2016).

Drp1 is mostly cytosolic with only about 3% of the total protein content residing at the mitochondrial surface. *Drp1* requires activation such as increase in Ca^{2+} levels or initiation of apoptosis, in order to induce organelle fission. In brief, *Drp1* is recruited from cytosol to OMM (outer mitochondrial membrane), where it forms ring-like multimeric structure on prospective OMM fission sites. Further, GTP is hydrolyzed to GDP to power constriction of the *Drp1* oligomer. Finally, the *Drp1* oligomer disassembles and *Drp1* is released back into the cytosol (Ingerman et al., 2005, Mears et al., 2011). Integration of mutated *Drp1* molecules (e.g. K38A mutation with incapacitated GTP hydrolysis) inhibits their constriction through DN effects, resulting in blocked organelle fission (Smirnova et al., 2001).

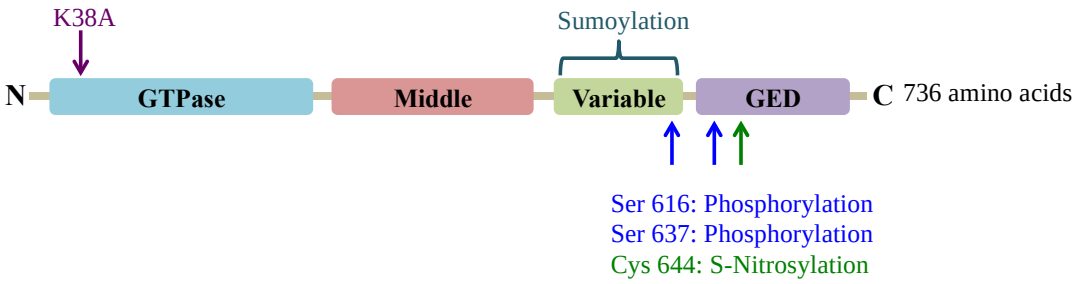

Figure 7: Domain structure and post-translational modification of *Drp1* (Figure adapted from (Cho et al., 2013)).

In yeast, *Fis1* was suggested to recruit *Drp1* to the OMM in mammalian cells (James et al., 2003). However, ablation of *Fis1* did not affect *Drp1* recruitment, but did cause mitochondrial elongation (Lee et al., 2004). Paradoxically, recent study showed that knockdown of *Fis1* in HeLa and HCT116 cells did not cause mitochondrial elongation (Otera et al., 2010). Interestingly, overexpression of *hFis1* caused pronounced fragmentation of mitochondria in both primary *β*-cell and INS-1E cells. Cells overexpressing *hFis1* showed reduced mitochondrial volume, lowered cellular ATP level, and as a consequence, impaired GSIS. In addition, inhibition of *Fis1* using RNAi displayed reduced maximal respiratory chain capacity and consequently suppressed GSIS as well as reduced reactive oxygen species (ROS) production (Park et al., 2008, Twig et al., 2008). Furthermore, recently three mammalian adaptor

proteins have been identified so far – Mff, MiD49 and MiD51– all of which can mediate *Drp1* recruitment and mitochondrial fission (Loson et al., 2013, Otera et al., 2010, Palmer et al., 2013, Richter et al., 2014).

Drp1 is essential for mitochondrial fission provoked by all cellular circumstances, like mitosis or stress. Inhibition of *Drp1* function by RNAi or expression of a DN allele causes severe elongation and interconnection of mitochondria, which can result in the formation of a perinuclear, collapsed mitochondrial mass (Lee et al., 2004, Smirnova et al., 2001). For instance, downregulation of *Drp1* expression leads to loss of mtDNA and a decrease in mitochondrial respiration in HeLa cells (Chang et al., 2010, Parone et al., 2008). However, another study demonstrated that inhibition of *Drp1* prevents the decrease in mitochondrial membrane potential and release of cytochrome *c* in COS-7 cells (Twig et al., 2008). Recently, a mutation in the fission gene *Drp1* (heterozygous mutation A395D in middle domain of *Drp1*) has been identified in a newborn child with abnormal brain development and optic atrophy. Cells derived from this patient showed aberrant elongation of mitochondria. Similarly, *Drp1* null mice have developmental abnormalities and die at midgestation (Chan, 2006, Chang et al., 2010). Apart from promoting mitochondrial fission, *Drp1* also regulate peroxisomal fission in mammals (Waterham et al., 2007). In hippocampal neurons, it has been shown that loss of *Drp1* function leads to misshaped synaptic vesicles (Huang et al., 2015). The disruption of mitochondrial morphology due to overexpression of *Drp1* leads to mitochondrial fragmentation, suppression of ETC activities, mitochondrial number and activation of apoptosis, whereas overexpression of DN isoform of *Drp1* (K38A) not only decreased mitochondrial autophagy but also reduced respiration (Frank et al., 2001). Several studies have implicated excessive mitochondrial fission as a key mediator of increased ROS production and cellular apoptosis under hyperglycemic conditions (Carneiro et al., 2012). Therefore, proper balance of fission/ fusion genes is prerequisite, since inappropriate disruption of either can be deleterious.

Post-translational modification of Drp1

The function of *Drp1* is also influenced by post-translational modifications. These covalent modifications include protein phosphorylation, S-nitrosylation, ubiquitination and sumoylation. It is well known that a distinct combination of both

post-translational modifications and protein effectors regulate the activity of *Drp1* in different physiological and pathological contexts (Santel and Frank, 2008).

Protein phosphorylation is mediated by protein kinases to modulate protein function and cellular signaling pathways. During mitosis, phosphorylation of *Drp1* at Ser616 by Cdk1/Cyclin B complex activates *Drp1*, triggering mitochondrial fission to enable even mitochondrial distribution to cellular progeny (Taguchi et al., 2007). Increased level of *Drp1* Ser616 phosphorylation was found recently in Alzheimer's disease (Wang et al., 2009). In neurons, the Ser616 site can also be phosphorylated by protein kinase C δ (PKCδ), where hypertensive encephalopathy was shown to be associated with mitochondrial fission (Qi et al., 2011). Another phosphorylation site widely studied has been *Drp1* Ser637. When activated by increased cAMP levels, protein kinase A (PKA) phosphorylates *Drp1* at residue Ser637, thereby inhibiting its GTPase activity as well as intermolecular *Drp1* interactions resulting in elongated mitochondria (Chang and Blackstone, 2007, Cribbs and Strack, 2007). This mechanism is being exploited during starvation where mitochondrial elongation can protect starving cells from autophagy (Gomes et al., 2011). In contrast, in response to increased cytosolic Ca^{2+} levels, *Drp1* dephosphorylation at Ser637 by calcineurin leads to fragmentation by boosting *Drp1* translocation to mitochondria (Cereghetti et al., 2008). Of note, increased calcineurin activity subsequent mitochondrial fission has been shown to participate in neuronal toxicity in a Huntington disease mouse model (Costa et al., 2010).

SUMOylation of *Drp1* is performed by the SUMO ligases Sumo1, Ubc9 and MAPL (Braschi et al., 2009, Figueroa-Romero et al., 2009, Harder et al., 2004), while deSUMOylation is mediated by the SUMO protease SenP5 (Zunino et al., 2007). Sumoylation of *Drp1* occurs within the variable domain of *Drp1* therefore, it may exert an effect on *Drp1* interactions with the OMM or other proteins (Figueroa-Romero et al., 2009). SUMO-1 linkage stabilizes *Drp1* on mitochondria, thereby supporting mitochondrial fragmentation (Harder et al., 2004). SUMO-2/3 conjugation stabilizes location of *Drp1* during ischemia. SUMO protease SenP3 is necessary for the removal of SUMO-2/3 conjugates of *Drp1* (Guo et al., 2013).

Drp1 can also be modified by ubiquitination. MARCH5-mediated K63-linked ubiquitination stabilizes *Drp1* on mitochondria, while parkin-mediated K48-linked ubiquitination promotes the proteasomal degradation of *Drp1* (Karbowski et al., 2007, Park et al., 2010, Wang et al., 2011).

Another modification that *Drp1* can undergo is nitrosylation. S-nitosylation of *Drp1* at residue Cys644 in AD brains triggers mitochondrial fission and subsequent synaptic loss and neuronal damage. Preventing S-nitosylation of *Drp1* through Cys644Ala mutation blocked the neurotoxicity (Cho et al., 2009). Lastly, O-linked-N-acetyl-glucosamine glycosylation (O-glcNAcylation) of *Drp1* at residues T585 and T586 activates its translocation to mitochondria in cardiomyocytes (Gawlowski et al., 2012). This discussion certainly underscores the importance of mitochondrial dynamics control and discerns *Drp1*-function contribution in mitochondrial fission.

Drp1 inhibitor: mdivi-1

The laboratory of Jodi Nunnari, UC Davis, USA identified mdivi-1 (for mitochondrial division inhibitor) as the selective inhibitor of *Drp1* in both yeast and mammalian cells. Mdivi-1, quinazolinone derivative, acts by attenuating the *Drp1* assembly in the early stages of division by preventing the polymerization of higher order structures (Cassidy-Stone et al., 2008, Lackner and Nunnari, 2010).

1.2.4 *Drp1* and pancreatic *β*-cell

Recent research in the field of diabetes and obesity recognizes the possible involvement of *Drp1* in causing mitochondrial fragmentation. Study in pancreatic insulin secreting INS1 cell line has shown that inhibition of mitochondrial fission by *Drp1-DN* resulted in the prevention of mitochondrial autophagy and accumulation of damaged mitochondrial material, leading to decreased metabolic function and insulin secretion (Twig et al., 2008). Several studies in islets and *β*-cells revealed that under gluco-lipotoxic condition the expression of *Drp1* is upregulated-initiating apoptotic signaling cascades. In contrast, suppression of *Drp1* function by *Drp1* K38A (DN mutant) significantly prevented high glucose and FFA induced *β*-cell apoptosis (Peng et al., 2011, Men et al., 2009, Peng et al., 2012). In addition, Rhein, an anthraquinone compound localizes at mitochondria in the *β*-cell and protected them from hyperglycemia-induced apoptosis by blocking ROS-*Drp1*-mitochondrial fission-apoptosis pathway (Liu et al., 2013). *Drp1* is an ER resident protein found to regulate ER morphology in stressed β-cell. Phosphorylation of *Drp1* at Ser637 by AMPK or inhibition of *Drp1* activity using GTP hydrolysis-defective mutant (Ad-K38A) prevented ER and mitochondrial morphology changes and improved *β*-cells function, induced due to saturated free fatty acid (FFA) (Wikstrom et al., 2013). Recently it has been demonstrated that inhibition of mitochondrial fission by *Drp1* K38A increased

the mitochondrial proton leak, and thus significantly blocked GSIS in INS-1E cells (Jhun et al., 2013).

Taken together, mitochondrial dynamics control the proper maintenance of tissues and organ systems, when misregulated progresses to pathologies associated with disease.

2 Aim of the Thesis

Rescuing insulin secretion of dysfunctional *β*-cells is of great therapeutic interest for individuals with diabetes. It is well accepted that mitochondria play an important role in metabolism–secretion coupling in pancreatic *β*-cells (Ashcroft et al., 1994, Kaufman et al., 2015). Emerging evidence suggests that mitochondrial morphology has an immense impact on diabetic pathophysiology. Considering the intricate relationship between mitochondrial function and morphology, it is likely that mitochondrial dynamics play a role in insulin secretion in *β*-cells (Sivitz and Yorek, 2010, Gomez-Valades et al., 2015). Among various proteins regulating mitochondrial dynamic, mitochondrial fission protein *Drp1* is important as it regulate shape, size, distribution and remodeling of cell mitochondria (Campello and Scorrano, 2010). Recent findings reinforce well-established role of *Drp1* in pancreatic *β*-cell apoptosis (Twig et al., 2008, Liu et al., 2013, Men et al., 2009, Peng et al., 2012, Peng et al., 2011), but its role in pancreatic hormone secretion, and in particular insulin secretion, remained elusive. Therefore, the specific aims of the present thesis were:

- To investigate the role of *Drp1* in GSIS in clonal *β*-cells (MIN6) and mouse and human pancreatic islets using genetical and pharmacological approaches.
- To delineate the mechanism involved in *Drp1*-mediated insulin secretion.
- To study the effect of nutrition on insulin secretion and mitochondrial bioenergetics in mouse pancreatic islets.
- To ascertain mitochondrial respiratory parameters that can quantitatively predict and classify dysfunctional properties of pancreatic insulin secretion.

3 Materials and Methods

3.1 Materials

3.1.1 Human islet donor's

Human islets were provided through the JDRF award 31-2008-416 (European Consortium for Islet Transplantation (ECIT) islet for basic research program). All the experiments were approved by Helmholtz Zentrum, Munich (Germany). Islet donor's information is given in the table below:

Table 1: Human islet donar's information

	Donar 1	**Donar 2**	**Donar 3**
Date of harvesting	November 4 2015 5:15 AM	February 10 2016 11.45 PM	October 25 2016 3.03 AM
Date of processing	November 4 2015 2:01 PM	February 11 2016 11.35 AM	October 25 2016 10.50 AM
Cold ischemic time	06:29	10.25	05:37
Age	65	55	55
Gender	Female	Female	Female
BMI (Kg/m^2)	20,8	30,1	24
ABO blood group	O	A	
HLA A	3/19 (31)	02/	2/31(19)
HLA B	7/18	40/	18/44(12)
HLA DR	13/15	13/	15/15
HIV I/II	Negative		Negative
HTLV I/II	Not done		Not done
CMV	Positive		Positive
EBV	Not done		Not done
HBsAg	Negative		Negative
Anti-HBc	Negative		Negative
Cause of death	Trauma		

3.1.2 Mouse strains

For islet isolation, male C57BL/6 mice provided by *Janvier lab* (Le Genest-Saint-Isle, France) were housed under a 12 h light dark cycle with *ad libitum* access to food and water. At the age of 8 weeks, mice were fed with either chow (5.6% fat, LM-485,

Harlan Teklad) or high-fat diet (HFD) (58% kcal fat; Research Diets Inc., New Brunswick, NJ, USA) for 16 weeks to develop diet-induced obesity (DIO). All the experiments were conducted according to the regulation of our institutional and state committees on animal experiments.

3.1.3 Cell line

MIN6 cells, a pancreatic mouse insulinoma cell line was provided by Prof. J. Miyazaki (Osaka University, Japan).

3.1.4 Laboratory equipment's

Table 2: Laboratory equipment's

Equipment	Supplier
Bacterial incubator multitron	Infors GmbH, Einsbach, Germany
Beckmann coulter	Beckmann coulter GmbH, krefeld, Germany
Centrifuge Mikro 200R	Hettrich Zentrifugen, Tuttlingen, Germany
CO_2 incubator	Thermo Fisher Scientific Inc., Waltham, MA, USA
Electroporator	Biorad, Hercules, CA, USA
Gel electrophoresis apparatus	Biorad, Hercules, CA, USA
Gene Amp pcr machine (Mastercycler pro)	Eppendorf, Mississauga, Ontario, Canada
Heating magnetic stirrer	VELP scientifica, Usmate, Italy
Incubator shaker	Thermo Fisher Scientific Inc., Waltham, MA, USA
LiCor Odyssey instrument	Lincoln, NE, USA
Mice weighing balance (Ranger 4000)	OHAUS Europe GmbH, Greifensee, Switzerland
Microscope DM6000 B	Leica Microsystems, Heerbrugg, Switzerland
Microscope Scope.A1	Zeiss, Oberkochen, Germany
Microscope SMZ1000	Nikon Instruments Europe BV, Postbus, Amsterdam, Netherlands
Nanodrop 2000 UV-Vis spectrophotometer	Thermo Fisher Scientific Inc., Waltham, MA, USA
PHERAstar FS	BMG Labtech, Ortenberg, Germany
pH meter LAB 850	Xylem Analytics Germany Sales GmbH & Co. KG, Weilheim, Germany
Scale M-prove	Sartorius, Goettingen, Germany
Scale New Classic MF	Mettler toledo, Gießen, Germany
Seahorse XF 24/96 extracellular flux analyzer	Seahorse Bioscience/Agilent technologies, Santa Clara, CA, USA
Shaker Reciprocal 30	Labnet international, Woodbridge, USA
Sonicator 150 V/T	BioLogics Inc., Manassas, Virginia, USA

SP5 confocal microscope	Leica Microsystems, Heerbrugg, Switzerland
Table centrifuge for 96well plates perfect spin P	PeQ Lab, Erlangen, Germany
Table centrifuge perfect spin mini	PeQ Lab, Erlangen, Germany
Taqman cycler Viia7	Applied biosystems, Foster City, USA
Tissue lyser II	Qiagen, Hilden, Germany
Trans Blot Turbo transfer apparatus	Biorad, Hercules, CA, USA
Vortex Mixer PeQ TWIST	PeQ Lab, Erlangen, Germany
Water bath	Thermo Fisher Scientific Inc., Waltham, MA, USA
Water installation Q-POD®	Merck Millipore, Darmstadt, Germany
XF preparation station	Seahorse Bioscience/Agilent technologies, Santa Clara, CA, USA
Zeiss LSM880 Airyscan	Carl Zeiss Microscopy GmbH, Göttingen, Germany

3.1.5 Media, buffers and antibiotics

Table 3: Media, buffers and antibiotics

Product	**Supplier**
Ampicillin	Gibco/Life Technologies/Thermo Fisher Scientific Inc., Massachusetts MA, USA
Antibiotic antimycotic solution (100 X)	Sigma-Aldrich Chemie GmbH, Taufkirchen, Germany
CMRL 1066	Gibco/Life Technologies/Thermo Fisher Scientific Inc., Massachusetts MA, USA
DMEM, high glucose, GlutaMAX(TM)	Gibco/Life Technologies/Thermo Fisher Scientific Inc., Massachusetts MA, USA
DMEM, no glucose	Gibco/Life Technologies/Thermo Fisher Scientific Inc., Massachusetts MA, USA
DPBS, no calcium, no magnesium	Gibco/Life Technologies/Thermo Fisher Scientific Inc., Massachusetts MA, USA
Fetal bovine serum (FBS)	Gibco/Life Technologies/Thermo Fisher Scientific Inc., Massachusetts MA, USA
Glutamine (200 mM)	Gibco/Life Technologies/Thermo Fisher Scientific Inc., Massachusetts MA, USA
Hank's Balanced Salt solution (HBSS)	Lonza Cologne GmbH, Cologne, Germany
HEPES (1 M)	Gibco/Life Technologies/Thermo Fisher Scientific Inc., Massachusetts MA, USA
Human serum	Sigma-Aldrich Chemie GmbH, Taufkirchen, Germany

Hyclone standard foetal bovine serum	GE healthcare /Thermo Fisher Scientific Inc., Massachusetts MA, USA
OptiPrep™ Density Gradient Medium	Sigma-Aldrich Chemie GmbH, Taufkirchen, Germany
Penicillin-Streptomycin (10,000 U/mL)	Gibco/Life Technologies/Thermo Fisher Scientific Inc., Massachusetts MA, USA
Puromycin	Gibco/Life Technologies/Thermo Fisher Scientific Inc., Massachusetts MA, USA
RIPA lysis buffer	Gibco/Life Technologies/Thermo Fisher Scientific Inc., Massachusetts MA, USA
Trypsin-EDTA (0.05%)	Gibco/Life Technologies/Thermo Fisher Scientific Inc., Massachusetts MA, USA
Versene solution	Gibco/Life Technologies/Thermo Fisher Scientific Inc., Massachusetts MA, USA

3.1.6 Chemicals

Table 4: Chemicals

Product	**Supplier**
Agar	Sigma-Aldrich Chemie GmbH, Taufkirchen, Germany
Albumin bovine Fraction V, Protease-free	SERVA Electrophoresis GmbH, Heidelberg, Germany
Amino - oxyacetate	Sigma-Aldrich Chemie GmbH, Taufkirchen, Germany
Antimycin A	Sigma-Aldrich Chemie GmbH, Taufkirchen, Germany
Bovine serum albumin (BSA), essentially fatty acid free	Sigma-Aldrich Chemie GmbH, Taufkirchen, Germany
Calcium chloride ($CaCl_2$)	Carl Roth GmbH + Co. KG, Karlsruhe, Germany
Chloroform	Applichem GmbH, Darmstadt, Germany
Collagenase P	Sigma-Aldrich Chemie GmbH, Taufkirchen, Germany
2-Deoxy-D-Glucose	Sigma-Aldrich Chemie GmbH, Taufkirchen, Germany
D- (+)- Glucose solution 45%	Sigma-Aldrich Chemie GmbH, Taufkirchen, Germany
Dimethyl sulfoxide (DMSO)	Carl Roth GmbH + Co. KG, Karlsruhe, Germany
DTT	SERVA Electrophoresis GmbH, Heidelberg, Germany
EDTA	Carl Roth GmbH + Co. KG, Karlsruhe, Germany
Ethanol, absolute	Merck KGaA, Darmstadt, Germany
FCCP	R&D Systems, Minneapolis, MN, USA
Glucokinase activator GKA50	Santacruz, CA, USA
Glycerol	Sigma-Aldrich Chemie GmbH, Taufkirchen, Germany
2 - Mercapethanol	Carl Roth GmbH + Co. KG, Karlsruhe, Germany
Magnesium sulfate ($MgSO_4$)	Carl Roth GmbH + Co. KG, Karlsruhe, Germany

mdivi-1	Sigma-Aldrich Chemie GmbH, Taufkirchen, Germany
Methyl pyruvate	Sigma-Aldrich Chemie GmbH, Taufkirchen, Germany
Methyl succinate	Sigma-Aldrich Chemie GmbH, Taufkirchen, Germany
MitoTrackerRed FM	Invitrogen GmbH, Karlsruhe, Germany
Nuclease free water	Carl Roth GmbH + Co. KG, Karlsruhe, Germany
Nu-PAGE LDS sample buffer	Novex, San Diego, CA, USA
Oligomycin	Sigma-Aldrich Chemie GmbH, Taufkirchen, Germany
Potassium chloride (KCl)	Carl Roth GmbH + Co. KG, Karlsruhe, Germany
Protease Phosphatase inhibitor cocktail	Thermo Fisher Scientific Inc., Massachusetts MA, USA
Puromycin	Sigma-Aldrich Chemie GmbH, Taufkirchen, Germany
Qiazol	Qiagen GmbH, Hilden, Germany
Rotenone	Sigma-Aldrich Chemie GmbH, Taufkirchen, Germany
Sodium bicarbonate ($NaHCO_3$)	Carl Roth GmbH + Co. KG, Karlsruhe, Germany
Sodium chloride (NaCl)	Carl Roth GmbH + Co. KG, Karlsruhe, Germany
Sodium lactate	Sigma-Aldrich Chemie GmbH, Taufkirchen, Germany
Sodium pyruvate	Sigma-Aldrich Chemie GmbH, Taufkirchen, Germany
Stripping buffer	Thermo Fisher Scientific Inc., Massachusetts MA, USA
TRIS	Carl Roth GmbH + Co. KG, Karlsruhe, Germany
TRIS HCL	Carl Roth GmbH + Co. KG, Karlsruhe, Germany
Trition X-100	Sigma-Aldrich Chemie GmbH, Taufkirchen, Germany
Tryptone	Sigma-Aldrich Chemie GmbH, Taufkirchen, Germany
Tween 20	Sigma-Aldrich Chemie GmbH, Taufkirchen, Germany
Yeast extract	Sigma-Aldrich Chemie GmbH, Taufkirchen, Germany

3.1.7 Primary antibodies

All the primary antibodies were diluted in TBST containing 5% BSA.

Table 5: Primary antibodies

Antibody	**Dilution**	**Supplier**
Actin	1:10,000	Cell Signaling, Danvers, MA, USA
p-Drp1 Ser616	1:2000	Cell Signaling, Danvers, MA, USA
p-Drp1 Ser637	1:2000	Cell Signaling, Danvers, MA, USA
Total *Drp1*	1:10,000	BD Bioscience Laboratories, Heidelberg, Germany
Total OXPHOS antibody cocktail	1:5000	Abcam, Cambridge, MA, USA
alpha - Tubulin	1:10,000	Santacruz, CA, USA

3.1.8 Secondary antibodies

All the secondary antibodies were purchased from Santacruz, CA, USA. Horseradish peroxidase (HRP) labeled anti-mouse and anti-rabbit secondary antibodies were used for western blotting at dilutions of 1:10,000 - 1:15,000 in TBST containing 5% BSA.

3.1.9 Primers

All the primers for qPCR were purchased from Sigma-Aldrich Chemie GmbH, Taufkirchen, Germany. SYBR Green PCR Master Mix was purchased from Life Technologies / Thermo Fisher Scientific Inc., Waltham, MA, USA.

Table 6: Primers

Target gene	Forward primer	Reverse primer
Drp1	TAAGCCCTGAGCCAATCCATC	CATTCCCGGTAAATCCACAAGT
Gck	AACGACCCCTGCTTATCCTC	CTTCTGCATCCGGCTCATCA
Glut1	CAGTTCGGCTATAACACTGGTG	GCCCCCGACAGAGAAGATG
Glut2	TCAGAAGACAAGATCACCGGA	GCTGGTGTGACTGTAAGTGGG
Ins1	CACTTCCTACCCCTGCTGG	ACCACAAAGATGCTGTTTGACA
Ins2	GCTTCTTCTACACACCCATGTC	AGCACTGATCTACAATGCCAC
Mfn1	CCTACTGCTCCTTCTAACCCA	AGGGACGCCAATCCTGTGA
Mfn2	ACCCCGTTACCACAGAAGAAC	AAAGCCACTTTCATGTGCCTC
Opa1	TGGAAAATGGTTCGAGAGTCAG	CATTCCGTCTCTAGGTTAAAGCG

3.1.10 Kits

Table 7: Kits

Kit	Supplier
EnzyLight™ ATP Assay kit	Bioassay system, Biotrend Chemikalien GmbH, Cologne, Germany
Glucose Uptake assay kit	Abcam, Cambridge, MA, USA
Mouse Ultrasensitive Insulin ELISA kit	Alpco Diagnostics, Salem, NH, USA
Nucleofector kit V	Lonza Cologne GmbH, Cologne, Germany
PierceTM BCA Protein Assay kit	Thermo Fisher Scientific Inc., Massachusetts MA, USA
Plasmid Mini and Maxi preparation	Qiagen GmbH, Hilden, Germany
QuantiTect Reverse Transcription kit	Qiagen GmbH, Hilden, Germany
Quant-iT™ PicoGreen™ dsDNA Assay kit	Thermo Fisher Scientific Inc., Massachusetts MA, USA
RNeasy Mini kit	Qiagen GmbH, Hilden, Germany

3.2 Methods

Human islets

3.2.1 *In vitro* glucose-stimulated insulin secretion

Human islets were cultured overnight in culture medium (See Appendix-Solutions) at 37°C and 5% CO_2. Batches of 10 size-matched human islets were handpicked in a volume of 10 µl and plated into a v-shaped bottom 96-well plate containing 90 µl of culture medium. Five replicate of 10 islets batches were used per stated conditions. The islets were then washed twice with HEPES balanced Krebs-ringer (KRH) buffer (See Appendix-Solutions) supplemented with 2 mM glucose. The islets were starved in 100 µl of the same buffer for 1 h at 37^{o}C with/without 100 µM mdivi-1. Latter, starvation buffer was aspirated and islets were incubated in 100 µl KRH buffer with indicated glucose concentrations with/without 100 µM mdivi-1 for 1 h at 37^{o}C. Thereafter, 80 µl of the supernatants were collected, centrifuged at 760g for 5 mins and the samples were immediately frozed at -20^{o}C for determination of insulin concentration using Mouse Ultrasensitive Insulin ELISA kit. Following the secretion assay, islets were incubated with 200 µl of ice-cold RIPA lysis buffer. Latter, the buffer along with the islets was transferred to 2 ml eppendrof tube already containing 300 µl ice-cold RIPA lysis buffer and bead. The eppendrof tubes were then placed in tissue lyser. Islet homogenates were centrifuged at 12000g for 10 mins and supernatants assayed for total insulin content by RIA. For normalization, DNA content was measured.

3.2.2 Determination of DNA content

At the end of experiment, the homogenates/ lysates are centrifuged at 12000g for 10 mins. Later, 20 µl of each supernatant was transferred into black 96-well plate and assayed for DNA content using Quant-iT™ PicoGreen™ dsDNA Assay kit according to the manufacturer's instructions.

Animals

3.2.3 Determination of body weight

Body weights of mice were measured after 16 weeks of chow and high fat diet using ranger 4000 from OHAUS.

3.2.4 Determination of blood glucose levels

A drop of blood was collected from the tail vein for blood glucose measurement using a handheld glucometer (Freestyle freedom Lite, Abbott Diabetes Care, Alameda, CA, USA).

3.2.5 Determination of plasma insulin levels

Blood samples were collected in EDTA-containing centrifuge tubes. Samples were kept on ice and then centrifuged for 10 mins at 2000g. Insulin was measured using Mouse Ultrasensitive Insulin ELISA kit according to the manufacturer's instructions.

3.2.6 Pancreatic islet isolation

Mice were killed by cervical dislocation. Immediately afterwards the abdominal cavity was opened and the bile duct and hepatic portal vein were clamped adjacent to liver. A 30½ G needle was inserted into the bile duct immediately before the junction of duodenum/-bile duct. The pancreas was perfused with 4 ml of ice-cold collagenase P solution (See Appendix-Solutions) and immediately dissected out and placed in 15 ml falcon tube containing 4 ml of ice-cold G-solution (See Appendix-Solutions). The pancreas was then incubated at 37^{o}C water bath for 7.5 mins with intermittent shaking. Shaking was done vigorously to dissociate exocrine tissue from the islets. After incubation the sample was placed on ice and 10 ml of ice-cold G-solution was added and centrifuged at 290g for 2 mins. The supernatant was discarded and pellet was resuspended in 10 ml G-solution (room temperature). The digest was poured through a mesh into 50 ml falcon tube. The tissue digest was centrifuged at 290g for 2 mins. The supernatant was discarded and the pellet was resuspended in 5.5 ml of 15% optiprep (See Appendix-Solutions). The solution was added carefully along the side of the tube in the remaining 15% optiprep solution. 6 ml of G-solution was carefully added along the side of the tube and incubated for 10 mins at room temperature. The tube was then centrifuged at 336g for 15 mins (settings acceleration: 5 and deacceleration: 0). After the centrifugation step islets were floating between the optiprep (2^{nd} layer) and G-solution (1^{st} layer). Using a 25 ml serological pipette, the supernatant along with the islets was collected and passed through a 70 μm cell strainer that was placed upside down on top of a 50 ml falcon. Islets stayed on top of the cell strainer and they were washed three times with 5 ml G-solution. After washing, the cell strainer was put on a petri dish, islets side facing the bottom of the dish and washed onto dish with 15 ml islet culture medium (See Appendix-Solutions)

to release the islets into the petri dish. The islets were then picked to a fresh petri dish and incubated overnight in culture medium at 37°C before performing experiments.

3.2.7 *In vitro* glucose-stimulated insulin secretion

Isolated islets were cultured overnight in culture medium (See Appendix-Solutions) at 37°C and 5% CO_2 before performing experiment. Three replicate of 8 size-matched islets batches were used per stated conditions. The islets were processed for insulin secretion assay, total insulin content and DNA content using the same procedure as employed for human islets.

3.2.8 Islet bioenergetics

The extracellular flux analyzer XF24 was used to measure the change in dissolved O_2 concentration from within a fixed volume of media over a desired time period. The resulting metric is the oxygen consumption rate (OCR), which is an indicator of mitochondrial respiration and is expressed as picomols per minute (pmol/min). Absolute OCR measurements are recorded at 7 mins intervals, giving a mix/wait/measure setting of 1/2/3 mins.

On the day prior to the assay, the XF24 sensor cartridge was hydrated by adding 1 ml of the XF calibrant solution to the utility plate and lowering the sensor cartridge to submerge the sensors. The cartridge was placed in a non-CO_2 incubator at 37^{o}C overnight until required.

Isolated islets were cultured overnight in culture medium (See Appendix-Solutions) at 37°C and 5% CO_2, before performing experiment. Batches of 25-30 size-matched islets were picked in a volume of 20 µl and plated into islet capture 24-well plate containing 480 µl of culture medium. Three replicate of 25-30 islets batches were used per stated conditions. Four wells were remained unseeded to be used for background temperature and pH determination. The islets were then washed twice with bicarbonate-free KRH buffer (See Appendix-Solutions) supplemented with 2 mM glucose. The islets were starved in 500 µl of the same buffer for 1 h at 37^{o}C with/without 100 µM mdivi-1 in non-CO_2 incubator. Thereafter, pre-wetted islet capture screens were placed into wells using the capture screen islet tool. While the plate was incubating, the compounds were diluted in bicarbonate-free KRH buffer at 10X the desired final concentration. The cartridge was then filled with compounds for injection and loaded into the machine for calibration. After the completion of

calibration, the islet plate was placed into machine (controlled at 37°C) for a 10 mins calibration and four measurement cycles to record steady basal respiration before injecting the compounds. The islets were then treated sequentially with indicated concentrations of glucose and/or other substrates (10 cycles), oligomycin 10 μg/ml (3 cycles) to inhibit ATP synthase and a mixture of rotenone/antimycin A 2/2 μM (3 cycles) to block complexes I and III.

The individual bioenergetics parameters of OXPHOS were calculated as follows: **Non-mitochondrial respiration** = minimum rate measured after injection of respiratory chain inhibitors rotenone/antimycin A. **Basal mitochondrial respiration** = (last rate measured before glucose and /or other secretagogues injection) – (non-mitochondrial respiration rate). **Mitochondrial respiration** = (last rate measured before oligomycin injection) – (non-mitochondrial respiration rate). **Proton leak-linked respiration** = (minimum rate measured after oligomycin injection) - (non-mitochondrial respiration rate). **ATP-linked respiration** = mitochondrial respiration – proton leak-linked respiration. **Coupling efficiency** = represents the fraction of respiration used to drive ATP synthesis for each run, calculated as CE = 1- (proton leak-linked respiration / mitochondrial stimulated respiration).

Following the run, buffer was aspirated and islets were incubated with 200 μl of ice-cold RIPA lysis buffer. Latter, the lysis buffer along with the islets were transferred to 2 ml eppendrof tube already containing 300 μl ice-cold RIPA lysis buffer and bead. The eppendrof tubes were then placed in tissue lyser. Islet homogenates were centrifuged at 12000g for 10 mins and supernatants were assayed for DNA content as described above in human islet section.

Cell culture

MIN6 cells were maintained in culture medium (See Appendix-Solutions) at 37°C in a humidified 5% CO_2, 95% air environment. The culture medium was changed every 72 h and subcultured when 80-90% confluent.

3.2.9 Production of lentivirus

The lentiviral transfer and packaging vector were obtained from Addgene (Cambridge, MA, USA). Lentivirus production was conducted by co-transfection of HEK293T cells with three plasmid, i.e. a packaging-defective helper construct (pCMV-ΔR8.91, 900 ng), a vesicular stomatitis virus glycoprotein envelope-coding

construct (pMD2.G, 100 ng) and a transfer vector (pLKO.1, 1000 ng) harboring a specific hairpin siRNA sequence. A control vector (pLKO.1, without insertion of the hairpin siRNA expression cassettes) expressing EGFP was also used in the study. Transfection was conducted using X-tremeGENE HP (Sigma-Aldrich Chemie GmbH, Taufkirchen, Germany) according to manufacturer's suggested method. At 48 h, supernatants containing the lentiviral recombinants were collected. The viruses obtained were stored at -80^{o}C. Viral titer was assessed by transducing 293T cells with the control GFP-expressing virus and measuring the percentage of EGFP-positive cells.

3.2.10 Infection with lentivirus

The premade lentiviral pLKO.1 plasmid expressing shRNA for mouse *Drp1* (Sigma-Aldrich Chemie GmbH, Taufkirchen, Germany) was used to knockdown expression of mouse *Drp1* in MIN6 cell line. Viral infection was carried out in 96-well plate with 1000 cells/well. At 24 h, cells were infected with shRNA lentivirial particles to give a MOI of approximately 1. The cells were then incubated for 24 h at 37^{o}C and medium was replaced with selection medium containing 1 μg/ml puromycin. The puromycin selection was continued until stable puromycin resistant cell population was obtained.

3.2.11 Plasmid DNA extraction

The plasmids pcDNA3.1 and pcDNA3.1(+)*Drp1* (latter was a gift from David Chan plasmid # 34706) were purchased from Addgene (Cambridge, MA, USA). The Luria broth (LB) agar plates were prepared by mixing precooled LB media (See Appendix-Solutions) to 55^{o}C with ampicillin 100 μg/ml. Strains were streaked onto LB agar plates and spread evenly. The plates were then incubated at 37°C for 16 h. The next day single colony was picked from LB plates and suspended in 5 ml LB media containing ampicillin and incubated at 37°C with shaking overnight. After overnight culturing, bacterial culture was centrifuged and DNA plasmid mini isolation was performed using QIAprep Spin Miniprep kit according to the manufacturer's protocol. Plasmid DNA concentration was measured on Nanodrop 2000 UV-Visible spectrophotometer.

3.2.12 Transient transfection

For overexpression studies, transient transfection of MIN6 cells was achieved by electroporation using Nucleofector kit V as per the manufacturer's protocol. For

transfection 5 μg of plasmid DNA/ cuvette was used and tested 72 h later at protein level.

3.2.13 *In vitro* glucose-stimulated insulin secretion

Cells were seeded into 96-well plate at a density of 30,000 cells/well in 100 μl of standard culture medium (See Appendix-Solutions). After 48 h of culture, the standard culture medium was replaced with 100 μl of fresh medium (See Appendix-Solutions) supplemented with 5 mM glucose for 16 h. The cells were subsequently washed twice with KRH buffer (See Appendix-Solutions) supplemented with 2 mM glucose. The cells were starved in 100 μl of the same buffer for 2 h with/without 50 μM mdivi-1. Latter, starvation buffer was aspirated and cells were incubated in 100 μl KRH buffer with indicated concentrations of glucose and/or other substrates with/without 50 μM mdivi-1 for 2 h at 37^{o}C. The supernatants were collected, centrifuged at 760g for 5 mins and amount of secreted insulin was measured using Mouse Ultrasensitive Insulin ELISA Assay kit. Following the secretion assay, cells were incubated with 200 μl of ice-cold RIPA lysis buffer. Cell lysates were collected, centrifuged at 12000g for 10 mins and assayed for total insulin content and DNA content.

3.2.14 Cellular bioenergetics

In brief, cells were seeded into XF24-well plate at a density of 40,000 cells/well in 250 μl of standard culture medium (See Appendix-Solutions). After 48 h of culture, the standard culture medium was replaced with 250 μl of fresh medium (See Appendix-Solutions) supplemented with 5 mM glucose for 16 h. The cells were subsequently washed twice with bicarbonate-free KRH buffer (See Appendix-Solutions) supplemented with 2 mM glucose. The cells were starved in 500 μl of the same buffer for 2 h with/without 50 μM mdivi-1 in non-CO_2 incubator. The plate was then placed into machine (controlled at 37°C) for a 10 mins calibration and four measurement cycles to record steady basal cellular respiration. The cells were then treated sequentially with indicated concentrations of glucose and/or other substrates (20 cycles), oligomycin 2 μg/ml (3 cycles) and a mixture of rotenone/antimycin A 1/2 μM (3 cycles). Mitochondrial respiration was calculated as described above in islet section. Following the run, buffer was aspirated and cells were incubated with 200 μl of ice-cold RIPA lysis buffer. Cell lysates were collected, centrifuged at 12000g for 10 mins and assayed for DNA content.

3.2.15 Intracellular ATP content

Cells were seeded into white 96-well plate at a density of 10,000 cells/well in 100 µl of standard culture medium (See Appendix-Solutions) and processed using the same procedure as employed for determination of insulin secretion. At the end of experiment, the medium was aspirated; cells were washed twice with ice-cold DPBS and ATP content was determined using EnzyLight^{TM} ATP Assay kit according to the manufacture's protocol. Results were corrected for DNA content.

3.2.16 Western blotting

The treated cells were rinsed with ice-cold DPBS and then incubated with required volume of ice-cold RIPA lysis buffer containing protease and phosphatase inhibitors cocktail. The cell lysates were collected in 2 ml eppendrof tube and kept on ice. After sonication for 10 sec, cell lysates were centrifuged at 12000g for 10 mins. The supernatants were collected and protein concentration was determined using Pierce^{TM} BCA Protein Assay kit according to the manufacturer's protocol. Protein lysates were prepared in Nu-PAGE LDS sample buffer, boiled for 10 mins cooled on ice and pulse spun. Equal amount of total cell protein was separated by 10 or 12% sodium dodecyl sulfate polyacrylamide gel electrophoresis (SDS-PAGE) and transferred to nitrocellulose membrane using a Trans Blot Turbo transfer apparatus. The membrane was blocked for 1 h shaking at room temperature in TBST containing 5% BSA and then probed overnight at 4^{o}C with following appropriate primary antibodies. After the incubation with primary antibody, the membrane was washed for 15 mins three times with TBST and then incubated with horseradish peroxidase (HRP) conjugated secondary antibodies for 1 h at room temperature. After the incubation, three washes for 15 mins with TBST, the membrane was detected using ECL or prime ECL (Amersham Biosciences, Piscataway, NJ, USA) on LiCor Odyssey instrument. Quantification of band density was performed by densitometric analysis and normalized against alpha Tubulin/ Actin values. When membrane was used for detection of multiple proteins it was stripped off antibodies by incubating the membrane for 30 mins at 37^{o}C shaking using stripping buffer. The membrane was washed twice with TBST and then blocked for 1 h with TBST containing 5% BSA.

3.2.17 RNA isolation and qPCR

The treated cells were rinsed with ice-cold DPBS and total RNA was extracted using an RNeasy Mini kit according to the manufacture's instructions. RNA concentrations

were determined using a Nanodrop 2000 UV-Visible spectrophotometer. RNA purity was checked by measurement of the $A_{260/280\ nM}$ ratio, which was routinely in the range of 1.8-2.0. cDNA was synthesized from 1 μg total RNA using a QuantiTect Reverse Transcription kit. qPCRs were carried out using a ViiA 7 Real-Time PCR system. Gene expression was analyzed using primers and SYBR Green premix. *HPRT* was used as an internal control and gene expression was evaluated using the delta-delta Ct method.

3.2.18 Glucose uptake

The cells were treated using the same procedure as employed for determination of insulin secretion. Cells were then stimulated with 10 mM glucose and 5 mM 2-deoxyglucose (2-DG) for 2 h. Later, the medium was removed and cells were washed. 2-DG was determined using the calorimetric Glucose Uptake assay kit according to the manufacturer's protocol. Results were corrected for DNA content.

3.2.19 Confocal microscopy

Mitochondrial morphology was examined in live MIN6 cells. Cells were seeded in ibidi 8-wells chamber at a density of 60-70,000 cells/well. After 24 h, cells were incubated with 40 nM MitoTrackerRed FM for 30 mins. After three washes, mitochondria were visualized using a SP5 confocal microscope with 63X objective lens. Similarly, mitochondrial morphology was also studied by stimulating cells with glucose in the presence/absence of mdivi-1. For this, cells were incubated with 75 nM MitoTrackerRed CMXRos for 30 mins and after three washes, mitochondria were visualized using a Zeiss LSM880 Airyscan with 63X objective lens. The images were processed using image analyst MKII (www.imageanalyst.net) to filter and binarize the images. The morphological pipeline "mean mitochondrial shape parameters" was applied to assess mean mitochondrial length of processed images.

3.3 Statistical analysis

Data was collected from several independent experiments, with 3-5 replicates per experiment. Results are expressed as mean ± SEM. Unpaired two-tailed student t-tests was used to compare two variables, and one-way ANOVA (Boniferoni) was used for multiple comparisons using prism version 6.0 (Graph-Pad software). Statistically significant differences were considered at $p<0.05$ (*), $p<0.01$ (**), $p<0.001$ (***).

4 Results

4.1 Direct substrate delivery rescues impaired insulin secretion in *Drp1*-deficient cells and islets

4.1.1 Glucose stimulation leads to transient phosphorylation of *Drp1* in MIN6 cells

It is well documented that β-cell mitochondria fragment when cells are stimulated with nutrients (Molina et al., 2009, Jhun et al., 2013). *Drp1* appears to mediate this nutrient response as observed by strong effects of glucose on phosphorylation of its serine residues 616 (regulates recruitment into mitochondria) and 637 (inhibits translocation to mitochondria) (Chang and Blackstone, 2007, Kashatus et al., 2011, Taguchi et al., 2007, Wikstrom et al., 2013, Cribbs and Strack, 2007) in MIN6 cells respectively (Fig. 8A). Glucose leads to acute, short-lasting phosphorylation of S616 and to a gradual phosphorylation of S637 (Fig. 8A and B). The S616/S637 phosphorylation ratio is increased steeply, but transiently in response to glucose (Fig. 8C) indicating involvement of *Drp1*-induced mitochondrial fragmentation during glucose stimulation. To evaluate the functional significance of this fragmentation during GSIS, *Drp1* levels were reduced either by using shRNA approach or pharmacological inhibition by mdivi-1 in MIN6 cells and pancreatic islets.

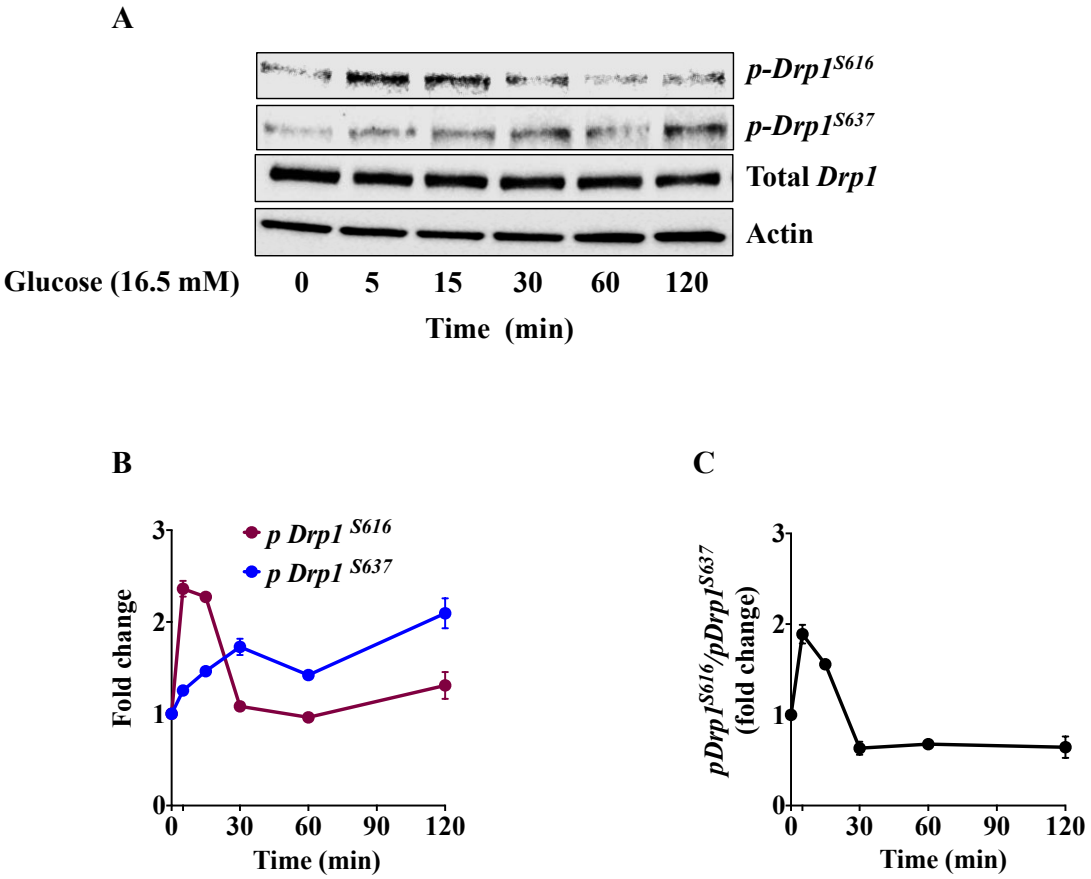

Figure 8: Glucose-stimulated transient phosphorylation of *Drp1*. MIN6 cells were treated with 16.5 mM glucose and sampled at different time points. The level of *Drp1* phosphorylation at different serine residues was examined by Western blotting using specific antibodies. (A) Representative Western blot. (B) Quantification of $pDrp1^{S616}$ and $pDrp1^{S637}$ bands. Actin was used as a loading control and (C) Phosphorylation ratio expressed as fraction of $pDrp1^{S616}$ / $pDrp1^{S637}$. Data are represented as mean ±SEM (n=3) and n-values represent independent experiments.

4.1.2 *Drp1* knockdown altered mitochondrial morphology with no effects on OXPHOS complexes and insulin content in MIN6 cells

Drp1 specific shRNA resulted in ~50% decrease of mRNA levels (Fig. 9A) and ~80% decrease of protein levels (Fig. 9B), as compared to the non-target shRNA (control) in MIN6 cells. *Drp1* knockdown (*Drp1* KD) did not affect *Mfn1* and *Opa1* mRNA levels but caused increase in *Mfn2* mRNA level (Fig. 9C), supporting the notion of mitochondrial elongation. Moreover, fluorescent visualization of the mitochondrial network exhibited elongated mitochondria in the *Drp1* KD cell (Fig. 9D), clearly explaining the expected changes in the mitochondrial network. The densitometric analysis of representative subunit from respiratory chain complexes using a cocktail of antibodies revealed no genotypic differences (Fig. 9E), confirming that *Drp1* KD does not alter the components of ETC. Although *Ins2*, but not *Ins1*, mRNA levels were

reduced (Fig. 9F), no differences was observed in the insulin protein content upon *Drp1* KD (Fig. 9G).

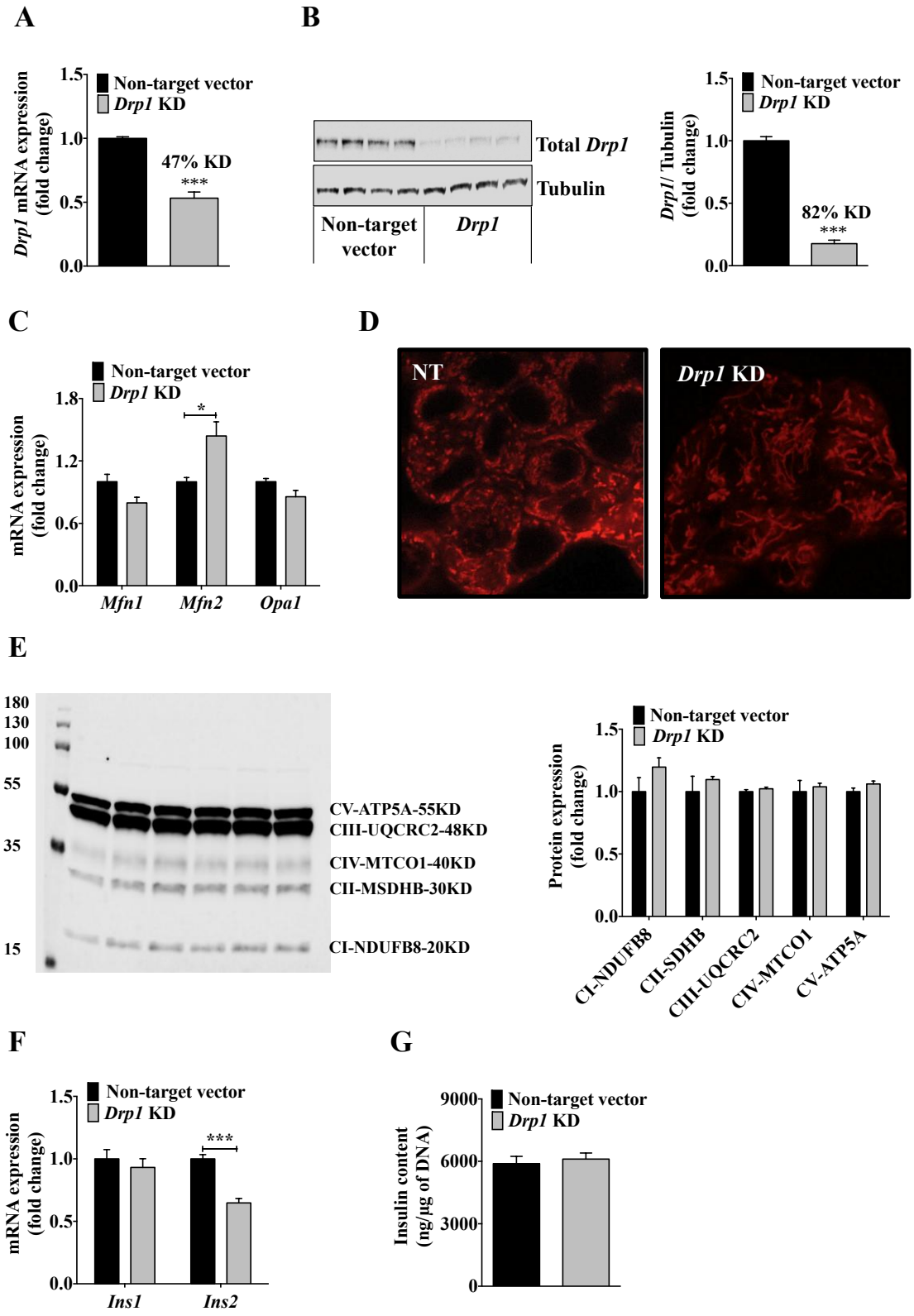

Figure 9: Alteration of mitochondrial morphology by *Drp1* KD in MIN6 cells. MIN6 cells were stably infected with non-target control (black bars) and *Drp1* shRNA (grey bars) lentivirus. (A) The

knockdown efficiency of *Drp1* was confirmed by qPCR. *HPRT* was used as control. Data is represented as mean ±SEM (n=3). (B) Immunoblot and densitometric quantification of *Drp1* protein content. Tubulin was used as a loading control. Data is represented as mean ±SEM (n=4). (C) Relative levels of *Mfn1*, *Mfn2* and *Opa1* mRNA were measured by qPCR. *HPRT* was used as a control for each sample. Data are represented as mean ±SEM (n=3). (D) Live confocal imaging of stably infected MIN6 cells that were stained with MitoTrackerRed FM for 30 mins. Representative confocal images of the non-targeted control and *Drp1* KD cells. (E) Immunoblot and densitometric quantification of OXPHOS complexes. (F) Relative levels of *Ins1* and *Ins2* mRNA were measured by qPCR. *HPRT* was used as a control for each sample. Data are represented as mean ±SEM (n=3) and (G) Insulin content. Data is represented as mean ±SEM (n=4) and n-values represent independent experiments. Statistical significance of mean differences was tested by unpaired two-tailed student t-test. $P<0.05$ (*), $P<0.01$ (**), $P<0.001$ (***).

4.1.3 *Drp1* knockdown decreases GSIS by lowering coupling efficiency of OXPHOS in MIN6 cells

Under basal glucose condition (2 mM) insulin release was not affected in *Drp1* KD cells (Fig. 10A). However, stimulation with 16.5 mM glucose significantly reduced GSIS in *Drp1* KD cells (Fig. 10A), strongly suggesting functional contribution of mitochondrial morphology in controlling nutrients metabolism-secretion coupling in pancreatic *β*-cells. Additionally, *Drp1* KD inferred no direct defects on insulin secretion mechanisms downstream of mitochondria: as neither 30 mM potassium chloride (depolarizes the plasma membrane bypassing the ATP-dependent potassium channel) nor 100 mM glyburide (binding the SUR1 subunit of the K_{ATP} channel resulting in channel closure) triggered insulin secretion was changed (Fig. 10A). These findings confirmed that *Drp1* KD solely decreases GSIS by mechanisms upstream of mitochondria.

Furthermore, mitochondrial bioenergetics was measured using Seahorse technology to monitor mitochondrial function in intact cells. Plate-based respirometry was used to measure basal mitochondrial respiration, followed by glucose injection to monitor glucose-stimulated mitochondrial respiration, followed by inhibition of ATP synthase by injecting oligomycin to estimate to what extent respiration is used to make ATP and how much of it is linked to mitochondrial proton leak and finally mixture of rotenone and antimycin A was injected to get non-mitochondrial respiration. The oxygen consumption traces were corrected for non-mitochondrial respiration, thus illustrating only mitochondrial respiration plotted over the time-course of the experiments (Fig. 10B). In the following graphs, “2 mM” low-glucose conditions were always time-matched, running in separate wells. The basal respiration at 2 mM glucose was not different between *Drp1* KD and non-target control (Fig. 10C). In response to glucose injection, glucose-stimulated respiration appeared slightly, but not

significantly, lower in *Drp1* KD cells (Fig. 10C). Interestingly, ATP-linked respiration at high glucose was significantly lowered in *Drp1* KD cells (Fig. 10D). A robust insight into mitochondrial energy efficiency is given by calculating coupling efficiency (CE) that internally standardizes each measurement. CE was found to be decreased in response to glucose in *Drp1* KD cells (Fig. 10E). This relatively low coupling efficiency also reflects an increase in mitochondrial proton leak that is provoked by *Drp1* KD at high glucose (Fig. 10F). The simultaneous changes in OCR linked to proton leak (increase) and ATP synthesis (decrease) counteracts each other, such that the overall glucose-stimulated respiration does not differ between *Drp1* KD and non-target control cells (Fig. 10C). Since, the bioenergetics effects in response to glucose was not caused by changes in ETC components (Fig. 10G) therefore, in the MIN6 cells culture system, impaired GSIS upon *Drp1* KD can be mechanistically explained by the decrease in coupling efficiency of glucose-stimulated OXPHOS. Consequently, intracellular ATP content was found to be decrease upon glucose stimulation by ~30% in *Drp1* KD cells (Fig. 10H).

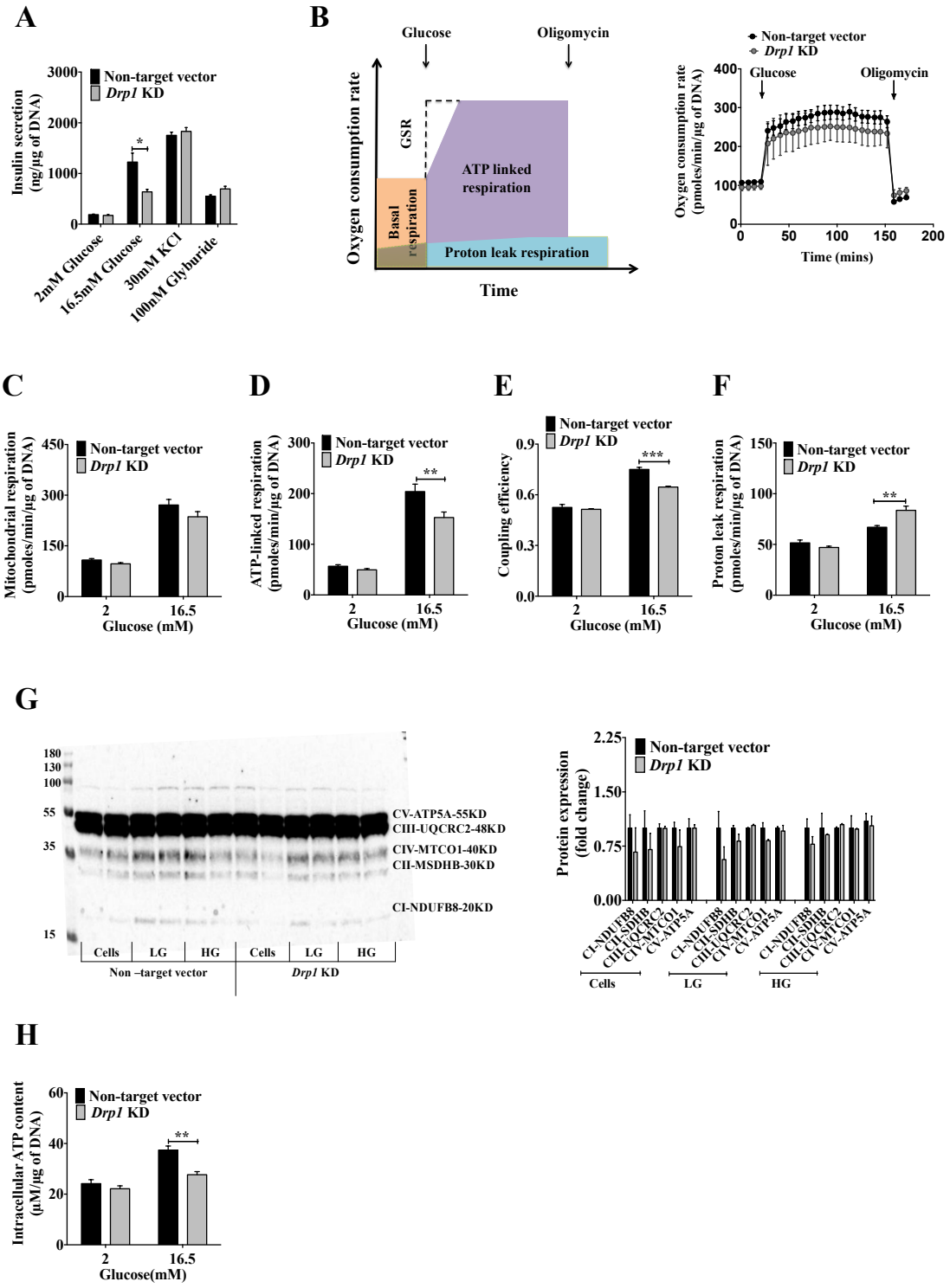

Figure 10: GSIS and mitochondrial bioenergetics of *Drp1* KD in MIN6 cells. MIN6 cells were stably infected with non-target control (black bars) and *Drp1* shRNA (grey bars) lenti-virus and exposed to glucose and other substrates for 2 h to measure (A) Insulin release. Data are represented as mean ±SEM (n=4). (B) Right panel: Averaged time-resolved oxygen consumption traces measured using the XF24 extracellular flux analyzer as described in the method section. Left panel: Schematic representation marking different oxygen consumption modules. (C) Mitochondrial respiration. (D) ATP-linked respiration. (E) Coupling efficiency. (F) Proton leak respiration. Data are represented as mean ±SEM (n=6). (G) A representative immunoblot and densitometric quantification of OXPHOS complexes. Data are represented as mean ±SEM (n= 3) and (H) ATP content. Data are represented as mean ±SEM (n=4) and n-values represent independent experiments. Statistical significance of mean

differences was tested by unpaired two-tailed student t-test to compare two variables, and one-way ANOVA (Bonferroni) was used for multiple comparisons. $P<0.05$ (*), $P<0.01$ (**), $P<0.001$ (***).

4.1.4 Pharmacological inhibition of *Drp1* by mdivi-1 validates the genetic *Drp1* KD phenotype

Genetic knockdown of *Drp1* induces mitochondrial elongation, inhibits mitochondrial autophagy and causes mitochondrial dysfunction (Kageyama et al., 2014, Frank et al., 2001, MacVicar and Lane, 2014). These consequences of long term genetic *Drp1* KD can lead to misinterpretation of its effect on GSIS. Therefore, the decrease in GSIS mediated by *Drp1* KD was further confirmed by using pharmacological selective chemical inhibitor of *Drp1*, mdivi-1 (mitochondrial division inhibitor-1). Mdivi-1, a small cell-permeable molecule, inhibits *Drp1* assembly and its GTPase activity. It has been suggested as therapeutic for stroke, myocardial infarction and neurodegenerative diseases (Lackner and Nunnari, 2010, Manczak and Reddy, 2015, Zaja et al., 2014, Zhao et al., 2014). To study mdivi-1 effects on insulin secretion, MIN6 cells were acutely pretreated with different concentrations of mdivi-1 (25, 50 and 100 µM) at basal (2 mM) and stimulatory (16.5 mM) glucose concentrations. No difference was observed on insulin content (Fig. 11A) and basal insulin release (Fig 11B) at all mdivi-1 concentrations. But GSIS was found to be decreased in a dose-dependent manner and reached statistical significant at 50 and 100 µM concentrations (Fig. 11B). To investigate whether mdivi-1 solely reduces GSIS by bioenergetic mechanism as found for the genetic *Drp1* KD, plate-based respirometry was performed in the presence of 50 and 100 µM mdivi-1 concentrations. Incubation with inhibitor did not significantly affect basal and glucose-stimulated respiration (Fig. 11C), but increased mitochondrial proton leak (Fig. 11D). Likewise, the ATP-linked respiration and CE was decreased after glucose stimulation by mdivi-1 treatment (Fig. 11E and F). Thus, pharmacological inhibitor mdivi-1 fully mimicked the effects on insulin secretion and bioenergetics of genetic *Drp1* KD. However, increasing concentration to 100 µM mdivi-1 had no further effects on the insulin secretion and bioenergetics of the MIN6 cells, suggesting that 50 µM mdivi-1 concentration as the fully inhibitory dose. Additionally, mitochondrial morphology was also studied at basal and stimulated glucose concentrations in the presence of mdivi-1. In mdivi-1 treated cells, mean mitochondrial length remained significantly increased even after glucose stimulation compared to the control cells (Fig. 11G). Thus, pharmacological inhibition by mdivi-1 induces a similar elongation phenotype as found in the stable *Drp1*-deficient cells.

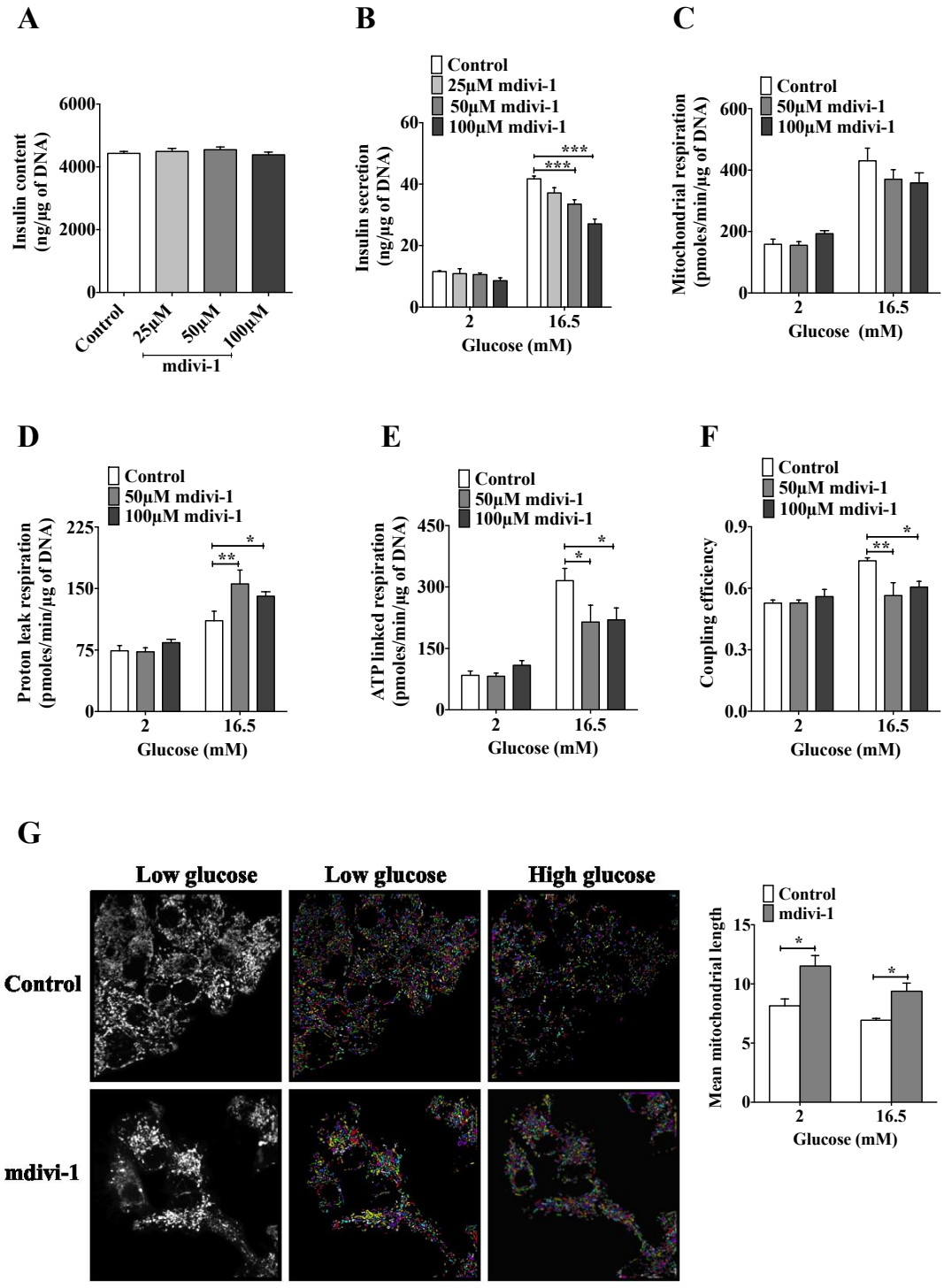

Figure 11: Effect of mdivi-1 on GSIS and mitochondrial bioenergetics in MIN6 cells. MIN6 cells were exposed to 2 and 16.5 mM glucose with/without different concentrations of mdivi-1 for 2 h to measure (A) Insulin content. (B) Insulin release. Data are represented as mean ±SEM (n=4). (C) Mitochondrial respiration. (D) Proton leak respiration. (E) ATP-linked respiration. (F) Coupling efficiency. Data are represented as mean ±SEM (n=5) and (G) Effect of mdivi-1 on mitochondrial morphology upon glucose stimulation. The morphological pipeline "mean mitochondrial shape parameters" was applied to assess mean mitochondrial length of processed images. Average mean mitochondrial length is depicted in the bar charts and consists of three viewfields. Values are given as mean ± SEM (n = 3) and n-values represent individual experiments. Statistical significance of mean differences was tested by unpaired two-tailed student t-test to compare two variables, and one-way ANOVA (Bonferroni) was used for multiple comparisons. $P<0.05$ (*), $P<0.01$ (**), $P<0.001$ (***).

4.1.5 *Drp1* inhibition by mdivi-1 reduces GSIS by decreasing glucose oxidation capacity in pancreatic islets

To explore the translational relevance of *Drp1*-dependent GSIS, human pancreatic islets were incubated with 100 µM mdivi-1. In accordance with the previous results in MIN6 cells, mdivi-1 did not impair insulin content and basal insulin release but significantly decreased GSIS (Fig. 12A and B).

To investigate the physiological and pathophysiological significance of *Drp1*, pancreatic islets isolated from mice were treated with 100 µM mdivi-1. Similar to human islet and MIN6 cell data, mdivi-1 treatment did not affect insulin content but reduced GSIS (Fig. 12C and D). To study mitochondrial bioenergetics, plate-based respirometry using islet-capture plates was performed as shown in the representative trace (Fig. 12E). Mdivi-1 had no effects on basal respiration (low glucose) (Fig. 12F). However, mdivi-1 significantly decreased glucose-stimulated respiration (Fig. 12F), and ATP-linked respiration (Fig. 12G). Unlike cells, there was no apparent effect on proton leak respiration (Fig. 12H), as the consequence, inhibitory effect on ATP-synthesis-coupled respiration is apparent from the overall glucose-stimulated oxygen consumption in islets. As a result of reduced glucose oxidation, CE was significantly reduced (Fig. 12I). Thus, *Drp1* strongly controls GSIS via glucose oxidation capacity and not proton leak, in pancreatic islets.

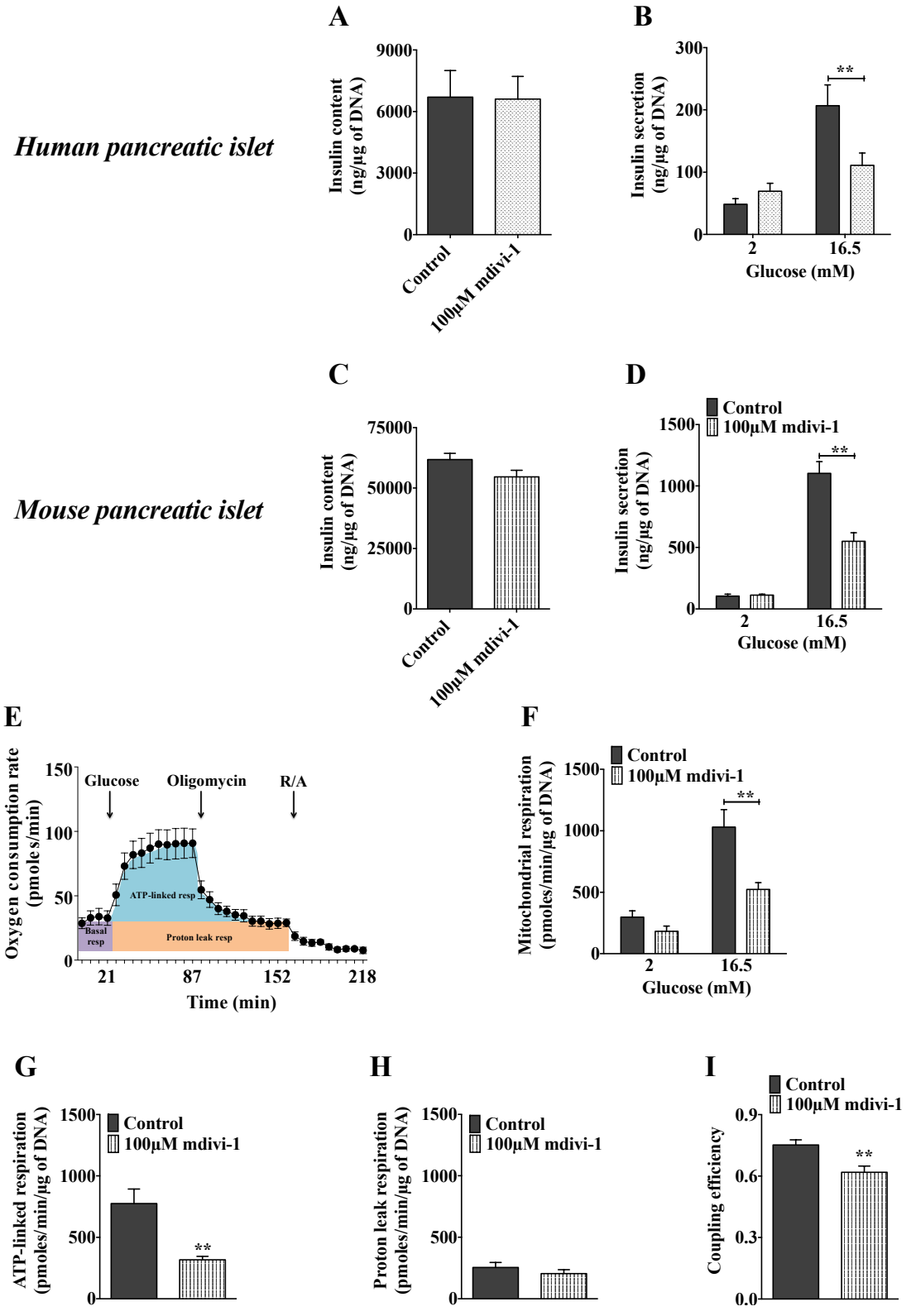

Figure 12: Effect of mdivi-1 on GSIS and mitochondrial bioenergetics in pancreatic islets. (A-B) Batches of size-matched human pancreatic islets were incubated with 2 and 16.5 mM glucose with/without mdivi-1 for 1 h to measure (A) Insulin content. (B) Insulin secretion. Data are represented as mean ±SEM (n=3). (C-I) Batches of size-matched mouse pancreatic islets were exposed 2 and 16.5 mM glucose with/without mdivi-1 for 1 h to measure (C) Insulin content. (D) Insulin secretion. Data are represented as mean ±SEM (n=3). (E) Representative scheme of time-resolved oxygen consumption traces using islet-capture plates of the XF24 extracellular flux analyzer. (F) Mitochondrial respiration. (G) ATP-linked respiration. (H) Proton leak respiration and (I) Coupling efficiency. Data are

represented as mean ±SEM (n=5) and n-values represent independent experiments. Statistical significance of mean differences was tested by unpaired two-tailed student t-test. $P<0.05$ (*), $P<0.01$ (**), $P<0.001$ (***).

4.1.6 Pyruvate rescues impaired GSIS and mitochondrial bioenergetics in *Drp1*-deficient MIN6 cells

It is possible that the impaired glucose oxidation effect is secondary to reduced mitochondrial substrate supply, and this can be easily assessed by directly providing substrate (pyruvate) to mitochondria. In *Drp1* KD MIN6 cells, insulin secretion was reduced by about 40% upon glucose stimulation (Fig. 13A). Interestingly, supplementing cells with exogenous pyruvate rescued the impaired GSIS (Fig. 13A and B), presumably either by circumventing deficiencies in ATP production or by initiating secretion-signaling cascades downstream of mitochondria. In MIN6 cells, exogenous pyruvate supply increased oxidation above control high-glucose condition irrespective of *Drp1* deficiency (Fig. 13C). Moreover, pyruvate stimulation restored ATP-linked respiration in *Drp1*-deficient cells to the same level as seen in control cells incubated at high glucose (Fig. 13D). The calculation of coupling efficiency (proton leak as the proportion of substrate oxidation) illustrates that *Drp1*-dependent efficiency differences remain upon pyruvate supplementation (Fig. 13E) presumably because of the persistently high mitochondrial proton leak exhibited by *Drp1* KD cells (Fig. 13F). This demonstrates that increased proton leak respiration is solely the result of increased substrate (pyruvate) oxidation [132-134] and has only minor control over GSIS. This notion is supported by highly increased ATP content in pyruvate-treated cells (Fig. 13G and H). Taken together, pyruvate increases substrate oxidation, resulting in increased absolute ATP-linked respiration and ATP content, which eventually rescues insulin secretion in *Drp1* KD cells. Additionally, glucose transporters genes expression except glucokinase and glucose uptake tends to be increased in *Drp1* KD cells, suggesting deficiencies downstream of glucose transport (Fig. 13I and J). Interestingly, pharmacologic activation of glucokinase by GKA50 rescued GSIS by improving glucose oxidation in *Drp1* KD cells (Fig. 13K and L). These results also support the concept of defect downstream of glucose transport/ lowered glucose catabolism in *Drp1* KD cells.

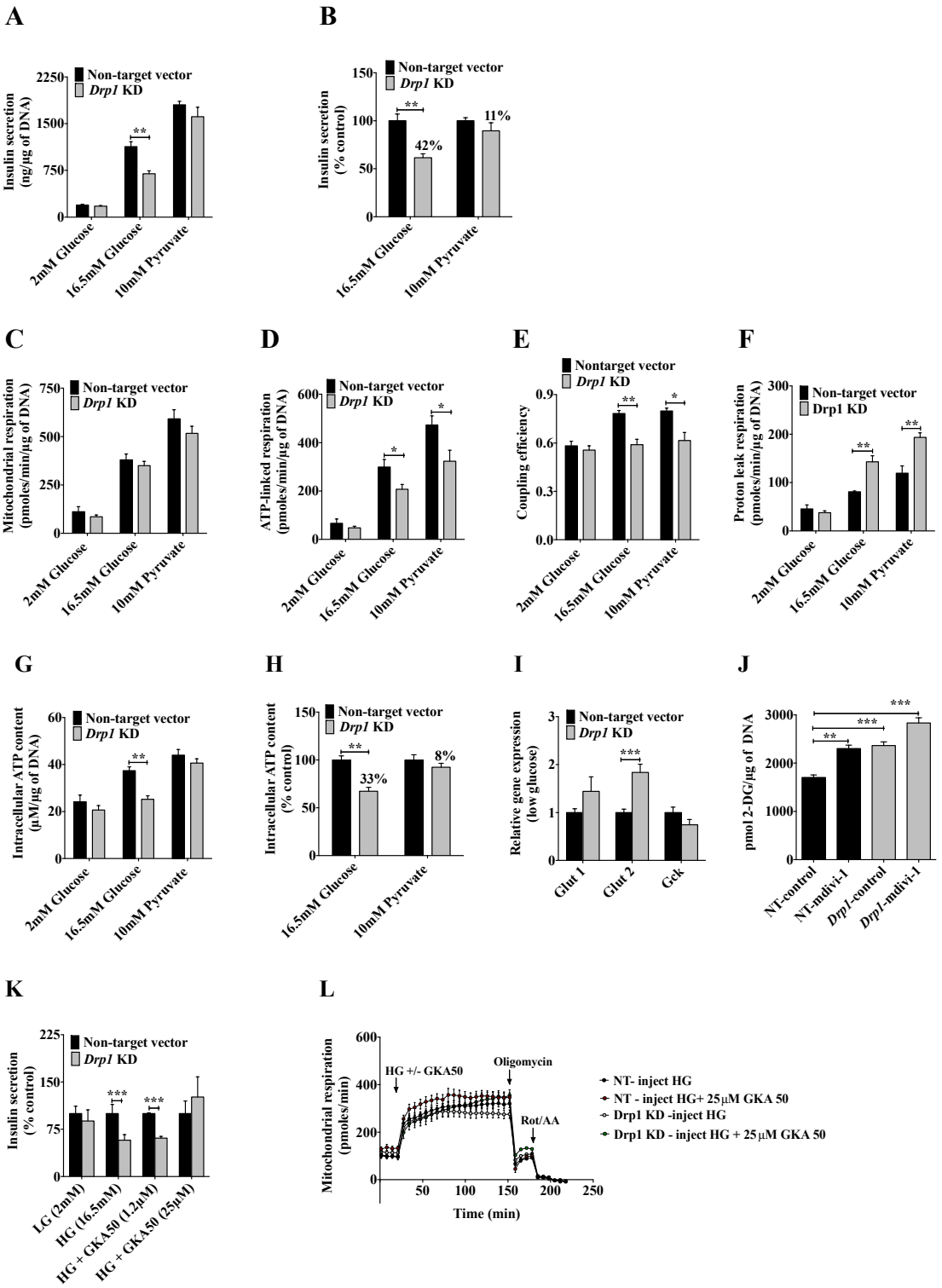

Figure 13: Pyruvate rescues *Drp1*-related deficiency in insulin secretion and mitochondrial bioenergetics in MIN6 cells. MIN6 cells were stably infected with non-target control (black bars) and *Drp1* shRNA (grey bars) lenti-virus. (A-H) Cells were incubated either with glucose or sodium pyruvate to measure (A) Insulin secretion. (B) Insulin secretion expressed as percentage of control. (C) Mitochondrial respiration. (D) ATP-linked respiration. (E) Coupling efficiency. (F) Proton leak respiration. (G) Intracellular ATP content. (H) Intracellular ATP content expressed as percentage of control. (I) Relative levels of *Glut1*, *Glut2* and *Gck* mRNA were measured by qPCR. *HPRT* was used as a control. (J) Glucose uptake. (K-L) Cells were incubated with either glucose or glucokinase activator GKA50 to measure (K) Insulin secretion and (L) Mitochondrial respiration. Data are represented as mean ±SEM (n=4) and n-values represent independent experiments. Statistical

significance of mean differences was tested by unpaired two-tailed student t-test to compare two variables, and one-way ANOVA (Bonferroni) was used for multiple comparisons. $P<0.05$ (*), $P<0.01$ (**), $P<0.001$ (***).

4.1.7 Methyl pyruvate overcomes impaired function of *Drp1*-deficient pancreatic mouse islets

Pancreatic insulinoma cells such as MIN6 expresses substantial amounts of monocarboxylate carrier protein (MCP) which allow pyruvate uptake; a characteristic that is absent in native β-cells, that tightly couple glucose to mitochondrial respiration. Thus, the cellular model is incompetent to determine the physiological relevance, whether rescue with pyruvate is solely mediated as intracellular substrate or it contributes *via* other effects (e.g. as extracellular secretagogues) (Dufer et al., 2002, Lembert et al., 2001, Mertz et al., 1996). To clarify this, methyl pyruvate, a membrane permeable ester analog was tested in mouse pancreatic islets. Mdivi-1 mediated GSIS deficiency was not rescued by sodium pyruvate in mouse pancreatic islets, thus demonstrating that pyruvate does not act as extracellular secretagogues (Fig. 14A and B). However, one-hour incubation with methyl pyruvate rescued impaired GSIS in *Drp1*-deficient islets, even in the absence of glucose (Fig. 14A and B). The respective respirometry analysis suggests that methyl pyruvate acts as a mitochondrial substrate as it increases mitochondrial respiration (Fig. 14C). Although proton leak respiration was increased when glucose and methyl-pyruvate were combined (Fig. 14D), methyl pyruvate treatment restored ATP-linked respiration in *Drp1*-deficient islets to the same level as seen in control islets incubated at high glucose (Fig. 14E). Furthermore, the mdivi-1 mediated difference in coupling efficiency was ameliorated by methyl pyruvate treatment (Fig. 14F). Collectively, all the above findings suggest a model (Fig. 14G) that direct substrate delivery to mitochondria can be considered as potential route for drug intervention rescuing fission-impaired GSIS.

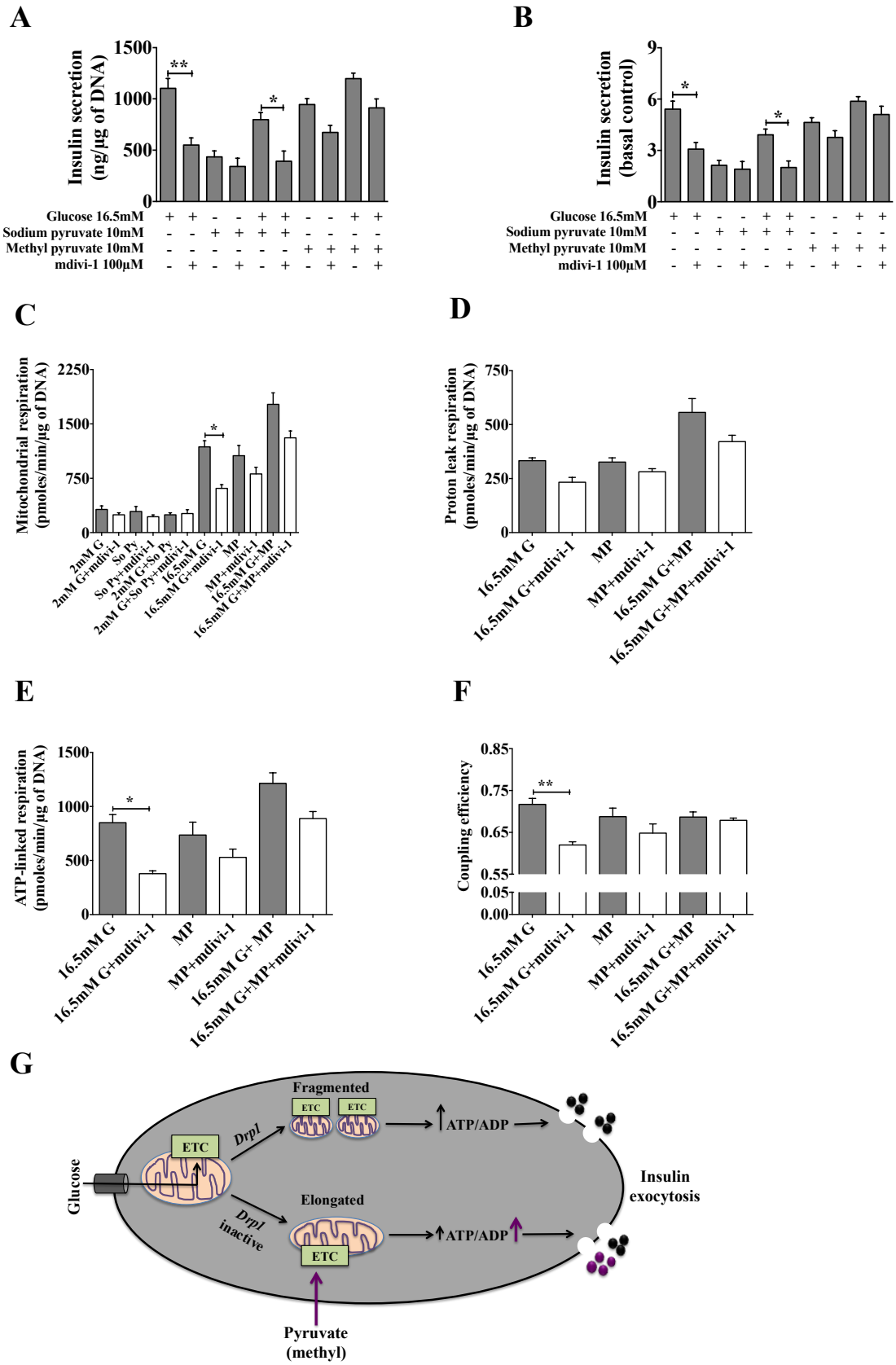

Figure 14: Methyl pyruvate rescues *Drp1*-related deficiency in insulin secretion and mitochondrial bioenergetics in pancreatic mouse islets. Batches of size-matched islets were exposed to glucose and different substrates with/without mdivi-1 for 1 h to measure (A) Insulin secretion. (B) Insulin secretion normalized to basal control. (C) Mitochondrial respiration. (D) Proton leak respiration. (E) ATP-linked respiration. (F) Coupling efficiency. Data are represented as mean ±SEM (n=3) and n-

values represent independent experiments and (G) Schematic model of the effect of *Drp1* on GSIS, emphasizing the rescue of insulin secretion with pyruvate. Statistical significance of mean differences was tested by unpaired two-tailed student t-test to compare two variables, and one-way ANOVA (with Bonferroni posthoc analysis) was used for multiple comparisons. $P<0.05$ (*), $P<0.01$ (**), $P<0.001$ (***).

4.2 *Drp1* overexpression restored impaired insulin secretion triggering in *Drp1* KD MIN6 cells

To explore further on the role of *Drp1* in pancreatic *β*-cells, *Drp1* was transiently overexpressed using electroporation technique in pancreatic MIN6 cells. Overexpression of *Drp1* resulted in ~6.5 fold increase of mRNA levels (Fig. 15A) and ~4 fold increase of protein levels (Fig. 15B) compared to the control cells. To follow mitochondrial morphology transiently transfected MIN6 cells were incubated with MitoTrackerRed FM for 30 mins. As shown in Fig. 15C, mitochondria in control cells showed an elongated pattern of mitochondria whereas overexpression of *Drp1* caused fragmentation of the mitochondria by promoting the fission process. *Drp1* overexpression did not affect *Mfn1* or *Opa1* mRNA levels but caused a decrease in *Mfn2* mRNA, consistent with the concept that mitochondrial fragmentation is supported (Fig. 15D). Western analysis of representative subunits from all respiratory complexes confirms that *Drp1* overexpression does not affect the components of the mitochondrial ETC (Fig. 15E).

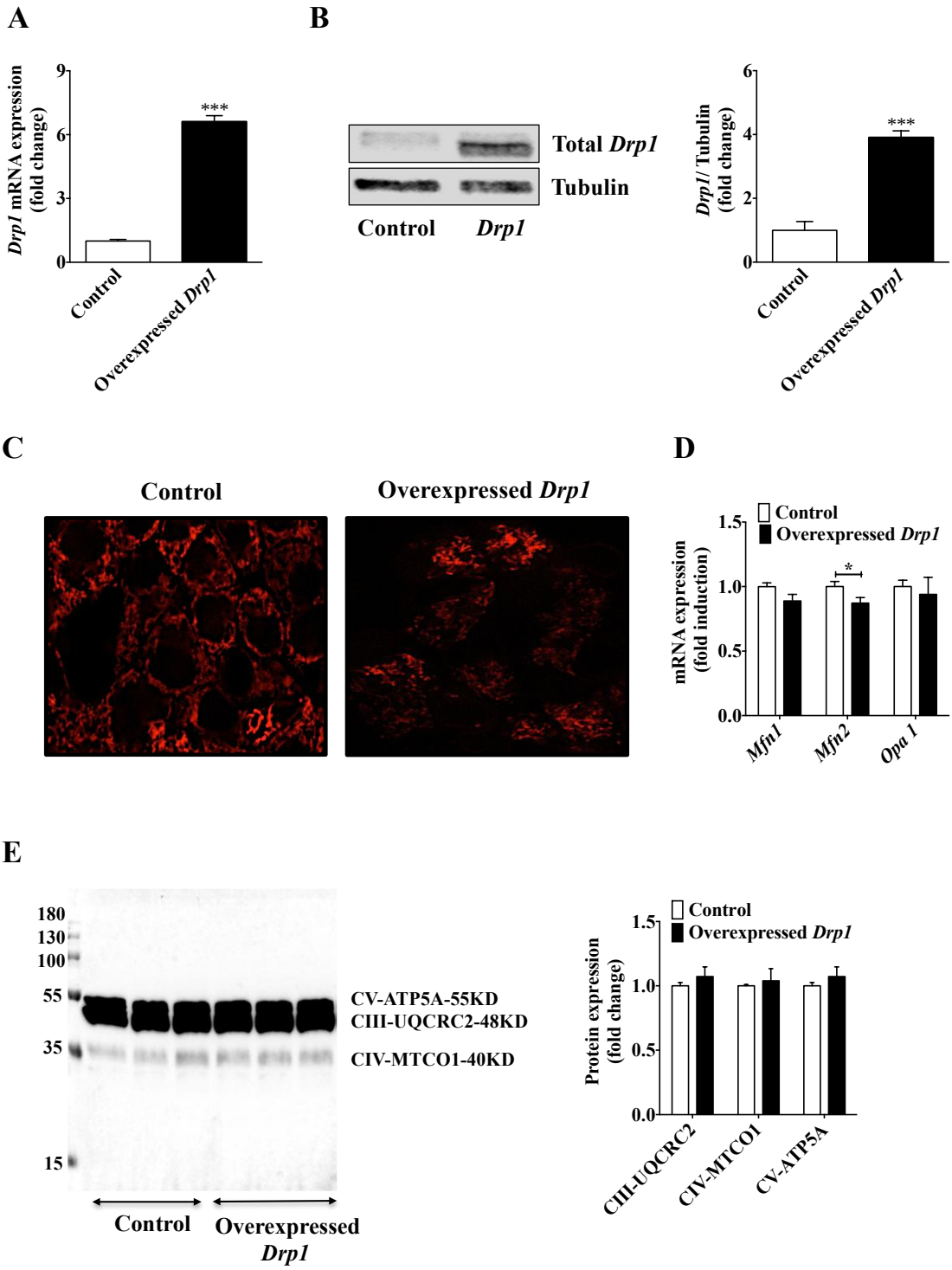

Figure 15: Alteration of mitochondrial morphology by *Drp1* overexpression in MIN6 cells. MIN6 cells were transiently transfected using *Drp1* plasmid by electroporation technique to overexpress *Drp1*: control (white bars) and overexpressed *Drp1* (black bars). (A) The overexpression efficiency of *Drp1* was confirmed by qPCR. *HPRT* was used as a control. (B) Representative immunoblot and densitometric quantification of *Drp1* protein content. Tubulin was used as a loading control. (C) Live confocal imaging of transiently transfected MIN6 cells that were stained with MitoTrackerRed FM for 30 mins. Representative confocal images of the control and *Drp1* overexpressed cells. (D) Relative levels of *Mfn1*, *Mfn2* and *Opa1* mRNA were measured by qPCR. *HPRT* was used as a control. (E) Immunoblot and densitometric quantification of OXPHOS complexes. Data are represented as mean ±SEM (n=3) and n-values represent independent experiments. Statistical significance of mean differences was tested by unpaired two-tailed student t-test. $P<0.05$ (*), $P<0.01$ (**), $P<0.001$ (***).

Furthermore, *Drp1* overexpression did not affect *Ins2* mRNA level, but significantly decreased *Ins1* mRNA level (Fig. 16A); consistently insulin content was also decreased in *Drp1* overexpressed cells (Fig. 16B). Normalizing insulin secretion to content showed no difference in basal insulin secretion (2 mM glucose), however insulin secretion at 16.5 mM glucose was significantly increased (Fig. 16C), demonstrating improved insulin secretion triggering in *Drp1* overexpressed cells. Comprehensive analysis of mitochondrial bioenergetics parameters revealed no differences between control and *Drp1* overexpressed cells (Fig. 15D-G). In agreement, *Drp1* overexpression leaves intracellular ATP content unaffected (Fig. 15H).

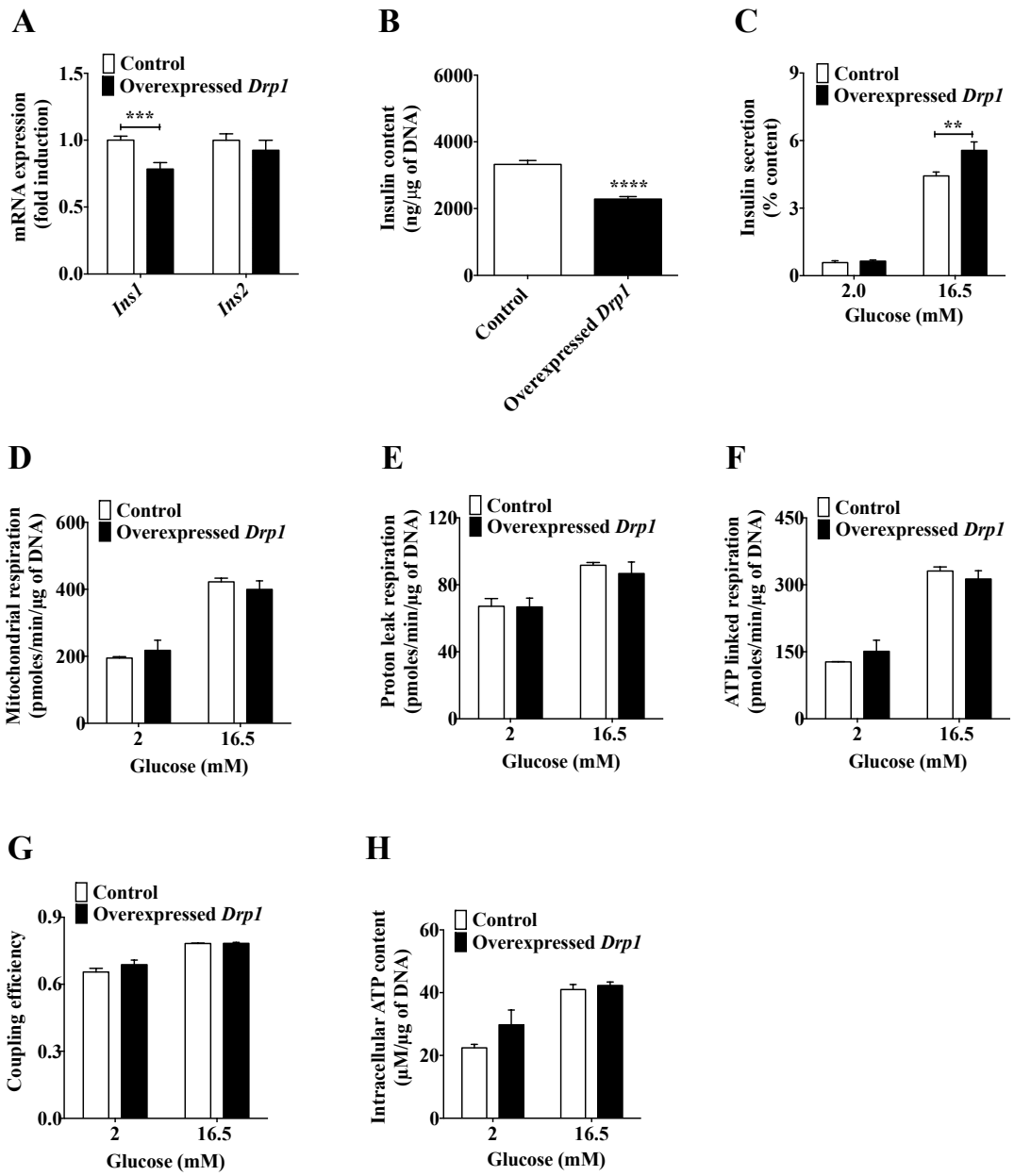

Figure 16: GSIS and mitochondrial bioenergetics of *Drp1* overexpressed MIN6 cells. MIN6 cells were transiently transfected using *Drp1* plasmid by electroporation technique to overexpress *Drp1;* control (white bars) and overexpressed *Drp1* (black bars) were exposed to glucose (2 and 16.5 mM) for 2 h. (A) Relative levels of *Ins1* and *Ins2* mRNA were measured by qPCR. *HPRT* was used as a control. Data are represented as mean ±SEM (n=3). (B) Insulin content. (C) Insulin release expressed as percentage of content. Data are represented as mean ±SEM (n=4). (D) Mitochondrial respiration. (E) Proton leak respiration. (F) ATP-linked respiration. (G) Coupling efficiency. Data are represented as mean ±SEM (n=6) and (H) Intracellular ATP content. Data are represented as mean ±SEM (n=4) and n-values represent independent experiments. Statistical significance of mean differences was tested by unpaired two-tailed student t-test to compare two variables. $P<0.05$ (*), $P<0.01$ (**), $P<0.001$ (***).

Additionally, to investigate whether *Drp1* overexpression can rescue impaired insulin secretion in *Drp1* KD cells, different concentration (2.5 and 5 µg DNA) of *Drp1* overexpressing plasmid were used to overexpress *Drp1* in stable *Drp1* KD MIN6 cells. Immunoblot and densitometric analysis revealed that 2.5 µg of overexpressor

DNA was sufficient to restore *Drp1* level in *Drp1* KD cells to the same level as in the non-target control (Fig. 17A). Normalizing insulin secretion to content showed no significant difference in basal insulin release (2 mM glucose), interestingly, GSIS was restored in *Drp1* KD cells upon *Drp1* overexpression (Fig. 17B). However, increasing the overexpressor DNA concentration to 5 µg did not further improve insulin secretion, suggesting that *Drp1* may not serve as therapeutic to increase GSIS beyond normal levels.

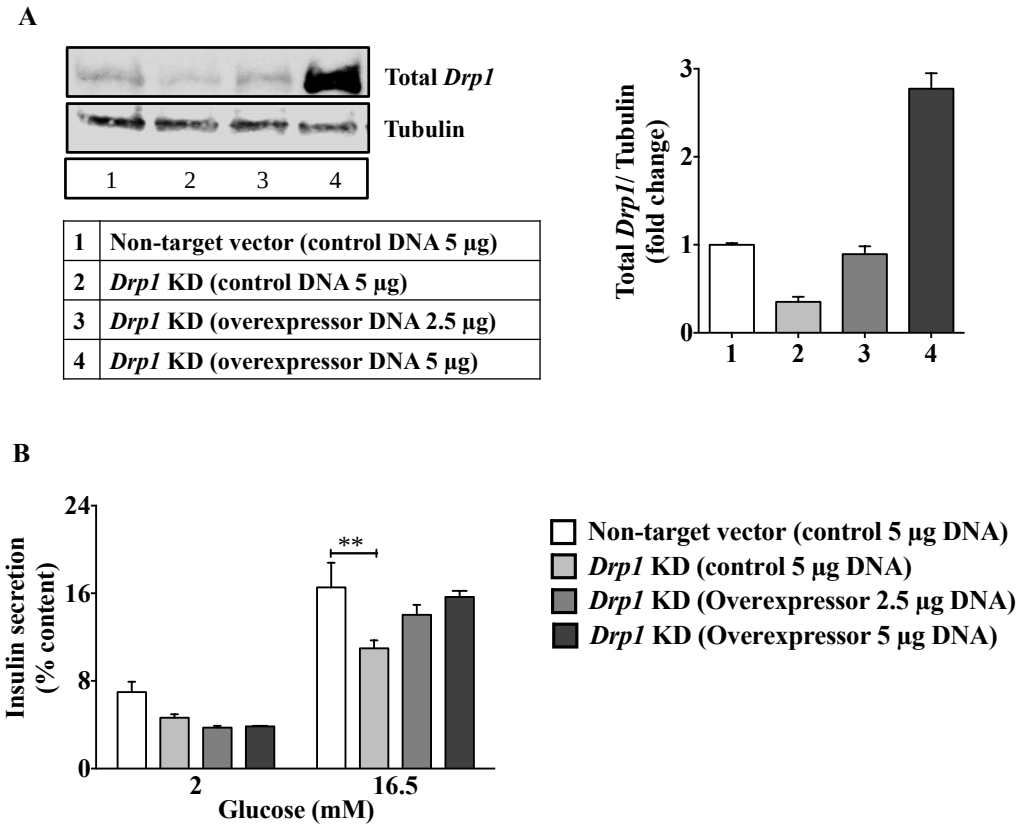

Figure 17: *Drp1* overexpression rescues impaired insulin secretion triggering in *Drp1* KD MIN6 cells. *Drp1* KD stable cell line were transiently transfected using electroporation technique with different concentration of *Drp1* plasmid to overexpress *Drp1*. After 48 h transfection (A) Overexpression efficiency in *Drp1* KD cells was confirmed by Western blotting. Representative immunoblot and densitometric quantification of *Drp1* protein content. Tubulin was used as a loading control. (B) Insulin secretion expressed as percentage of content. Data are represented as mean ±SEM (n=2) and n-values represent independent experiments. Statistical significance of mean differences was tested by one-way ANOVA (with Bonferroni posthoc analysis) for multiple comparisons. $P<0.05$ (*), $P<0.01$ (**), $P<0.001$ (***).

In the last part of my thesis, I explored the effect of nutrition (chow and high-fat diet) on insulin secretion and mitochondrial bioenergetics in pancreatic mouse islets. In addition, by correlating mitochondrial respiratory parameter vs. GSIS, I suggested a

model that can be used as tool to predict and classify impaired pancreatic insulin secretion.

4.3 Mitochondrial respiratory parameters classifies dysfunctional properties of pancreatic insulin secretion

4.3.1 Metabolic status of mice

Male C57BL/6 mice were kept on high-fat diet (HFD) for 16 weeks, to develop diet-induced obesity (DIO). At 16 weeks, HFD mice weighed around 45 grams compared to the chow diet mice, which weighed around 28 grams (Fig. 18A). Analysis of metabolic changes revealed no difference in plasma glucose levels (Fig. 1B) in contrast; plasma insulin levels were dramatically increased after 16-weeks of HFD (Fig. 1C). This suggests that hyperinsulinemia is sufficient to compensate insulin resistance in HFD mice.

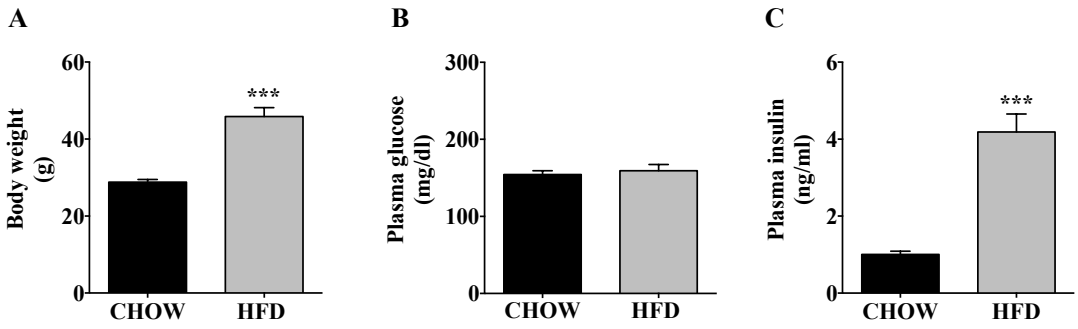

Figure 18: Characterization of chow and HFD fed C57BL/6 mice. At the age of 8 weeks, mice were fed with either chow or HFD for 16 weeks to develop diet-induced obesity (DIO). (A) Body weight. (B) Plasma glucose levels and (C) Plasma insulin levels. Data are represented as mean ± SEM (n=8) and n-values represent independent experiments. Statistical significance of mean differences was tested by unpaired two-tailed student t-test. $P<0.05$ (*), $P<0.01$ (**), $P<0.001$ (***).

4.3.2 Decreased glucose oxidation capacity resulted in compromised insulin secretion triggering in islets of DIO mice

To study the effect of nutrition on insulin secretion, islets isolated from chow and DIO mice were incubated with 2 and 16.5 mM glucose for 1 h. In islets from chow and DIO mice, insulin secretion increased when glucose was raised from 2 to 16.5 mM (Fig. 19A). No difference in basal and glucose-stimulated insulin secretion was observed in islets from DIO and chow mice (Fig. 19A). However, diet-induced increase in insulin content was observed in DIO islets (Fig. 19B). Normalizing to insulin content showed decreased GSIS (Fig. 19C), suggesting compromised triggering of insulin secretion in DIO islets. Furthermore, mitochondrial bioenergetics

was studied in response to glucose using islet-capture plate as shown in the representative trace (Fig. 19D). Analysis of real-time respiratory data revealed no difference in basal respiration between chow and DIO islets (Fig. 19E). However, glucose-stimulated respiration was markedly decreased resulting in reduced ATP-linked respiration in DIO islets compared to chow islets (Fig. 19F). Similarly, proton leak respiration was lowered in DIO islets (Fig. 19G). Notably, CE was not different between chow and DIO islets (Fig. 19H). Thus, apparent differences in proton leak respiration are presumably not fully caused by altered proton conductance but also affected by altered oxidation rates, which partially control proton leak respiration rates (Keipert and Jastroch, 2014).

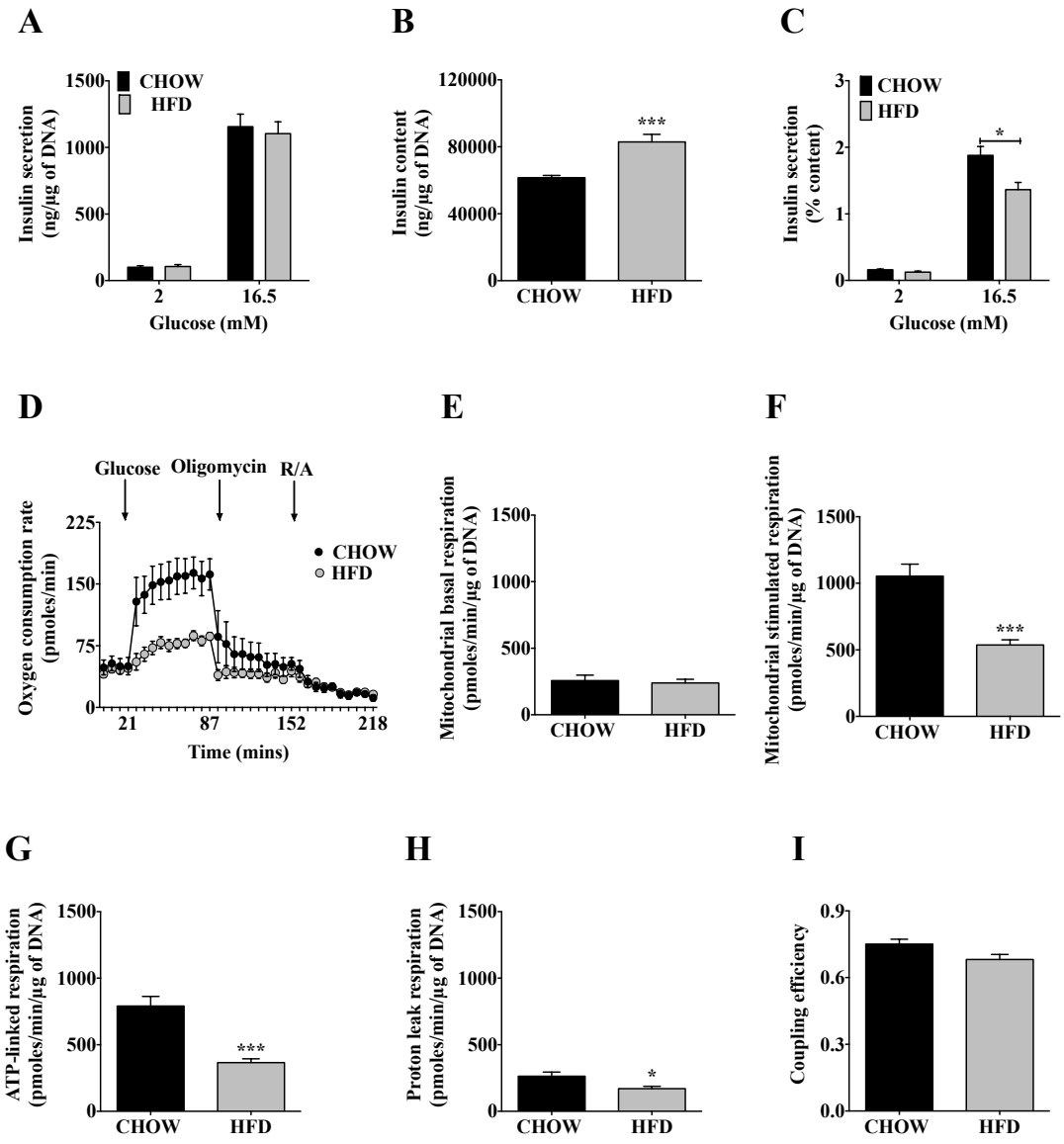

Figure 19: GSIS and mitochondrial bioenergetics in islets of chow and DIO mice. Batches of size-matched islets were exposed to 2 and 16.5 mM glucose for 1 h to measure. (A) Insulin secretion. (B)

Insulin content. (C) Insulin secretion expressed as percentage of content. (D) Representative scheme of time-resolved oxygen consumption traces using islet-capture plates of the XF24 extracellular flux analyzer. (E) Mitochondrial basal respiration at low glucose (2 mM). (F) Mitochondrial stimulated respiration at high glucose (16.5 mM). (G) ATP-linked respiration at high glucose. (H) Proton leak respiration at high glucose and (I) Coupling efficiency at high glucose. Data are represented as mean ± SEM (n=6) and n-values represent independent experiments. Statistical significance of mean differences was tested by unpaired two-tailed student t-test. $P<0.05$ (*), $P<0.01$ (**), $P<0.001$ (***).

4.3.3 Relationship between GSIS and mitochondrial respiration

Relationship between GSIS and mitochondrial respiratory parameters was derived by plotting GSIS vs. respiratory parameters and tested for correlation. The upper panel shows absolute secreted insulin levels plotted against ATP-linked respiration, GSR and CE (Fig. 20A-C). In the lower panel, GSIS is corrected for insulin content (Fig. 20D-F). In Fig. 20, it transpires that secreted insulin values requires normalization to insulin content to establish a robust linear relationship of secreted insulin to mitochondrial parameters such as ATP-linked respiration, GSR and CE. While all mitochondrial parameters possess predictive power for GSIS, the best prediction in this study is granted by GSR and ATP-linked respiration. The relationship between oxidative phosphorylation and GSIS leads to a simple correlation model to classify defects of insulin secretion (Fig. 20G). Descending from control values along the regression line suggests reduced oxidative power by either compromised substrate delivery or respiratory dysfunction, while ascending values suggests improved substrate delivery or oxidative phosphorylation. Upwards deviation from regression is explained by amplifying pathways, while downwards deviation points towards secretory dysfunction downstream or no mitochondrial impact. In the case of DIO islets, the model suggests defect in or upstream of oxidative phosphorylation.

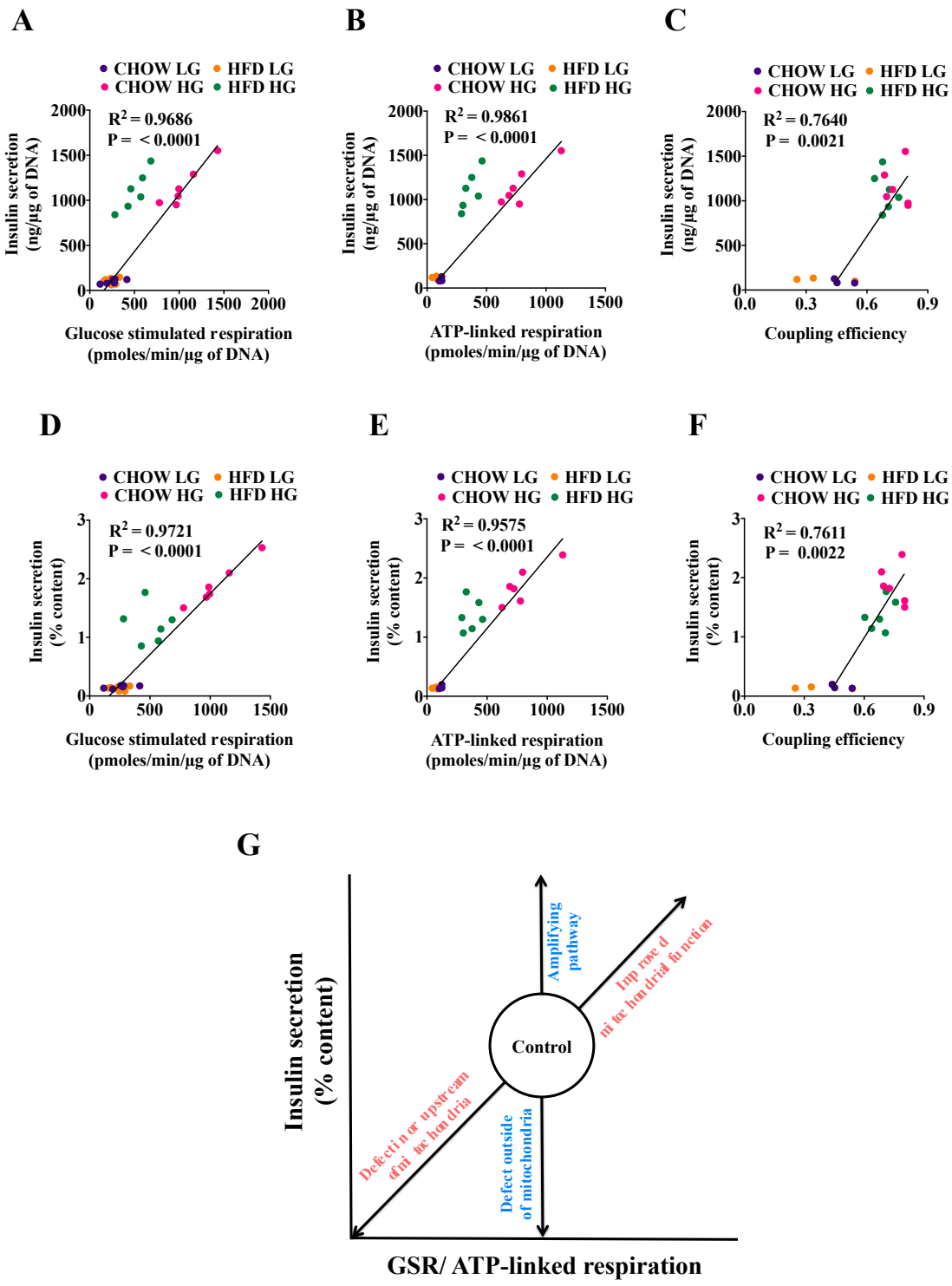

Figure 20: Correlation between GSIS and mitochondrial respiratory parameters. (A-C) Correlation of insulin secretion (absolute values) and (A) Glucose-stimulated respiration (GSR). (B) ATP-linked respiration. (C) Coupling efficiency. (D-F) Correlation of insulin secretion (% content) and (D) Glucose-stimulated respiration (GSR). (E) ATP-linked respiration. (F) Coupling efficiency and (G) Correlation model classifying defect of pancreatic insulin secretion.

4.3.4 Coupling efficiency parameter can predict GSIS across independent studies

Coupling efficiency has proven to uncover molecular mechanisms in mitochondria, e.g. the role of UCP2 in β-cells (Affourtit and Brand, 2009). Internally standardized parameter, coupling efficiency solely underlies the laws of thermodynamics that energy can only be converted from one form to another without gain or loss. Describing the fraction of energy that is converted to ATP (thus ranging from 0 to 1), coupling efficiency is less prone to variation between independent experiments. Coupling efficiency indeed correlates with GSIS but there appears a steeper relationship and higher variability concerning linear regression, as compared to ATP-linked respiration and GSR in our experimental setup (see Fig. 20D-F). Nevertheless, CE turns out to be more robust parameter when comparing independent studies, as absolute respiration rates are more prone to variation. Furthermore, the linear correlation of CE with GSIS enables to determine a "threshold" when to expect secretion triggering. The interception defines the CE threshold when triggering is expected. In this study, CE = 0.5 is required for triggering insulin secretion in islets as well as β -cell models.

5 Discussion

The present doctoral thesis provides novel mechanistic insights by which mitochondrial fission protein *Drp1* controls pancreatic insulin secretion. Previously, it has been well established that the function of *Drp1* is affected by post-translational modifications e.g. phosphorylation (Santel and Frank, 2008). Our study demonstrates that *Drp1* exhibits a distinct pattern of phosphorylation upon glucose stimulation at both the serine phosphorylation sites S616 and S637, indicating that glucose potentially influence *Drp1* function.

In particular, the data demonstrate that *Drp1* deficiency, either by genetic knockdown or pharmacological inhibition, decreases GSIS in MIN6 mouse insulinoma cells, consistent with previous finding in INS-1E rat insulinoma cells overexpressing dominant-negative *Drp1* (*DN-Drp1*) (Jhun et al., 2013). On dissecting the bioenergetic mechanisms upon *Drp1* inhibition, mitochondrial proton leak respiration was increased thus lowering coupling efficiency of oxidative phosphorylation in MIN6 cells, consistent with the conclusion of another study in INS-1E cells (Jhun et al., 2013). However, our plate-based respirometry analysis revealed decreased ATP-linked respiration by decreased glucose oxidation rates, an effect that contributes to the low coupling efficiency in *Drp1* KD MIN6 cells. These observations uncovered that *Drp1* influences both, glucose-fueled respiration used to make ATP and to drive proton leak. In a more physiologically relevant setup, the pancreatic mouse islet, *Drp1* deficiency impaired GSIS by limiting mitochondrial ATP synthesis-linked to glucose oxidation, with no effect on proton leak. Importantly, this *Drp1*-deficiency phenotype was also reproduced in human pancreatic islets, thus disclosing the translational relevance of *Drp1* control over GSIS.

Strikingly, our ‘substrate rescue’ experiments demonstrate that supply of exogenous pyruvate rescued GSIS defect exhibited by *Drp1*-deficient *β*-cells, despite of elevated proton leak. Similarly, our islet data provide compelling evidence that glucose-stimulated oxidative phosphorylation is largely controlled by substrate delivery, as supplementation with cell permeable methyl pyruvate rescued *Drp1*-related respiration, ATP output and eventually, insulin secretion, all of which were compromised after *Drp1* inhibition by mdivi-1. The ability to rescue impaired mitochondrial ATP output upstream of mitochondrial oxidative phosphorylation by direct substrate delivery opens a new window for the development of compounds to

treat mitochondrial diseases specifically, defect in insulin secretion associated with mitochondrial dysfunction. This important finding shed further light on the relationship between mitochondrial dynamics and function (Liesa and Shirihai, 2013) as it demonstrates that mitochondrial morphology can influence bioenergetic processes (glycolysis) that operate outside and upstream from the organelle itself. CE uncovers no difference between glucose- and pyruvate stimulated respiration in *Drp1*-inactivated cells (Fig. 14), thus elucidating no rescue of *Drp1*-related proton leak despite the rescue of ATP output and insulin secretion. It has recently been shown, in this respect, that cellular energy deficiency induces mitochondrial fission via AMPK-dependent *Fis1* and *Drp1* recruitment (Toyama et al., 2016). This fission has been interpreted as prerequisite for the removal of faulty mitochondria by mitophagy (Toyama et al., 2016), but our findings offer the alternative possibility that mitochondrial fragmentation enhances glycolytic metabolite delivery to mitochondria and thus maintains ATP output during times of high energetic demand. In conclusion, mitochondrial dynamics have profound effects on bioenergetics and immediately, may control upstream processes such as substrate delivery.

Additionally, our data show increased glucose uptake, excluding the possibility of compromised glucose availability in *Drp1*-deficient MIN6 cells. Glucokinase (GCK), a member of hexokinase family of enzymes, plays an integral role in glucose sensing. In pancreatic *β*-cells, GCK phosphorylate glucose and stimulate insulin secretion. Therefore, glucokinase activators could represent a viable treatment strategy in patients with T2D [135, 136]. Interestingly, glucokinase activator GKA50 rescued respiration and insulin secretion in *Drp1*-deficient MIN6 cells, an observation that supports the concept of lowered glucose catabolism but that requires further experimental confirmation in pancreatic islets. Furthermore, transient overexpression of *Drp1* rescued impaired insulin secretion triggering *in Drp1* KD MIN6 cells. At this stage, it can only be speculated that the complex machinery of fission-fusion requires several adjustments to improve insulin secretion beyond physiological levels. However, above findings confirms the critical role of *Drp1* in glucose homeostasis and *β*-cell function and also highlight modulation of mitochondrial dynamics as a mean to influence insulin secretion.

Besides, our data demonstrated diet-induced increase in insulin content of DIO islets, with no apparent pathologies in absolute GSIS compared to chow islets. Analysis of real-time respiratory data revealed marked decreases in glucose-stimulated respiration,

resulting in reduced ATP-linked respiration in DIO islets compared to chow islets. On the other hand, normalizing GSIS to insulin content uncovers compromised mitochondrial triggering of insulin secretion in DIO islets.

This study also highlights the importance of novel technologies such as real time multi-well plate-based respirometry for measuring cells and islets bioenergetics, to assess mechanisms of energy-coupled insulin secretion in pancreatic *β*-cell. Quantitative assessment of mitochondrial respiratory parameters like GSR, ATP-linked respiration, or CE identifies mitochondrial dysfunction and predicts insulin secretion, possibly serving as a biomarker for glucose responsiveness and islet health. Our model designed by plotting respiratory parameters vs. insulin secretion suggests defects in or upstream of oxidative phosphorylation in islets of DIO mice. Furthermore, coupling efficiency of oxidative phosphorylation is often an underestimated parameter that is very important for *β*-cell biology as it quantifies this proportion of glucose-fueled respiration that is coupled to ATP synthesis. As CE is an internally normalized parameter, it benefits from a comparably high signal-to-noise ratio that renders it exquisitely sensitive to *any* perturbation in proton leak, mitochondrial ATP synthesis and/or cellular substrate oxidation (Brand and Nicholls, 2011). CE reveals a bioenergetic threshold for insulin triggering that can be used to address mitochondrial failure across independent studies.

6 Conclusion and outlook

Collectively, the data of this thesis demonstrated that mitochondrial network fragmentation mediated by *Drp1* is necessary for glucose-mediated ATP synthesis and insulin secretion in MIN6 cells as well as in mouse and human pancreatic islets. *Drp1* mediates insulin secretion by controlling glycolytic substrate delivery to mitochondria, rather than directly affecting energy transduction at the mitochondrial inner membrane. Thus, mitochondrial dynamics exert profound control over cellular bioenergetics, and not only control mitochondrial activity *per se*, but also upstream energetic processes such as substrate delivery (e.g. glycolysis). Other players in the mitochondrial fission-fusion system also have profound effects on GSIS, such as *Opa1* (Zhang et al., 2011). Whether or not such effects on GSIS can be neutralized by substrate supplementation, or if pathological changes in mitochondrial dynamics may generally be rescued by increased substrate delivery, are questions that should be considered for future studies. Although my thesis suggests critical glycolytic steps being affected, in particular glucokinase activity, future studies should also consider compromised shuttling of glycolytic NADH to the mitochondrial matrix as this is immensely important in non-lactate producing *β*-cells. Furthermore, although the rescue by pyruvate argues against the role of mitochondrial pyruvate carrier (MPC) during limited substrate supply in *Drp1*-deficient systems, restricted pyruvate transport can also not be formally excluded at this stage.

Appendix-Solutions

All the media, buffers and solutions were prepared using demineralized, ultrapure water system and sterilized by filtration using 0.22 μm filter sets (Sarstedt, Nümbrecht, Germany).

Human islet culture medium

- 1X CMRL medium
- 10% human serum
- 1% penicillin/streptomycin
- 2 mM glutamine

HEPES-balanced Krebs-ringer (KRH) buffer

- 114 mM NaCl
- 4.7 mM KCl
- 2.5 mM $CaCl_2$
- 1.16 mM $MgSO_4$
- 1.2 mM KH_2PO_4
- 25.5 mM $NaHCO_3$
- 20 mM HEPES; supplemented with 0.2% BSA, pH 7.2-7.4

G-solution

- 1X Hank's Balanced Salt Solution (HBSS) solution
- 1% antibiotic anti-mycotic solution
- 1% Bovine serum albumin (BSA)

40% Optiprep solution

- 20 ml 60% Optiprep
- 9.7 ml DPBS
- 300 μl HEPES

Mouse islet culture medium

- RPMI 1640 GlutaMAX
- 10% Fetal bovine serum (FBS)
- 1% antibiotic anti-mycotic solution

10% RPMI

- 45 ml G-solution
- 5 ml mouse islet culture medium

15% Optiprep solution

- 3 ml/mouse 40% Optiprep solution
- 5 ml/mouse 10% RPMI

Collagenase P solution

- 10 mg collagenase powder/ mouse
- 8 ml G-solution/mouse (final concentration 1.25 mg/ml)

MIN6 standard culture medium

- 1X Dulbecco's modified Eagle's medium (DMEM) with glutaMAX containing 25 mM glucose
- 15% heat inactivated hyclone serum
- 72 μm 2-mercaptoethanol
- 1% penicillin/streptomycin

MIN6 culture medium without glucose

- 1X Dulbecco's modified Eagle's medium (DMEM) with glutaMAX containing 25 mM glucose
- 15% heat inactivated hyclone serum
- 72 μm 2-mercaptoethanol
- 1% penicillin/streptomycin

Luria broth (LB) agar plate medium

- 10 grams Typton
- 10 grams Nacl
- 5 grams Yeast extract
- 15 grams Agarose

Adjust the volume to 1 liter by water, pH-7. Sterilize by autoclaving for 20 mins at 15 psi (1.05 kg/cm^2) on liquid cycle.

Publications

- **Kabra UD,** Pfuhlmann K, Migliorini A, Keipert S, Lamp D, Korsgren O, Gegg M, Woods SC, Pfluger PT, Lickert H, Affourtit C, Tschöp MH, Jastroch M**.** Direct substrate delivery into mitochondrial fission-deficient pancreatic islets rescues insulin secretion (**In press** in **Diabetes**).
- **Kabra UD,** Affourtit C, Jastroch M**.** Mitochondrial respiratory parameters classify defective insulin secretion in pancreatic islets (in preparation).

Other contributions

- Kabra DG, Pfuhlmann K, García-Cáceres C, Schriever SC, Casquero García V, Kebede AF, Fuente-Martin E, Trivedi C, Heppner K, Uhlenhaut NH, Legutko B, **Kabra UD**, Gao Y, Yi CX, Quarta C, Clemmensen C, Finan B, Müller TD, Meyer CW, Paez-Pereda M, Stemmer K, Woods SC, Perez-Tilve D, Schneider R, Olson EN, Tschöp MH, Pfluger PT. Hypothalamic leptin action is mediated by histone deacetylase 5. Nat Commun. 2016 Feb 29; 7:10782.
- Tattikota SG, Rathjen T, Hausser J, Khedkar A, **Kabra UD**, Pandey V, Sury M, Wessels HH, Mollet IG, Eliasson L, Selbach M, Zinzen RP, Zavolan M, Kadener S, Tschöp MH, Jastroch M, Friedländer MR, Poy MN. miR-184 regulates pancreatic β-cell function according to glucose metabolism. J Biol Chem. 2015 Aug 14; 290(33): 20284-94.

References

AFFOURTIT, C. & BRAND, M. D. 2009. Measuring mitochondrial bioenergetics in INS-1E insulinoma cells. *Methods Enzymol,* 457**,** 405-24.

ALEXANDER, C., VOTRUBA, M., PESCH, U. E., THISELTON, D. L., MAYER, S., MOORE, A., RODRIGUEZ, M., KELLNER, U., LEO-KOTTLER, B., AUBURGER, G., BHATTACHARYA, S. S. & WISSINGER, B. 2000. OPA1, encoding a dynamin-related GTPase, is mutated in autosomal dominant optic atrophy linked to chromosome 3q28. *Nat Genet,* 26**,** 211-5.

ANELLO, M., LUPI, R., SPAMPINATO, D., PIRO, S., MASINI, M., BOGGI, U., DEL PRATO, S., RABUAZZO, A. M., PURRELLO, F. & MARCHETTI, P. 2005. Functional and morphological alterations of mitochondria in pancreatic beta cells from type 2 diabetic patients. *Diabetologia,* 48**,** 282-9.

ASHCROFT, F. M. 2005. ATP-sensitive potassium channelopathies: focus on insulin secretion. *J Clin Invest,* 115**,** 2047-58.

ASHCROFT, F. M., PROKS, P., SMITH, P. A., AMMALA, C., BOKVIST, K. & RORSMAN, P. 1994. Stimulus-secretion coupling in pancreatic beta cells. *J Cell Biochem,* 55 Suppl**,** 54-65.

BERGSTEN, P., LIN, J. & WESTERLUND, J. 1998. Pulsatile insulin release: role of cytoplasmic Ca2+ oscillations. *Diabetes Metab,* 24**,** 41-5.

BINDOKAS, V. P., KUZNETSOV, A., SREENAN, S., POLONSKY, K. S., ROE, M. W. & PHILIPSON, L. H. 2003. Visualizing superoxide production in normal and diabetic rat islets of Langerhans. *J Biol Chem,* 278**,** 9796-801.

BRAND, M. D. & NICHOLLS, D. G. 2011. Assessing mitochondrial dysfunction in cells. *Biochem J,* 435**,** 297-312.

BRASCHI, E., ZUNINO, R. & MCBRIDE, H. M. 2009. MAPL is a new mitochondrial SUMO E3 ligase that regulates mitochondrial fission. *EMBO Rep,* 10**,** 748-54.

BRZEZINSKI, P. & GENNIS, R. B. 2008. Cytochrome c oxidase: exciting progress and remaining mysteries. *J Bioenerg Biomembr,* 40**,** 521-31.

BUTLER, A. E., JANSON, J., BONNER-WEIR, S., RITZEL, R., RIZZA, R. A. & BUTLER, P. C. 2003. Beta-cell deficit and increased beta-cell apoptosis in humans with type 2 diabetes. *Diabetes,* 52**,** 102-10.

CABRERA, O., BERMAN, D. M., KENYON, N. S., RICORDI, C., BERGGREN, P. O. & CAICEDO, A. 2006. The unique cytoarchitecture of human pancreatic islets has implications for islet cell function. *Proc Natl Acad Sci U S A,* 103**,** 2334-9.

CAMPELLO, S. & SCORRANO, L. 2010. Mitochondrial shape changes: orchestrating cell pathophysiology. *EMBO Rep,* 11**,** 678-84.

CARNEIRO, L., ALLARD, C., GUISSARD, C., FIORAMONTI, X., TOURREL-CUZIN, C., BAILBE, D., BARREAU, C., OFFER, G., NEDELEC, E., SALIN, B., RIGOULET, M., BELENGUER, P., PENICAUD, L. & LELOUP, C. 2012. Importance of mitochondrial dynamin-related protein 1 in hypothalamic glucose sensitivity in rats. *Antioxid Redox Signal,* 17**,** 433-44.

CASSIDY-STONE, A., CHIPUK, J. E., INGERMAN, E., SONG, C., YOO, C., KUWANA, T., KURTH, M. J., SHAW, J. T., HINSHAW, J. E., GREEN, D. R. & NUNNARI, J. 2008. Chemical inhibition of the mitochondrial division dynamin reveals its role in Bax/Bak-dependent mitochondrial outer membrane permeabilization. *Dev Cell,* 14**,** 193-204.

CEREGHETTI, G. M., STANGHERLIN, A., MARTINS DE BRITO, O., CHANG, C. R., BLACKSTONE, C., BERNARDI, P. & SCORRANO, L. 2008. Dephosphorylation by calcineurin regulates translocation of Drp1 to mitochondria. *Proc Natl Acad Sci U S A,* 105**,** 15803-8.

CHAN, D. C. 2006. Mitochondria: dynamic organelles in disease, aging, and development. *Cell,* 125**,** 1241-52.

CHAN, D. C. 2012. Fusion and fission: interlinked processes critical for mitochondrial health. *Annu Rev Genet,* 46**,** 265-87.

CHANG, C. R. & BLACKSTONE, C. 2007. Cyclic AMP-dependent protein kinase phosphorylation of Drp1 regulates its GTPase activity and mitochondrial morphology. *J Biol Chem,* 282**,** 21583-7.

CHANG, C. R., MANLANDRO, C. M., ARNOULT, D., STADLER, J., POSEY, A. E., HILL, R. B. & BLACKSTONE, C. 2010. A lethal de novo mutation in the middle domain of the dynamin-related GTPase Drp1 impairs higher order assembly and mitochondrial division. *J Biol Chem,* 285**,** 32494-503.

CHEN, H. & CHAN, D. C. 2005. Emerging functions of mammalian mitochondrial fusion and fission. *Hum Mol Genet,* 14 Spec No. 2**,** R283-9.

CHEN, H., CHOMYN, A. & CHAN, D. C. 2005. Disruption of fusion results in mitochondrial heterogeneity and dysfunction. *J Biol Chem,* 280**,** 26185-92.

CHEN, H., DETMER, S. A., EWALD, A. J., GRIFFIN, E. E., FRASER, S. E. & CHAN, D. C. 2003. Mitofusins Mfn1 and Mfn2 coordinately regulate mitochondrial fusion and are essential for embryonic development. *J Cell Biol,* 160**,** 189-200.

CHEN, H., VERMULST, M., WANG, Y. E., CHOMYN, A., PROLLA, T. A., MCCAFFERY, J. M. & CHAN, D. C. 2010. Mitochondrial fusion is required for mtDNA stability in skeletal muscle and tolerance of mtDNA mutations. *Cell,* 141**,** 280-9.

CHENG, A. Y. & FANTUS, I. G. 2005. Oral antihyperglycemic therapy for type 2 diabetes mellitus. *CMAJ,* 172**,** 213-26.

CHO, B., CHOI, S. Y., CHO, H. M., KIM, H. J. & SUN, W. 2013. Physiological and pathological significance of dynamin-related protein 1 (drp1)-dependent mitochondrial fission in the nervous system. *Exp Neurobiol,* 22**,** 149-57.

CHO, D. H., NAKAMURA, T., FANG, J., CIEPLAK, P., GODZIK, A., GU, Z. & LIPTON, S. A. 2009. S-nitrosylation of Drp1 mediates beta-amyloid-related mitochondrial fission and neuronal injury. *Science,* 324**,** 102-5.

CIPOLAT, S., MARTINS DE BRITO, O., DAL ZILIO, B. & SCORRANO, L. 2004. OPA1 requires mitofusin 1 to promote mitochondrial fusion. *Proc Natl Acad Sci U S A,* 101**,** 15927-32.

COSTA, V., GIACOMELLO, M., HUDEC, R., LOPREIATO, R., ERMAK, G., LIM, D., MALORNI, W., DAVIES, K. J., CARAFOLI, E. & SCORRANO, L. 2010. Mitochondrial fission and cristae disruption increase the response of cell models of Huntington's disease to apoptotic stimuli. *EMBO Mol Med,* 2**,** 490-503.

CRIBBS, J. T. & STRACK, S. 2007. Reversible phosphorylation of Drp1 by cyclic AMP-dependent protein kinase and calcineurin regulates mitochondrial fission and cell death. *EMBO Rep,* 8**,** 939-44.

DAVIES, V. J., HOLLINS, A. J., PIECHOTA, M. J., YIP, W., DAVIES, J. R., WHITE, K. E., NICOLS, P. P., BOULTON, M. E. & VOTRUBA, M. 2007. Opa1 deficiency in a mouse model of autosomal dominant optic atrophy impairs mitochondrial morphology, optic nerve structure and visual function. *Hum Mol Genet,* 16**,** 1307-18.

DE BRITO, O. M. & SCORRANO, L. 2008. Mitofusin 2 tethers endoplasmic reticulum to mitochondria. *Nature,* 456**,** 605-10.

DE VOS, A., HEIMBERG, H., QUARTIER, E., HUYPENS, P., BOUWENS, L., PIPELEERS, D. & SCHUIT, F. 1995. Human and rat beta cells differ in glucose transporter but not in glucokinase gene expression. *J Clin Invest,* 96**,** 2489-95.

DEFRONZO, R. A. 2004. Pathogenesis of type 2 diabetes mellitus. *Med Clin North Am,* 88**,** 787-835, ix.

DIMAURO, S. & SCHON, E. A. 2003. Mitochondrial respiratory-chain diseases. *N Engl J Med,* 348**,** 2656-68.

DRUCKER, D. J. 2001. Minireview: the glucagon-like peptides. *Endocrinology,* 142**,** 521-7.

DUFER, M., KRIPPEIT-DREWS, P., BUNTINAS, L., SIEMEN, D. & DREWS, G. 2002. Methyl pyruvate stimulates pancreatic beta-cells by a direct effect on KATP channels, and not as a mitochondrial substrate. *Biochem J,* 368**,** 817-25.

FERNIE, A. R., CARRARI, F. & SWEETLOVE, L. J. 2004. Respiratory metabolism: glycolysis, the TCA cycle and mitochondrial electron transport. *Curr Opin Plant Biol,* 7**,** 254-61.

FIGUEROA-ROMERO, C., INIGUEZ-LLUHI, J. A., STADLER, J., CHANG, C. R., ARNOULT, D., KELLER, P. J., HONG, Y., BLACKSTONE, C. & FELDMAN, E. L. 2009. SUMOylation of the mitochondrial fission protein Drp1 occurs at multiple nonconsensus sites within the B domain and is linked to its activity cycle. *FASEB J,* 23**,** 3917-27.

FRANK, S., GAUME, B., BERGMANN-LEITNER, E. S., LEITNER, W. W., ROBERT, E. G., CATEZ, F., SMITH, C. L. & YOULE, R. J. 2001. The role of dynamin-related protein 1, a mediator of mitochondrial fission, in apoptosis. *Dev Cell,* 1**,** 515-25.

FREZZA, C., CIPOLAT, S., MARTINS DE BRITO, O., MICARONI, M., BEZNOUSSENKO, G. V., RUDKA, T., BARTOLI, D., POLISHUCK, R. S., DANIAL, N. N., DE STROOPER, B. & SCORRANO, L. 2006. OPA1 controls apoptotic cristae remodeling independently from mitochondrial fusion. *Cell,* 126**,** 177-89.

GAUTHIER, B. R., BRUN, T., SARRET, E. J., ISHIHARA, H., SCHAAD, O., DESCOMBES, P. & WOLLHEIM, C. B. 2004. Oligonucleotide microarray analysis reveals PDX1 as an essential regulator of mitochondrial metabolism in rat islets. *J Biol Chem,* 279**,** 31121-30.

GAWLOWSKI, T., SUAREZ, J., SCOTT, B., TORRES-GONZALEZ, M., WANG, H., SCHWAPPACHER, R., HAN, X., YATES, J. R., 3RD, HOSHIJIMA, M. & DILLMANN, W. 2012. Modulation of dynamin-related protein 1 (DRP1) function by increased O-linked-beta-N-acetylglucosamine modification (O-GlcNAc) in cardiac myocytes. *J Biol Chem,* 287**,** 30024-34.

GEMBAL, M., DETIMARY, P., GILON, P., GAO, Z. Y. & HENQUIN, J. C. 1993. Mechanisms by which glucose can control insulin release independently from its action on adenosine triphosphate-sensitive K+ channels in mouse B cells. *J Clin Invest,* 91**,** 871-80.

GLOYN, A. L. 2003. The search for type 2 diabetes genes. *Ageing Res Rev,* 2**,** 111-27.

GOMES, L. C., DI BENEDETTO, G. & SCORRANO, L. 2011. During autophagy mitochondria elongate, are spared from degradation and sustain cell viability. *Nat Cell Biol,* 13**,** 589-98.

GOMEZ-VALADES, A. G., GONZALEZ-FRANQUESA, A., GAMA-PEREZ, P., CLARET, M. & GARCIA-ROVES, P. M. 2015. Emerging concepts in Diabetes: mitochondrial dynamics and glucose homeostasis. *Curr Diabetes Rev*.

GREEN, A., CHRISTIAN HIRSCH, N. & PRAMMING, S. K. 2003. The changing world demography of type 2 diabetes. *Diabetes Metab Res Rev,* 19**,** 3-7.

GUO, C., HILDICK, K. L., LUO, J., DEARDEN, L., WILKINSON, K. A. & HENLEY, J. M. 2013. SENP3-mediated deSUMOylation of dynamin-related protein 1 promotes cell death following ischaemia. *EMBO J,* 32**,** 1514-28.

HARDER, Z., ZUNINO, R. & MCBRIDE, H. 2004. Sumo1 conjugates mitochondrial substrates and participates in mitochondrial fission. *Curr Biol,* 14**,** 340-5.

HENQUIN, J. C. 2000. Triggering and amplifying pathways of regulation of insulin secretion by glucose. *Diabetes,* 49**,** 1751-60.

HERMAN, M. A. & KAHN, B. B. 2006. Glucose transport and sensing in the maintenance of glucose homeostasis and metabolic harmony. *J Clin Invest,* 116**,** 1767-75.

HIRIART, M. & AGUILAR-BRYAN, L. 2008. Channel regulation of glucose sensing in the pancreatic beta-cell. *Am J Physiol Endocrinol Metab,* 295**,** E1298-306.

HOPPINS, S., LACKNER, L. & NUNNARI, J. 2007. The machines that divide and fuse mitochondria. *Annu Rev Biochem,* 76**,** 751-80.

HUANG, S., WANG, Y., GAN, X., FANG, D., ZHONG, C., WU, L., HU, G., SOSUNOV, A. A., MCKHANN, G. M., YU, H. & YAN, S. S. 2015. Drp1-mediated mitochondrial abnormalities link to synaptic injury in diabetes model. *Diabetes,* 64**,** 1728-42.

HUGHES, S. J., FAEHLING, M., THORNELEY, C. W., PROKS, P., ASHCROFT, F. M. & SMITH, P. A. 1998. Electrophysiological and metabolic characterization of single beta-cells and islets from diabetic GK rats. *Diabetes,* 47**,** 73-81.

IN'T VELD, P. & MARICHAL, M. 2010. Microscopic anatomy of the human islet of Langerhans. *Adv Exp Med Biol,* 654**,** 1-19.

INGERMAN, E., PERKINS, E. M., MARINO, M., MEARS, J. A., MCCAFFERY, J. M., HINSHAW, J. E. & NUNNARI, J. 2005. Dnm1 forms spirals that are structurally tailored to fit mitochondria. *J Cell Biol,* 170**,** 1021-7.

ISHIHARA, N., NOMURA, M., JOFUKU, A., KATO, H., SUZUKI, S. O., MASUDA, K., OTERA, H., NAKANISHI, Y., NONAKA, I., GOTO, Y., TAGUCHI, N., MORINAGA, H., MAEDA, M., TAKAYANAGI, R., YOKOTA, S. & MIHARA, K. 2009. Mitochondrial fission factor Drp1 is essential for embryonic development and synapse formation in mice. *Nat Cell Biol,* 11**,** 958-66.

JAMES, D. I., PARONE, P. A., MATTENBERGER, Y. & MARTINOU, J. C. 2003. hFis1, a novel component of the mammalian mitochondrial fission machinery. *J Biol Chem,* 278**,** 36373-9.

JAMES, P. & MCFADDEN, R. 2004. Understanding the processes behind the regulation of blood glucose. *Nurs Times,* 100**,** 56-8.

JHUN, B. S., LEE, H., JIN, Z. G. & YOON, Y. 2013. Glucose stimulation induces dynamic change of mitochondrial morphology to promote insulin secretion in the insulinoma cell line INS-1E. *PLoS One,* 8**,** e60810.

KABALEESWARAN, V., PURI, N., WALKER, J. E., LESLIE, A. G. & MUELLER, D. M. 2006. Novel features of the rotary catalytic mechanism revealed in the structure of yeast F1 ATPase. *EMBO J,* 25**,** 5433-42.

KAGEYAMA, Y., HOSHIJIMA, M., SEO, K., BEDJA, D., SYSA-SHAH, P., ANDRABI, S. A., CHEN, W., HOKE, A., DAWSON, V. L., DAWSON, T. M., GABRIELSON, K., KASS, D. A., IIJIMA, M. & SESAKI, H. 2014. Parkin-independent mitophagy requires Drp1 and maintains the integrity of mammalian heart and brain. *EMBO J,* 33**,** 2798-813.

KARBOWSKI, M., NEUTZNER, A. & YOULE, R. J. 2007. The mitochondrial E3 ubiquitin ligase MARCH5 is required for Drp1 dependent mitochondrial division. *J Cell Biol,* 178**,** 71-84.

KASHATUS, D. F., LIM, K. H., BRADY, D. C., PERSHING, N. L., COX, A. D. & COUNTER, C. M. 2011. RALA and RALBP1 regulate mitochondrial fission at mitosis. *Nat Cell Biol,* 13**,** 1108-15.

KAUFMAN, B. A., LI, C. & SOLEIMANPOUR, S. A. 2015. Mitochondrial regulation of beta-cell function: maintaining the momentum for insulin release. *Mol Aspects Med,* 42**,** 91-104.

KEIPERT, S. & JASTROCH, M. 2014. Brite/beige fat and UCP1 - is it thermogenesis? *Biochim Biophys Acta,* 1837**,** 1075-82.

KENNEDY, E. D., MAECHLER, P. & WOLLHEIM, C. B. 1998. Effects of depletion of mitochondrial DNA in metabolism secretion coupling in INS-1 cells. *Diabetes,* 47**,** 374-80.

KOMATSU, M., TAKEI, M., ISHII, H. & SATO, Y. 2013. Glucose-stimulated insulin secretion: A newer perspective. *J Diabetes Investig,* 4**,** 511-6.

KOSHIBA, T., DETMER, S. A., KAISER, J. T., CHEN, H., MCCAFFERY, J. M. & CHAN, D. C. 2004. Structural basis of mitochondrial tethering by mitofusin complexes. *Science,* 305**,** 858-62.

KUZUYA, T., NAKAGAWA, S., SATOH, J., KANAZAWA, Y., IWAMOTO, Y., KOBAYASHI, M., NANJO, K., SASAKI, A., SEINO, Y., ITO, C., SHIMA, K., NONAKA, K., KADOWAKI, T. & COMMITTEE OF THE JAPAN DIABETES SOCIETY ON THE DIAGNOSTIC CRITERIA OF DIABETES, M. 2002. Report of the Committee on the classification and diagnostic criteria of diabetes mellitus. *Diabetes Res Clin Pract,* 55**,** 65-85.

LACKNER, L. L. & NUNNARI, J. 2010. Small molecule inhibitors of mitochondrial division: tools that translate basic biological research into medicine. *Chem Biol,* 17**,** 578-83.

LAYBUTT, D. R., SHARMA, A., SGROI, D. C., GAUDET, J., BONNER-WEIR, S. & WEIR, G. C. 2002. Genetic regulation of metabolic pathways in beta-cells disrupted by hyperglycemia. *J Biol Chem,* 277**,** 10912-21.

LEE, Y. J., JEONG, S. Y., KARBOWSKI, M., SMITH, C. L. & YOULE, R. J. 2004. Roles of the mammalian mitochondrial fission and fusion mediators Fis1, Drp1, and Opa1 in apoptosis. *Mol Biol Cell,* 15**,** 5001-11.

LEIBIGER, B., WAHLANDER, K., BERGGREN, P. O. & LEIBIGER, I. B. 2000. Glucose-stimulated insulin biosynthesis depends on insulin-stimulated insulin gene transcription. *J Biol Chem,* 275**,** 30153-6.

LEMBERT, N., JOOS, H. C., IDAHL, L. A., AMMON, H. P. & WAHL, M. A. 2001. Methyl pyruvate initiates membrane depolarization and insulin release by metabolic factors other than ATP. *Biochem J,* 354**,** 345-50.

LESNEFSKY, E. J. & HOPPEL, C. L. 2006. Oxidative phosphorylation and aging. *Ageing Res Rev,* 5**,** 402-33.

LIESA, M. & SHIRIHAI, O. S. 2013. Mitochondrial dynamics in the regulation of nutrient utilization and energy expenditure. *Cell Metab,* 17**,** 491-506.

LIN, Y. & SUN, Z. 2010. Current views on type 2 diabetes. *J Endocrinol,* 204**,** 1-11.

LIU, J., CHEN, Z., ZHANG, Y., ZHANG, M., ZHU, X., FAN, Y., SHI, S., ZEN, K. & LIU, Z. 2013. Rhein protects pancreatic beta-cells from dynamin-related protein-1-mediated mitochondrial fission and cell apoptosis under hyperglycemia. *Diabetes,* 62**,** 3927-35.

LOSON, O. C., SONG, Z., CHEN, H. & CHAN, D. C. 2013. Fis1, Mff, MiD49, and MiD51 mediate Drp1 recruitment in mitochondrial fission. *Mol Biol Cell,* 24**,** 659-67.

MACDONALD, P. J., FRANCY, C. A., STEPANYANTS, N., LEHMAN, L., BAGLIO, A., MEARS, J. A., QI, X. & RAMACHANDRAN, R. 2016. Distinct Splice Variants of Dynamin-related Protein 1 Differentially Utilize Mitochondrial Fission Factor as an Effector of Cooperative GTPase Activity. *J Biol Chem,* 291**,** 493-507.

MACVICAR, T. D. & LANE, J. D. 2014. Impaired OMA1-dependent cleavage of OPA1 and reduced DRP1 fission activity combine to prevent mitophagy in cells that are dependent on oxidative phosphorylation. *J Cell Sci,* 127**,** 2313-25.

MAECHLER, P. & WOLLHEIM, C. B. 2001. Mitochondrial function in normal and diabetic beta-cells. *Nature,* 414**,** 807-12.

MANCZAK, M. & REDDY, P. H. 2015. Mitochondrial division inhibitor 1 protects against mutant huntingtin-induced abnormal mitochondrial dynamics and neuronal damage in Huntington's disease. *Hum Mol Genet,* 24**,** 7308-25.

MARTY, N., DALLAPORTA, M. & THORENS, B. 2007. Brain glucose sensing, counterregulation, and energy homeostasis. *Physiology (Bethesda),* 22**,** 241-51.

MATSCHINSKY, F. M. 1996. Banting Lecture 1995. A lesson in metabolic regulation inspired by the glucokinase glucose sensor paradigm. *Diabetes,* 45**,** 223-41.

MATSUNO-YAGI, A. & HATEFI, Y. 2001. Ubiquinol:cytochrome c oxidoreductase (complex III). Effect of inhibitors on cytochrome b reduction in submitochondrial particles and the role of ubiquinone in complex III. *J Biol Chem,* 276**,** 19006-11.

MEARS, J. A., LACKNER, L. L., FANG, S., INGERMAN, E., NUNNARI, J. & HINSHAW, J. E. 2011. Conformational changes in Dnm1 support a contractile mechanism for mitochondrial fission. *Nat Struct Mol Biol,* 18**,** 20-6.

MEN, X., WANG, H., LI, M., CAI, H., XU, S., ZHANG, W., XU, Y., YE, L., YANG, W., WOLLHEIM, C. B. & LOU, J. 2009. Dynamin-related protein 1 mediates high glucose induced pancreatic beta cell apoptosis. *Int J Biochem Cell Biol,* 41**,** 879-90.

MERTZ, R. J., WORLEY, J. F., SPENCER, B., JOHNSON, J. H. & DUKES, I. D. 1996. Activation of stimulus-secretion coupling in pancreatic beta-cells by specific products of glucose metabolism. Evidence for privileged signaling by glycolysis. *J Biol Chem,* 271**,** 4838-45.

MOLINA, A. J., WIKSTROM, J. D., STILES, L., LAS, G., MOHAMED, H., ELORZA, A., WALZER, G., TWIG, G., KATZ, S., CORKEY, B. E. & SHIRIHAI, O. S. 2009. Mitochondrial networking protects beta-cells from nutrient-induced apoptosis. *Diabetes,* 58**,** 2303-15.

NEUSPIEL, M., ZUNINO, R., GANGARAJU, S., RIPPSTEIN, P. & MCBRIDE, H. 2005. Activated mitofusin 2 signals mitochondrial fusion, interferes with Bax activation, and reduces susceptibility to radical induced depolarization. *J Biol Chem,* 280**,** 25060-70.

NODA, M., YAMASHITA, S., TAKAHASHI, N., ETO, K., SHEN, L. M., IZUMI, K., DANIEL, S., TSUBAMOTO, Y., NEMOTO, T., IINO, M., KASAI, H., SHARP, G. W. & KADOWAKI, T. 2002. Switch to anaerobic glucose metabolism with NADH accumulation in the beta-cell model of mitochondrial diabetes. Characteristics of betaHC9 cells deficient in mitochondrial DNA transcription. *J Biol Chem,* 277**,** 41817-26.

OTERA, H., WANG, C., CLELAND, M. M., SETOGUCHI, K., YOKOTA, S., YOULE, R. J. & MIHARA, K. 2010. Mff is an essential factor for mitochondrial recruitment of Drp1 during mitochondrial fission in mammalian cells. *J Cell Biol,* 191**,** 1141-58.

PALMER, C. S., ELGASS, K. D., PARTON, R. G., OSELLAME, L. D., STOJANOVSKI, D. & RYAN, M. T. 2013. Adaptor proteins MiD49 and

MiD51 can act independently of Mff and Fis1 in Drp1 recruitment and are specific for mitochondrial fission. *J Biol Chem,* 288**,** 27584-93.

PAPA, S., DE RASMO, D., SCACCO, S., SIGNORILE, A., TECHNIKOVA-DOBROVA, Z., PALMISANO, G., SARDANELLI, A. M., PAPA, F., PANELLI, D., SCARINGI, R. & SANTERAMO, A. 2008. Mammalian complex I: a regulable and vulnerable pacemaker in mitochondrial respiratory function. *Biochim Biophys Acta,* 1777**,** 719-28.

PAPA, S., MARTINO, P. L., CAPITANIO, G., GABALLO, A., DE RASMO, D., SIGNORILE, A. & PETRUZZELLA, V. 2012. The oxidative phosphorylation system in mammalian mitochondria. *Adv Exp Med Biol,* 942**,** 3-37.

PARK, K. S., WIEDERKEHR, A., KIRKPATRICK, C., MATTENBERGER, Y., MARTINOU, J. C., MARCHETTI, P., DEMAUREX, N. & WOLLHEIM, C. B. 2008. Selective actions of mitochondrial fission/fusion genes on metabolism-secretion coupling in insulin-releasing cells. *J Biol Chem,* 283**,** 33347-56.

PARK, Y. Y., LEE, S., KARBOWSKI, M., NEUTZNER, A., YOULE, R. J. & CHO, H. 2010. Loss of MARCH5 mitochondrial E3 ubiquitin ligase induces cellular senescence through dynamin-related protein 1 and mitofusin 1. *J Cell Sci,* 123**,** 619-26.

PARONE, P. A., DA CRUZ, S., TONDERA, D., MATTENBERGER, Y., JAMES, D. I., MAECHLER, P., BARJA, F. & MARTINOU, J. C. 2008. Preventing mitochondrial fission impairs mitochondrial function and leads to loss of mitochondrial DNA. *PLoS One,* 3**,** e3257.

PENG, L., MEN, X., ZHANG, W., WANG, H., XU, S., FANG, Q., LIU, H., YANG, W. & LOU, J. 2012. Involvement of dynamin-related protein 1 in free fatty acid-induced INS-1-derived cell apoptosis. *PLoS One,* 7**,** e49258.

PENG, L., MEN, X., ZHANG, W., WANG, H., XU, S., XU, M., XU, Y., YANG, W. & LOU, J. 2011. Dynamin-related protein 1 is implicated in endoplasmic reticulum stress-induced pancreatic beta-cell apoptosis. *Int J Mol Med,* 28**,** 161-9.

PORTHA, B., GIROIX, M. H., SERRADAS, P., WELSH, N., HELLERSTROM, C., SENER, A. & MALAISSE, W. J. 1988. Insulin production and glucose metabolism in isolated pancreatic islets of rats with NIDDM. *Diabetes,* 37**,** 1226-33.

QI, X., DISATNIK, M. H., SHEN, N., SOBEL, R. A. & MOCHLY-ROSEN, D. 2011. Aberrant mitochondrial fission in neurons induced by protein kinase C{delta} under oxidative stress conditions in vivo. *Mol Biol Cell,* 22**,** 256-65.

REASNER, C. A. 2008. Reducing cardiovascular complications of type 2 diabetes by targeting multiple risk factors. *J Cardiovasc Pharmacol,* 52**,** 136-44.

RICHTER, V., PALMER, C. S., OSELLAME, L. D., SINGH, A. P., ELGASS, K., STROUD, D. A., SESAKI, H., KVANSAKUL, M. & RYAN, M. T. 2014.

Structural and functional analysis of MiD51, a dynamin receptor required for mitochondrial fission. *J Cell Biol,* 204**,** 477-86.

RIDDERSTRALE, M. & GROOP, L. 2009. Genetic dissection of type 2 diabetes. *Mol Cell Endocrinol,* 297**,** 10-7.

SANTEL, A. & FRANK, S. 2008. Shaping mitochondria: The complex posttranslational regulation of the mitochondrial fission protein DRP1. *IUBMB Life,* 60**,** 448-55.

SCHAGGER, H. & PFEIFFER, K. 2000. Supercomplexes in the respiratory chains of yeast and mammalian mitochondria. *EMBO J,* 19**,** 1777-83.

SCHUIT, F., DE VOS, A., FARFARI, S., MOENS, K., PIPELEERS, D., BRUN, T. & PRENTKI, M. 1997. Metabolic fate of glucose in purified islet cells. Glucose-regulated anaplerosis in beta cells. *J Biol Chem,* 272**,** 18572-9.

SCHWARTZ, M. W., SEELEY, R. J., TSCHOP, M. H., WOODS, S. C., MORTON, G. J., MYERS, M. G. & D'ALESSIO, D. 2013. Cooperation between brain and islet in glucose homeostasis and diabetes. *Nature,* 503**,** 59-66.

SIVITZ, W. I. & YOREK, M. A. 2010. Mitochondrial dysfunction in diabetes: from molecular mechanisms to functional significance and therapeutic opportunities. *Antioxid Redox Signal,* 12**,** 537-77.

SMIRNOVA, E., GRIPARIC, L., SHURLAND, D. L. & VAN DER BLIEK, A. M. 2001. Dynamin-related protein Drp1 is required for mitochondrial division in mammalian cells. *Mol Biol Cell,* 12**,** 2245-56.

SMIRNOVA, E., SHURLAND, D. L., RYAZANTSEV, S. N. & VAN DER BLIEK, A. M. 1998. A human dynamin-related protein controls the distribution of mitochondria. *J Cell Biol,* 143**,** 351-8.

SOEJIMA, A., INOUE, K., TAKAI, D., KANEKO, M., ISHIHARA, H., OKA, Y. & HAYASHI, J. I. 1996. Mitochondrial DNA is required for regulation of glucose-stimulated insulin secretion in a mouse pancreatic beta cell line, MIN6. *J Biol Chem,* 271**,** 26194-9.

SOLDATOS, G. & COOPER, M. E. 2008. Diabetic nephropathy: important pathophysiologic mechanisms. *Diabetes Res Clin Pract,* 82 Suppl 1**,** S75-9.

SONG, Z., CHEN, H., FIKET, M., ALEXANDER, C. & CHAN, D. C. 2007. OPA1 processing controls mitochondrial fusion and is regulated by mRNA splicing, membrane potential, and Yme1L. *J Cell Biol,* 178**,** 749-55.

STEINER, D. J., KIM, A., MILLER, K. & HARA, M. 2010. Pancreatic islet plasticity: interspecies comparison of islet architecture and composition. *Islets,* 2**,** 135-45.

STRACK, S., WILSON, T. J. & CRIBBS, J. T. 2013. Cyclin-dependent kinases regulate splice-specific targeting of dynamin-related protein 1 to microtubules. *J Cell Biol,* 201**,** 1037-51.

STRAUB, S. G. & SHARP, G. W. 2002. Glucose-stimulated signaling pathways in biphasic insulin secretion. *Diabetes Metab Res Rev,* 18**,** 451-63.

TAGUCHI, N., ISHIHARA, N., JOFUKU, A., OKA, T. & MIHARA, K. 2007. Mitotic phosphorylation of dynamin-related GTPase Drp1 participates in mitochondrial fission. *J Biol Chem,* 282**,** 11521-9.

THORENS, B. 2008. Glucose sensing and the pathogenesis of obesity and type 2 diabetes. *Int J Obes (Lond),* 32 Suppl 6**,** S62-71.

TOYAMA, E. Q., HERZIG, S., COURCHET, J., LEWIS, T. L., JR., LOSON, O. C., HELLBERG, K., YOUNG, N. P., CHEN, H., POLLEUX, F., CHAN, D. C. & SHAW, R. J. 2016. Metabolism. AMP-activated protein kinase mediates mitochondrial fission in response to energy stress. *Science,* 351**,** 275-81.

TRIPLITT, C. L. 2012. Examining the mechanisms of glucose regulation. *Am J Manag Care,* 18**,** S4-10.

TSUKIHARA, T., SHIMOKATA, K., KATAYAMA, Y., SHIMADA, H., MURAMOTO, K., AOYAMA, H., MOCHIZUKI, M., SHINZAWA-ITOH, K., YAMASHITA, E., YAO, M., ISHIMURA, Y. & YOSHIKAWA, S. 2003. The low-spin heme of cytochrome c oxidase as the driving element of the proton-pumping process. *Proc Natl Acad Sci U S A,* 100**,** 15304-9.

TWIG, G., ELORZA, A., MOLINA, A. J., MOHAMED, H., WIKSTROM, J. D., WALZER, G., STILES, L., HAIGH, S. E., KATZ, S., LAS, G., ALROY, J., WU, M., PY, B. F., YUAN, J., DEENEY, J. T., CORKEY, B. E. & SHIRIHAI, O. S. 2008. Fission and selective fusion govern mitochondrial segregation and elimination by autophagy. *EMBO J,* 27**,** 433-46.

UO, T., DWORZAK, J., KINOSHITA, C., INMAN, D. M., KINOSHITA, Y., HORNER, P. J. & MORRISON, R. S. 2009. Drp1 levels constitutively regulate mitochondrial dynamics and cell survival in cortical neurons. *Exp Neurol,* 218**,** 274-85.

WAI, T. & LANGER, T. 2016. Mitochondrial Dynamics and Metabolic Regulation. *Trends Endocrinol Metab,* 27**,** 105-17.

WANG, H., SONG, P., DU, L., TIAN, W., YUE, W., LIU, M., LI, D., WANG, B., ZHU, Y., CAO, C., ZHOU, J. & CHEN, Q. 2011. Parkin ubiquitinates Drp1 for proteasome-dependent degradation: implication of dysregulated mitochondrial dynamics in Parkinson disease. *J Biol Chem,* 286**,** 11649-58.

WANG, X., SU, B., LEE, H. G., LI, X., PERRY, G., SMITH, M. A. & ZHU, X. 2009. Impaired balance of mitochondrial fission and fusion in Alzheimer's disease. *J Neurosci,* 29**,** 9090-103.

WARNOTTE, C., GILON, P., NENQUIN, M. & HENQUIN, J. C. 1994. Mechanisms of the stimulation of insulin release by saturated fatty acids. A study of palmitate effects in mouse beta-cells. *Diabetes,* 43**,** 703-11.

WATERHAM, H. R., KOSTER, J., VAN ROERMUND, C. W., MOOYER, P. A., WANDERS, R. J. & LEONARD, J. V. 2007. A lethal defect of mitochondrial and peroxisomal fission. *N Engl J Med,* 356**,** 1736-41.

WEIR, G. C., LAYBUTT, D. R., KANETO, H., BONNER-WEIR, S. & SHARMA, A. 2001. Beta-cell adaptation and decompensation during the progression of diabetes. *Diabetes,* 50 Suppl 1**,** S154-9.

WEYER, C., TATARANNI, P. A., BOGARDUS, C. & PRATLEY, R. E. 2001. Insulin resistance and insulin secretory dysfunction are independent predictors of worsening of glucose tolerance during each stage of type 2 diabetes development. *Diabetes Care,* 24**,** 89-94.

WIKSTROM, J. D., ISRAELI, T., BACHAR-WIKSTROM, E., SWISA, A., ARIAV, Y., WAISS, M., KAGANOVICH, D., DOR, Y., CERASI, E. & LEIBOWITZ, G. 2013. AMPK regulates ER morphology and function in stressed pancreatic beta-cells via phosphorylation of DRP1. *Mol Endocrinol,* 27**,** 1706-23.

YANG, S. N. & BERGGREN, P. O. 2006. The role of voltage-gated calcium channels in pancreatic beta-cell physiology and pathophysiology. *Endocr Rev,* 27**,** 621-76.

ZAJA, I., BAI, X., LIU, Y., KIKUCHI, C., DOSENOVIC, S., YAN, Y., CANFIELD, S. G. & BOSNJAK, Z. J. 2014. Cdk1, PKCdelta and calcineurin-mediated Drp1 pathway contributes to mitochondrial fission-induced cardiomyocyte death. *Biochem Biophys Res Commun,* 453**,** 710-21.

ZHANG, C. Y., BAFFY, G., PERRET, P., KRAUSS, S., PERONI, O., GRUJIC, D., HAGEN, T., VIDAL-PUIG, A. J., BOSS, O., KIM, Y. B., ZHENG, X. X., WHEELER, M. B., SHULMAN, G. I., CHAN, C. B. & LOWELL, B. B. 2001. Uncoupling protein-2 negatively regulates insulin secretion and is a major link between obesity, beta cell dysfunction, and type 2 diabetes. *Cell,* 105**,** 745-55.

ZHANG, Z., WAKABAYASHI, N., WAKABAYASHI, J., TAMURA, Y., SONG, W. J., SEREDA, S., CLERC, P., POLSTER, B. M., AJA, S. M., PLETNIKOV, M. V., KENSLER, T. W., SHIRIHAI, O. S., IIJIMA, M., HUSSAIN, M. A. & SESAKI, H. 2011. The dynamin-related GTPase Opa1 is required for glucose-stimulated ATP production in pancreatic beta cells. *Mol Biol Cell,* 22**,** 2235-45.

ZHAO, Y. X., CUI, M., CHEN, S. F., DONG, Q. & LIU, X. Y. 2014. Amelioration of ischemic mitochondrial injury and Bax-dependent outer membrane permeabilization by Mdivi-1. *CNS Neurosci Ther,* 20**,** 528-38.

ZIMMET, P., ALBERTI, K. G. & SHAW, J. 2001. Global and societal implications of the diabetes epidemic. *Nature,* 414**,** 782-7.

ZUCHNER, S., MERSIYANOVA, I. V., MUGLIA, M., BISSAR-TADMOURI, N., ROCHELLE, J., DADALI, E. L., ZAPPIA, M., NELIS, E., PATITUCCI, A., SENDEREK, J., PARMAN, Y., EVGRAFOV, O., JONGHE, P. D., TAKAHASHI, Y., TSUJI, S., PERICAK-VANCE, M. A., QUATTRONE, A.,

BATTALOGLU, E., POLYAKOV, A. V., TIMMERMAN, V., SCHRODER, J. M. & VANCE, J. M. 2004. Mutations in the mitochondrial GTPase mitofusin 2 cause Charcot-Marie-Tooth neuropathy type 2A. *Nat Genet,* 36**,** 449-51.

ZUNINO, R., SCHAUSS, A., RIPPSTEIN, P., ANDRADE-NAVARRO, M. & MCBRIDE, H. M. 2007. The SUMO protease SENP5 is required to maintain mitochondrial morphology and function. *J Cell Sci,* 120**,** 1178-88.